Copyright Undertaking

This thesis is protected by copyright, with all rights reserved.

By reading and using the thesis, the reader understands and agrees to the following terms:

1. The reader will abide by the rules and legal ordinances governing copyright regarding the use of the thesis.
2. The reader will use the thesis for the purpose of research or private study only and not for distribution or further reproduction or any other purpose.
3. The reader agrees to indemnify and hold the University harmless from and against any loss, damage, cost, liability or expenses arising from copyright infringement or unauthorized usage.

If you have reasons to believe that any materials in this thesis are deemed not suitable to be distributed in this form, or a copyright owner having difficulty with the material being included in our database, please contact lbsys@polyu.edu.hk providing details. The Library will look into your claim and consider taking remedial action upon receipt of the written requests.

Pao Yue-kong Library, The Hong Kong Polytechnic University, Hung Hom, Kowloon, Hong Kong

http://www.lib.polyu.edu.hk

CHARACTERIZATION OF SURFACE ACOUSTIC WAVE (SAW) FILTERS GROWN ON ALUMINUM NITRIDE AND ZINC OXIDE THIN FILMS

By

Lai Pak Kin

A Thesis Submitted to

The Hong Kong Polytechnic University

in Partial Fulfillment of the Requirements for

the Degree of Master of Philosophy

in Department of Electronic and Information Engineering

January 2004, Hong Kong

Pao Yue-kong Library
PolyU • Hong Kong

Certificate of Originality

I hereby declare that this thesis is my own work and that, to the best of my knowledge and belief, it reproduces no material previously published or written, nor material that has been accepted for the award of any other degree or diploma, except where due acknowledgement has been made in the text.

LAI PAK KIN (Lai Pak Kin)

Abstract

The study on the influences of the aluminum nitride (AlN) and zinc oxide (ZnO) film quality on the SAW filter performances were conducted. In our studies the phase velocity (V_P) and electromechanical coupling coefficient (K^2) are the most important considerations. Both AlN and ZnO piezoelectric thin films were selected for their high V_P and K^2. The AlN and ZnO thin films were grown by rf magnetron sputtering technique and the influences of different sputtering conditions on the structure and the surface morphology of the thin films were investigated. Sputtering power and substrate temperature were found to be the most important factors affecting the crystal structure and the surface roughness of the thin films respectively. To further study the relationship between the quality and the surface roughness of the thin films and the SAW filter performances, AlN and ZnO thin films, grown with different sputtering powers and substrate temperatures, were fabricated into SAW filters and the devices were systematically characterized. Detailed characterizations of the frequency response, K^2, phase noise and insertion loss of the SAW filters were conducted as a function of the full width half maximum of the x-ray diffraction pattern and the surface roughness of both the AlN and ZnO thin films. From the experiment results, V_P, K^2, insertion loss and phase noise of the SAW filters were strongly affected by the sputtering power and the substrate temperature at which the films were grown. In the second part of this thesis, MBE technique was used to further improve the material quality. From the measurement results, AlN SAW filters grown by MBE technique were much better than those grown by rf magnetron sputtering. This clearly demonstrates the significant influence of the material quality of the thin film on device performance.

Acknowledgements

I am grateful to Professor P. K. Alex Wai, Head of Department of Electronic and Information Engineering, for offering an opportunity to join the department and a studentship for the financial support.

It is a pleasure for me to acknowledge my indebtedness to both my chief supervisor Professor Charles Surya and co-supervisor Dr. W.Y. Tam for their patient understanding, helpful discussions and stimulating guidance. My special thanks also go to Dr. W.Y. Tam for his financial support during the extended study period.

I would like to thank Dr. W. K. Fong for providing the AlN substrate samples together with helpful discussions and Dr Martin chow for helpful discussion on phase noise measurement. I also wish to thank the members of the Thin Film Optoelectronics Research Group, Professor Alex Wai, Dr. W. S. Li, Dr. W. K. Fong, Mr. B. H. Leung, Mr. Leo Tung, Mr. Hardy Lui and Mr. C. W. Lip. I wish to express my gratitude to Dr. C. F. Zhu for his help, guidance and enlightening discussions.

I deeply thank my parents for their love, patience and non-stop support. Last but not least I thank my girlfriend, Ellen Ho, for her understanding and perseverance.

Abstract ii

Acknowledgements iii

Table of Contents iv

List of Tables vi

List of Figures vii

1. Introduction 1
   - 1.1 Overview of SAW devices 1
     - 1.1.1 Historical background of SAW devices 1
     - 1.1.2 Principle of SAW devices 8
     - 1.1.3 Applications of SAW devices 13
     - 1.1.4 Current status of SAW materials development 15
   - 1.2 Use of AlN and ZnO as SAW materials 20
     - 1.2.1 Introduction 20
     - 1.2.2 The structure of AlN and ZnO 20
       - 1.2.2.1 Properties of aluminum nitride 20
       - 1.2.2.2 Properties of zinc oxide 21
     - 1.2.3 Piezoelectric effect 21

2. Experimental process 24
   - 2.1 Introduction 24
   - 2.2 Growth of AlN and ZnO thin films on sapphire by rf magnetron sputtering and MBE techniques 26
     - 2.2.1 AlN and ZnO deposition by rf magnetron sputtering technique 26
       - 2.2.1.1 Principle of rf magnetron sputtering 26
       - 2.2.1.2 Samples preparation 30
     - 2.2.2. AlN thin film deposition by MBE technique 32
       - 2.2.2.1 Principle of MBE growth 32
       - 2.2.2.2 Samples preparation 33
   - 2.3 Thin film characterization 34
     - 2.3.1 X-ray diffraction (XRD) 34
     - 2.3.2 Atomic force microscopy (AFM) 35
     - 2.3.3 Scanning electron microscopy (SEM) 36
   - 2.4 SAW filters fabrication and characterization 37
     - 2.4.1. SAW filters fabrication 37
     - 2.4.2 SAW filters measurements 41
       - 2.4.2.1 Frequency response and insertion loss 41
       - 2.4.2.2 Phase noise measurement 47

3. Experimental Results 55
- 3.1 Experimental results on AlN and ZnO SAW filters deposition on sapphire grown by rf magnetron sputtering technique 55
  - 3.1.1 Characterization of AlN and ZnO thin films deposition on sapphire grown by rf sputtering technique 55
  - 3.1.2 Characterization of AlN and ZnO SAW filters grown by rf magnetron sputtering technique 76
- 3.2 Experimental results on AlN SAW filters grown by rf magnetron sputtering and MBE techniques 90
  - 3.2.1 Characterization of AlN thin films deposition on sapphire grown by MBE technique 90
  - 3.2.2 Characterization of AlN SAW filters grown by MBE technique 94

4. Discussion 99
- 4.1 Analysis of AlN and ZnO based SAW filters grown by rf magnetron sputtering technique 99
  - 4.1.1 Effect of sputtering parameters on the quality of the AlN and ZnO thin films 99
  - 4.1.2 The relationship between surface roughness, crystallinity and AlN and ZnO SAW filter performance 105
- 4.2 The relationship between AlN SAW filters grown by rf sputtering and MBE techniques 113
  - 4.2.1 Comparison between the material quality of AlN thin films deposition by rf magnetron sputtering and MBE techniques 113
  - 4.2.2 Comparison between crystallinity and SAW filters performance grown by rf magnetron sputtering and MBE techniques 115

5. Conclusion 119

Reference 121

List of Tables

Table 1.1 Common parameters substrates for SAW devices 19
Table 2.1 Variation of sputtering conditions for ZnO 31
Table 2.2 Variation of sputtering conditions for AlN 31
Table 2.3 Summary of growing conditions of AlN by MBE 33
Table 2.4 Parameters of the designed SAW filter 40
Table 3.1 The summary of the operation frequency of both AlN and ZnO SAW filters under different IDT electrode linewidth. 77
Table 4.1 Optimal sputtering conditions for ZnO 104
Table 4.2 Optimal sputtering conditions for AlN 104

List of Figures

Fig. 1.1	Schematic diagram of the SAW filter	3
Fig. 1.2	Schematic diagram of a convolver	3
Fig. 1.3	A schematic diagram of single phase unidirectional transducers (SPUDT)	6
Fig. 1.4	Propagation of the surface acoustic wave	12
Fig. 2.1	A schematic diagram of zone model of film deposition	28
Fig. 2.2	Fabrication of IDT using liftoff process	39
Fig. 2.3	Schematic diagram of the SAW filter	40
Fig. 2.4	The measurement setup of the frequency response and insertion loss	42
Fig. 2.5	A equivalent circuit of a SAW filter	42
Fig. 2.6	Thin metal film on the top of the piezoelectric substrate	46
Fig. 2.7	The schematic diagram of Leeson's model	51
Fig. 2.8	Phase noise measurement setup	53
Fig. 3.1	Influence of different sputtering powers to the FWHM and growth rates on the sputtering AlN grown with 0.5Pa., 400°C and 50% N_2	57
Fig. 3.2	Influence of different sputtering pressures to the FWHM and growth rates on the sputtering AlN grown with 350W, 400°C and 50% N_2.	57
Fig. 3.3	Influence of different gas ratios to the FWHM and growth rates on the sputtering AlN grown with 0.5Pa., 400°C and 350W	58
Fig. 3.4	Influence of different substrate temperatures to the FWHM and growth rate on the sputtering AlN grown with 0.5Pa., 50% N_2 and 350W	58
Fig. 3.5	The 2th-th scanning of AlN / sapphire grown at 0.5 Pa., 50% N_2, 400°C and 350W	60
Fig. 3.6	The rocking curve of AlN / sapphire grown at 0.5 Pa., 50% N_2, 400°C and 350W	60
Fig. 3.7	Influence of different sputtering powers to the FWHM and growth rates on the sputtering ZnO grown with 1.5Pa. 100°C and 50% O_2	61
Fig. 3.8	Influence of different sputtering pressures to the FWHM and growth rates on the sputtering ZnO grown with 100W, 100°C and 50% O_2	61
Fig. 3.9	Influence of different gas ratios to the FWHM and growth rates on the sputtering ZnO grown with 1.5Pa. , 100°C and 100W	63
Fig. 3.10	Influence of different substrate temperatures to the FWHM and growth rates on the sputtering ZnO grown with 1.5Pa. , 50% O_2 and 100W	63
Fig. 3.11	The 2th-th scanning of ZnO / sapphire grown at 1.5Pa. , 50% O_2, 100°C and 100W	64
Fig. 3.12	The rocking curve scanning of ZnO / sapphire grown at 1.5Pa, 50% O_2, 100°C and 100W	64
Fig. 3.13	The SEM picture of the cross-section of both (a) AlN (b) ZnO thin films	66
Fig. 3.14	The FWHM of XRD peak from the AlN films grown by different sputtering powers	68
Fig. 3.15	The FWHM of XRD peak from the ZnO films grown by different sputtering powers	68
Fig. 3.16	The FWHM of XRD peak from the AlN films grown by different substrate temperatures	69
Fig. 3.17	The FWHM of XRD peak from the ZnO films grown by different substrate temperatures	69
Fig. 3.18	The effect of the different substrate temperatures on the surface morphology of AlN / sapphire at (a) 200°C (b) 300°C (c) 400°C	70

Fig. 3.19	The effect of the different substrate temperatures on the surface morphology of ZnO / sapphire at (a) 50°C (b) 100°C (c) 200°C	71
Fig. 3.20	The surface morphology of the AlN thin films deposited at different sputtering powers	73
Fig. 3.21	The surface morphology of the AlN thin films deposited at different substrate temperatures	73
Fig. 3.22	The surface morphology of the ZnO thin films deposited at different sputtering powers	74
Fig. 3.23	The surface morphology of the ZnO thin films deposited at different substrate temperatures	74
Fig. 3.24	The surface morphology of the AlN thin film grown at 400°C under AFM measurement	75
Fig. 3.25	The surface morphology of the ZnO thin film grown at 100°C under AFM measurement	75
Fig. 3.26	The picture of SAW filter under optical microscope	77
Fig. 3.27	The frequency response of AlN SAW filters fabricated with various electrode linewidths (a) 4 μm (b) 2μm (c) 1μm	78
Fig. 3.28	The frequency response of ZnO SAW filters fabricated with various electrode linewidths (a) 4 μm (b) 2μm (c) 1μm	79
Fig. 3.29	The phase velocity of SAW filters grown with different sputtering powers (a) AlN SAW filters and (b) ZnO SAW filters	81
Fig. 3.30	The phase velocity of SAW filters grown with different substrate temperatures (a) AlN SAW filters and (b) ZnO SAW filters	82
Fig. 3.31	The electromechanical coupling coefficient of SAW filters grown with different sputtering powers (a) AlN SAW filters and (b) ZnO SAW filters	83
Fig. 3.32	The electromechanical coupling coefficient of SAW filters grown with different substrate temperatures (a) AlN SAW filters and (b) ZnO SAW filters	84
Fig. 3.33	The phase noise of SAW filters grown with different sputtering powers (a) AlN SAW filters and (b) ZnO SAW filters	86
Fig. 3.34	The phase noise of SAW filters grown with different substrate temperatures (a) AlN SAW filters and (b) ZnO SAW filters	87
Fig. 3.35	The insertion loss of SAW filters grown with different sputtering powers (a) AlN SAW filters and (b) ZnO SAW filters	88
Fig. 3.36	The insertion loss of SAW filters grown with different substrate temperatures (a) AlN SAW filters and (b) ZnO SAW filters	89
Fig. 3.37	Influence of different aluminum cell temperatures to the FWHM on the AlN thin films grown by MBE	91
Fig. 3.38	The 2th-th scanning of XRD peak of AlN / sapphire grown by MBE at 1122°C	92
Fig. 3.39	The omega scanning of XRD peak of AlN / sapphire grown by MBE at 1122°C	92
Fig. 3.40	The SEM picture of AlN thin film grown by MBE (a) surface morphology (b) cross-section	93
Fig. 3.41	The roughness of AlN thin films grown by MBE at various Al cell temperature	95
Fig. 3.42	The AFM picture of the surface morphology of AlN thin film grown by MBE at 1125°C	95
Fig. 3.43	The frequency response of AlN SAW filters grown by MBE fabricated with various electrode linewidths (a) 4 μm (b) 2μm (c) 1μm	96

Fig. 3.44	The phase velocity of AlN SAW filters grown by MBE at various Al cell temperatures	97
Fig. 3.45	The electromechanical coupling coefficient of AlN SAW filters grown by MBE at various Al cell temperatures	97
Fig. 3.46	The phase noise of AlN SAW filters grown by MBE at various Al cell temperatures	98
Fig. 3.47	The insertion loss of AlN SAW filters grown by MBE at various Al cell temperatures	98
Fig. 4.1	The phase velocity of the SAW filters grown at different condition (a) AlN and (b) ZnO SAW filters	109
Fig. 4.2	The electromechanical coupling coefficient of the SAW filter grown at different conditions (a) AlN and (b) ZnO SAW filters	110
Fig. 4.3	The phase noise of the SAW filters grown at different conditions (a) AlN and (b) ZnO SAW filters	111
Fig. 4.4	The insertion loss of the SAW filters grown at different conditions (a) AlN and (b) ZnO SAW filters	112
Fig. 4.5	The phase velocity of the AlN SAW filters grown by MBE with different qualities.	117
Fig. 4.6	The electromechanical coupling coefficient of the AlN SAW filters grown by MBE with different qualities.	117
Fig. 4.7	The phase noise of the AlN SAW filters grown by MBE with different qualities.	118
Fig. 4.8	The insertion loss of the AlN SAW filters grown by MBE with different qualities.	118

1. Introduction

1.1 Overview of SAW devices

1.1.1 History background of SAW devices

Surface acoustic wave (SAW) can be generated on the free surface of an elastic solid. This phenomenon has been utilized in various devices and systems for consumers, commercial and military applications over the past 20 years with a multimillion-dollar. SAW was discovered over a century ago. The first report on SAW was given by Lord Rayleigh in 1885 [1] and hence SAW was also called "Rayleigh wave". Rayleigh was particularly interested in the seismic signals after the ground shock [2]. The presence of SAW in earthquake shocks was later verified using seismography recording techniques. The property of SAW propagation was first explored for applications in electronic devices in 1965. White and Voltmer [3] realized that a special pattern of electrode called interdigital transducer (IDT) that was the most efficient technique for the generation and detection of SAW waves on a piezoelectric surface. IDT is made of rectangular comb-liked electrodes as shown in Fig. 1.1. In 1969, Tancrell *et al.* suggested that the overlapping of the IDT electrodes could be designed to obtain different frequency response. This technique was later called 'apodization' which provides variable weighting factor [4] to the electrodes overlapping. They also showed that different pattern of the electrodes could reduce the time-sidelobes of the radar output pulse. This is a vital factor in the application

of SAW device.

The reflection of SAW was also utilized in the SAW device. SAW reflection was first demonstrated by Court *et al.* [5]. They found that the degree of reflectivity of SAW depends on the geometry of the reflector, such as the etched grooves and metal strip. This idea was then reviewed by Ash *et al* [6,7] who showed that good SAW reflectivity can be obtained, over a limited bandwidth, by using a regular array of rectangular reflectors, resulting in the maximum SAW reflectivity when the width is $\lambda/2$. Maine *et al.* [8] then successfully applied this idea and the first SAW oscillator was produced in 1970. A SAW oscillator would have two reflective gratings forming a resonating cavity with two IDT's in between, one serving as the input and the other as the output. Two arrays of metal strips with $\lambda/2$ width are located behind two inputs and output IDTs such that the metal strips acted as a reflective grating. While the output of the IDT is fed back to the input IDT via an amplifier, an oscillation therefore occurs.

SAW propagates from the input IDT to the output IDT while the energy is confined on the surface of the substrate. The variation of the surface condition means varying the propagation condition of SAW. The idea of a convolver is the best illustration of this idea. The first SAW convolver was reported by LuuKKala and Kino *et al.* [9] and is shown in Fig. 1.2. In a basic convolver, two SAWs propagating in two different directions are generated by two input transducers located at the two ends of the substrate, so that the generated SAWs interfere in the region between the two

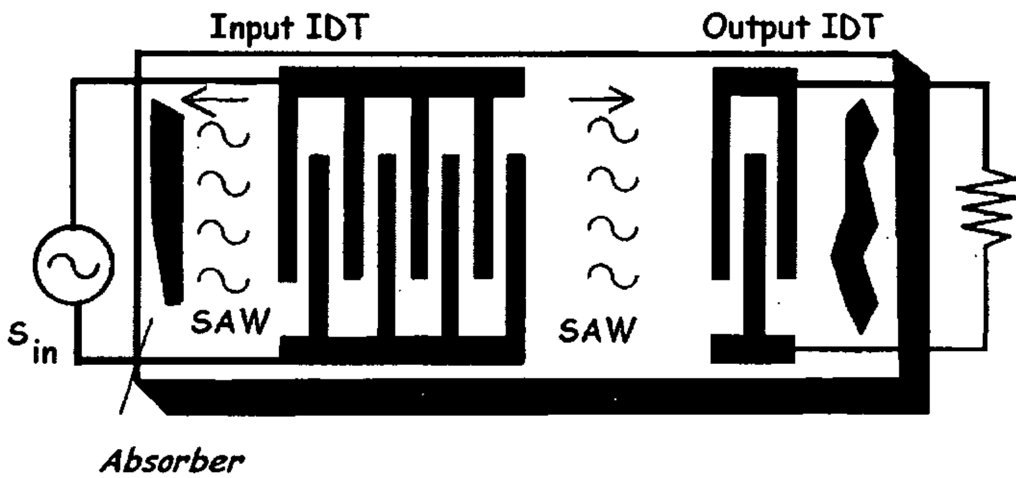

Fig. 1.1 Schematic diagram of the SAW filter

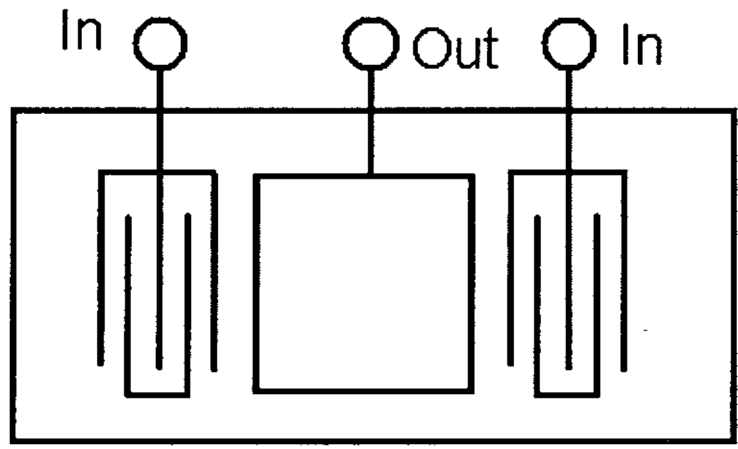

Fig 1.2 Schematic diagram of a convolver

transducers. The non-linearity gives rise to an electric field proportional to the product of the two SAW amplitudes as given by the equation below:

$$V_{out} = \int_{-\infty}^{\infty} S_1(\tau) \bullet S_2(2t - \tau) d\tau \qquad (1.1)$$

where S_1, S_2 are the two input signals and τ is the time delay due to the output electrode. The field is then sensed and spatially averaged by a uniform electrode on the surface between the two input transducers. For general input wavefronts, it can be shown that the output is ideally the convolution of the two input waveforms, hence the name 'convolver'.

One of the main problems of SAW devices is their high insertion loss, which is typically about 6dB. The problem arises since SAW excited by IDT propagates in two different directions. One way is toward the receiving IDT and the other is away from the receiving IDT. It is obvious that there is an energy loss of about 3dB due to the propagation of SAW in opposite direction. The other 3 dB loss is the same as that in the input IDT. In addition, another spurious signal source is induced. Since another SAW will be generated by the output IDT, it will interfere with the SAW generated by input IDT in the second period and finally reach the output IDT again. After the interference of SAW, from the point of view of the output input, the reflected SAW becomes a spurious signal and when couple with the unwanted multiple-transit signals, it causes serious adverse effects in the device characteristics. The earliest SAW filters had high insertion loss, typically more than 20dB.

Unidirectional transducer (UDT) was designed to solve this problem. A schematic diagram of this transducer is demonstrated in Fig. 1.3. The initial structure of UDT, introduced by Hartmann *et al.* [16], was a double electrode transducer made by alternate electrodes with different thickness shown in Fig. 1.3a. As the metal electrode thickness is increased, this enhances the loading of the acoustic impedance and reduces the inter-electrode reflection of SAW. Thus, there is no reflected wave, generation and propagation take place in one direction only. As shown in Figs. 1.3b and c, the electrodes are designed with different widths and reflective gratings introduced by Lewis [17] and Kodama [18] respectively. In these SPUDTs, the internal reflection of SAW inside the electrodes can be further reduced such that SAW is forced to propagate in one-direction only. A device with two transducers ideally gives a 0 dB insertion loss with no reflection at the center frequency.

Modeling tools for the devices are necessary for device designers. The first theoretical approach for modeling IDT in a SAW device is a 'delta-function' model derived by Holland *et al.* [20], which considers a localized source at the edge of each electrode. A localized source can be represented using a spatial delta function. To simplify the modeling, the source was considered to exist where the electrodes have different polarities. Excitation of SAW is analyzed by adding the waves, which is generated by an electrode. The disadvantage of this model is that it ignores the presence of other electrodes, hence excluding SAW reflection in between electrode. The analysis of IDT behaviors on piezoelectric substrates were further studied by

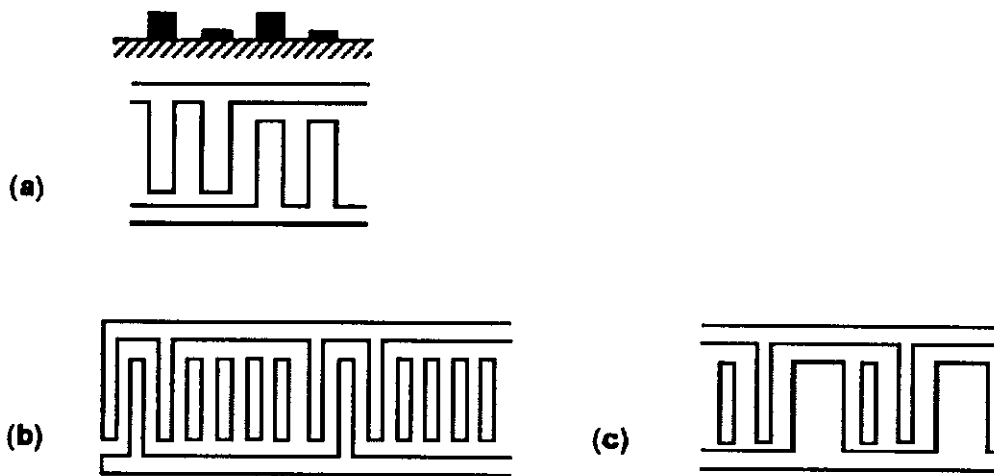

Fig. 1.3 A schematic diagram of single phase unidirectional transducers (SPUDT)

Conquin and Tiersten *et al.* [21], Joshi and White *et al.* [22] and Skeie *et al.* [23], utilizing several different approaches. However, the model was not widely adopted by design engineers. The main reason was due to the complexities and the limitations of unweighted electrode transducers. These deficiencies were overcame using an equivalent circuit model introduced in 1969 by Smith *et al.*[24]. It employs a Mason equivalent circuit which is most often used to model bulk acoustic wave piezoelectric devices. Using the idea of transmission line models, Mason's model included all the basic phenomena present - capacitance, transduction, propagation and reflection – though appropriate parameters need to be supplied from either experimental results or more basic theories. Another equivalent circuit model called the "impulse response" model was developed by Hartmann, Bell and Rosenfeld [25] to yield additional information on the SAW transducer response beyond that given by the simple delta function model, the circuit impedances and matching networks are also included in this impulse response model. The model also provides insight into frequency scaling that must be employed in the determination of apodization quantities for broadband or chirp SAW filters.

Due to the development of new devices, there were more demands on various analysis techniques, leading to further development of different designs of SAW devices [26-36]. Since 1980, many new devices developed not only utilized the reflection of SAW between two IDTs, but new wave modes, leaky wave and surface transverse wave (STW), were also being widely explored. Coupling-of-modes method (COM) is another convenient and widely adopted technique for modeling

and the design of SAW devices [37-39]. The technique complements the earlier network model, it deals with acoustic wave propagating in the forward and reverse directions in a distributed structure and incorporates their coupling interactions as they pass though the IDT structure. This is the deficiency of the previous two modeling techniques and the addition of SAW reflection leads to more accurate of the calculated results of the SAW devices.

1.1.2 Principles of SAW devices

A SAW includes both the "True" SAW known as Raleigh wave, the pseudo-SAW, such as the leaky-SAW, and the surface skimming bulk wave. The name, pseudo-SAW is attributed to its propagation inside the piezoelectric substrate but is still quite close to the surface of the substrate. Both types of SAW are used in filters, oscillators and resonators. SAW can be generated utilizing the piezoelectric property of the material. To generate SAW, electrodes are first fabricated on the piezoelectric materials. The metal film is deposited and patterned into a comb-like structure that called interdigital transducer as shown in Fig. 1.1. The propagation of acoustic waves in a piezoelectric crystal can be described by the following equations:

$$D = eS + \varepsilon E \tag{1.2}$$

$$T = cS - eE \tag{1.3}$$

where D is the electrical displacement density, e is the piezoelectric coefficient, S is the materials strain, ε is the dielectric permittivity, E is the external electric field, T is the mechanical stress and c is the elastic stiffness coefficient

The solutions for the mechanical surface wave propagation are quite complicated. Using static field approximation, the elastic wave equations for the particle displacements along the propagation axis are inter-coupled with the anisotropic Laplace's equation for the electric potential, ϕ, by the piezoelectric tensor, e_{ijk}, as shown below.

$$\rho \frac{\partial^2 u_j}{\partial t^2} - c_{ijkl} \frac{\partial^2 u_k}{\partial x_i \partial x_l} - e_{kij} \frac{\partial^2 \phi}{\partial x_i \partial x_k} = 0 \tag{1.4}$$

$$e_{ikl} \frac{\partial^2 u_k}{\partial x_i \partial x_l} - \varepsilon_{ik} \frac{\partial^2 \phi}{\partial x_i \partial x_k} = 0 \qquad \text{for } i, j, k, l = 1, 2, 3 \tag{1.5}$$

in which ρ is the density of the medium, c_{ijkl} is the elastic stiffness tensor measured at constant electric field and ε_{ik} is the dielectric permittivity tensor measured at constant strain.

The particle displacements and the electric potential can be calculated in each medium as reported by Conquin and Tiersten *et al.* [21] in 1967. The solutions sought after are straight-crested propagating waves. Thus, the particle displacements and the potential are assumed to be linear combinations of partial waves of the form,

$$u_j = \alpha_j \exp(ikbx_3)\exp(ik(x_1 - vt)) \quad (1.6)$$

$$\phi = \alpha_4 \exp(ikbx_3)\exp(ik(x_1 - vt)) \qquad \text{for } i, j, k, l = 1, 2, 3 \quad (1.7)$$

The wave propagation in a single substrate or in different layers can be described and calculated using the equations above. This model can be used to investigate the different types of acoustic wave with different thicknesses for the various materials.

When an electric field is applied on the IDT for the excitation of the material, there are polarity differences between the adjacent electrodes and will induce a longitudinal compressive and tensile stress. At the same time, the transversal compressive and tensile forces are coupled to the substrate due to the formation of a capacitor between the IDT and the bottom of the material. When the compressive and shear forces are coupled together, there are alternate regions of compression and dilation. In the compression region, the substrate will be bent downwards and the dilation region will be pulled upwards. The resultant motion making the particles in that region forms an elliptical motion and SAW is formed. This process is the reverse of the piezoelectric effect where the electrical energy converts into mechanical energy. Therefore, SAW comes out from the input IDT and the wave propagates in two directions. One direction propagates toward the output IDT and the other is away from it, which leads to a 3db insertion loss. After the wave arrives at the output IDT, the mechanical energy of the SAW is being converted back to electrical energy through the output IDT electrode. While an electrical field is built up at the output IDT, another SAW is generated leading to another 3 dB insertion

loss. Therefore, a total of 6dB insertion loss is found in SAW devices. Fig. 1.4 shows the propagation of SAW. In addition, one of SAW's interesting properties is that it is mainly concentrated on the surface of the substrate. The vertical component of SAW decays exponentially and diminishes after about one wavelength away from the surface.

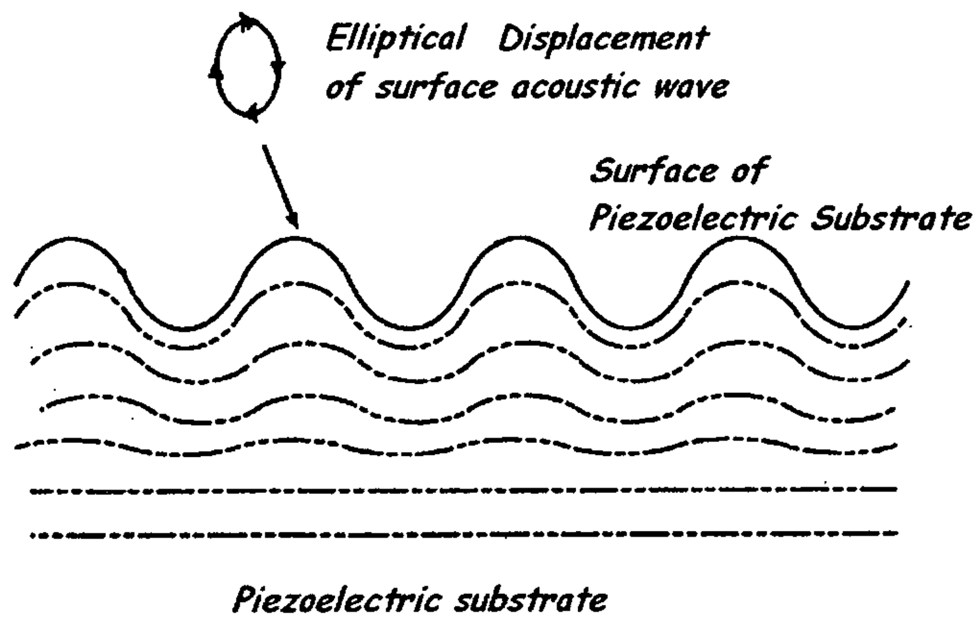

Fig. 1.4 Propagation of the surface acoustic wave

1.1.3 Applications of SAW devices

Surface acoustic wave devices can be designed with a center frequency of operation from few MHz to several GHz, which is in the VHF to UHF range. Since the size of the SAW element is proportional to the wavelength, the lower frequency limit is governed by the size of the substrates, and the upper limit is determined by the fabrication process. More and more electronic components utilize SAW technology rather than conventional techniques for signal processing in communication systems. Firstly, one of the most important applications is for implementation in small, rugged, light and power efficient modules such as filters, resonators and delay line etc. The demand for SAW components has been increasing yearly, especially in mobile and satellite communications systems. Secondly, SAW components can be made to operate efficiently at higher harmonic modes. Therefore, gigaherz-frequency devices can be fabricated using relatively inexpensive photolithographic techniques. Thirdly, SAW devices can be mass-produced using semiconductor microfabrication techniques. As a result, they can be produced in a large volume with a cost-effective process. Finally, SAW devices can generally be designed to provide complex signal processing functions through different design patterns of IDT. To achieve the same response, conventional LC-filters require several hundred inductors and capacitors in designs. Hence, SAW device can achieve different specifications without increasing the size of circuit.

SAW devices have also been used to improve existing systems such as pulse

compression filters for FM signals used in radar systems, and they are being merged into new systems such as matched filters for phase coded applications in spread spectrum communications systems. SAW devices are finding applications in radar, spread spectrum communications, air traffic control, electronic warfare, microwave radio relays, data handling systems, sonar, and IF filters for TV, such as bandpass filters, UHF oscillator control elements, programmable devices for frequency and time domain filtering, frequency synthesizers, correlators etc. In many cases the performance of SAW devices exceeds that of its best electromagnetic counterparts.

In addition, there are other areas of applications or potential applications which are currently still in the research and development stage. Examples of such areas, which may well become important, are imaging and nondestructive evaluation (NDE). With respect to imaging, it has been shown that acoustic surface waves can be used to scan an optical image as well as to scan and focus an acoustic image. Further studies need to be conducted before these techniques become practical or competitive to other imaging techniques. In the meantime, there are future implications for medical electronics and for nondestructive evaluation of materials. With respect to NDE, until recently simple techniques for testing and interpretation are believed to be adequate for most applications. The recent demands for more quantitative characterizations, which have resulted in the change from NDT (nondestructive testing) to NDE, have imposed the need for more complicated approaches, which the acoustic surface wave field can contribute in the form of better transducers, better theoretical descriptions of wave scattering from defects,

novel imaging approaches, and new adaptations of signal processing techniques.

1.1.4 Current status of SAW materials development

The potential advantages of SAW devices over the traditional components have been discussed and have been found to fulfill the requirements for high speed communication systems. Both the design of the IDT pattern and the material selection for the SAW devices has become an important topic in the research of SAW. The basic requirements for SAW materials are good piezoelectricity and smooth surface morphology. The root mean square (rms) roughness should be, at most, in the order of a few microns, otherwise, fine patterns of IDT cannot be fabricated on it. The third condition is the high value of electromechanical coupling coefficient for practical devices. Typically, 2% or higher is the minimum acceptable value for the electromechanical coupling coefficient. The fourth is the low insertion loss and temperature coefficient of frequency (TCF). Strong dependence of the operation frequency may significantly impair the performance of the devices. Finally the ability of mass production is required for the development of cost effective devices.

Selection of the substrate material is a determining factor for SAW device performance. Since piezoelectric materials commonly used as the substrate are intrinsically anisotropic, their properties are dependent not only on the cut angle but also the SAW propagation direction. The mismatch of the SAW propagation with the orientation of substrate materials results in losses of the steering beam and the

dissipation of SAW energy etc.

Piezoelectric materials commonly used as the substrates of the SAW filter are shown in Table 1.1 [41]. From the table, YZ-lithium niobate ($LiNbO_3$) substrate (i.e. Y-axis crystal cut, Z-axis propagation) with relatively high values of K^2 are generally applied in wideband SAW filters, such as in radio pulse compression filters with very large time-bandwidth (TB) products. Moreover, $LiNbO_3$ crystals have a nonzero temperature coefficient of delay. The propagation time τ between the input and output IDT's, separated by a distance L, is given by $\tau = L / v$. However, the SAW velocity, v, will be dependent on the elasticity, density and piezoelectric properties of the substrate used. These parameters change with temperature. When the material is utilized as a filter, the influence of temperature variation is not crucial to the filter application. If the filter is used in the feedback loop of an oscillator, temperature variation will result in phase shifts around the operation frequency, which reduces the stability of the oscillator.

K2 value of ST cut -X axis quartz is about forty times less than that of lithium niobate. It is mainly applied in narrowband ($BW \leq 5$ %) filters and delay lines. Moreover, it is widely employed in SAW oscillator designs, because of its zero temperature coefficient of delay about room temperature. The stability of SAW oscillators using ST-X quartz may be high enough without having an additional oven stabilization treatment. Lithium tantalite ($LiTaO_3$) with higher K^2 than ST-X quartz, has also found some use in oscillator designs. Another new material of SAW

piezoelectric materials is langasite. While it also has a low TCD for temperature stable device applications, it has a much higher K^2 than quartz, with a slightly smaller SAW phase velocity (Vp = 2400 ms^{-1}).

Good crystallinity for SAW material usually accomplishes high K^2, and nearly zero TCF can be achieved using different cutting angles. Because of the high reliability and reproducibility of the bulk type SAW oscillator and resonator, the single bulk type SAW substrate is widely used in industry. In order to fabricate high frequency SAW devices using bulk materials, one of the methods is to minimize the thickness of the substrate and the transducer line width. However, it leads to the risk of low yield. Thin film type SAW device is another method to compensate the deficiency of the bulk type. Piezoelectric film has also shown to be promising for use in conjunction with high velocity substrates to achieve high frequency SAW filter while maintaining reasonable electrode linewidth geometries. Actually, piezoelectric thin films have been used for over three decades as high frequency bulk acoustic wave (BAW) and surface acoustic wave (SAW) transducer and resonators, and also as a SAW medium for acousto-optic, acoustoelectronic, and sensor interactions.

Sputtered aluminum nitride (AlN) and zinc oxide (ZnO) films have been widely studied for acoustic wave device applications. Following the introduction of the interdigital transducer in 1965, thin piezoelectric films were used for the excitation of surface waves on non-piezoelectric substrates such as glass, silicon, and sapphire. [41] This led to the introduction of ZnO based SAW filters for consumer and

communication products. In addition, piezoelectric films have been used with piezoelectric substrates to enhance K^2, and TCF. The advantage of thin film substrate is the variation of acoustic velocity, TCF and K^2. These parameters vary with different combinations of substrates and thin films.

Material	Crystal Cut	SAW Axis	Velocity (ms^{-1})	K^2 (%)	Temperature Coefficient (ppm/°C)
Quartz	ST	X	3158	0.11	~0 (about 5°C)
Lithium niobate ($LiNbO_3$)	Y	Z	3488	4.5	94
Lithium niobate ($LiNbO_3$)	128°	X	3992	5.3	75
Lithium tantalite ($LiTaO_3$)	77.1° Rotated Y	Z	3254	0.72	35
Bismuth germanium oxide ($Bi_{12}GeO_{20}$)	110	001	1681	1.4	120
Gallium arsenide (GaAs)	100	<110>	2841	<0.06	35

Table 1.1 Common parameters substrates for SAW devices

1.2 Use of AlN and ZnO as SAW materials

1.2.1 Introduction

Piezoelectric films for SAW applications have received much attention over the past four decades. High crystallinity binary compounds such as ZnO and AlN are grown by sputtering method. Sputtered AlN and ZnO have been used for over three decades for the fabrication of high frequency bulk acoustic wave devices by utilizing their high acoustic velocity (AlN) [42-45] and high piezoelectricity coupling coefficient (ZnO) [46-49]. In this chapter, we will investigate of the relationship of piezoelectricity and crystalline structure of AlN and ZnO.

1.2.2 The structure of AlN and ZnO

1.2.2.1 Properties of aluminum nitride

Aluminum nitride thin films have broad applications because they possess excellent properties such as chemical stability, high thermal conductivity, electrical isolation, a wide band gap (6.2eV), a thermal expansion coefficient similar to that of GaAs, and a high acoustic velocity [50-56]. It is a hard material with bulk hardness similar to quartz, about 2.000 kg / mm. Pure AlN is chemically stable and is attacked only by an alkali solution. Therefore, AlN thin films are applied not only in surface passivation of semiconductors and insulators, but also in optical devices in the

ultraviolet spectral region, acousto-optic devices, and SAW devices. Polycrystalline films exhibiting piezoelectric properties can be used for the transduction of both BAW and SAW. When compared to other piezoelectric films, such as ZnO, AlN shows a slightly lower piezoelectric coupling (~2.5%), but the Rayleigh wave velocity of AlN is the highest among the piezoelectric materials at about 5600ms^{-1}.

1.2.2.2 Properties of zinc oxide (ZnO)

ZnO has a tetrahedral structure. The most common crystal structure of ZnO are the wurtzite structure and the zinc blende structure. For zinc blende structure, its lattice energy is slightly higher than other crystal structure [57-61]. A third possible crystal structure, which is stable at higher pressures, is the rocksalt structure. The experimentally derived values for the a and the c unit cell distances are 3.243 and 5.195 Å for rocksalt structure, respectively. This is the orientation in which the (002) surface is perpendicular to the c-axis.

1.2.3 Piezoelectric effect

If a stress is applied to a certain type of crystal, it develops an electric dipole moment with magnitude proportional to the applied stress. This phenomenon is called the direct piezoelectric effect. However, the inverse piezoelectric effect happens when an electric field is applied to a certain crystal, and the shape of the crystal changes. Eq (1.7) shows the equation for the direct piezoelectric effect:

$$D = dT \tag{1.7}$$

where D is the electric displacement, d is the piezoelectric coefficient and T is the applied mechanical stress

Existence of the inverse piezoelectric effect is a thermodynamic consequence of the direct effect and the coefficients relating the field and the strain in the inverse effect are the same as those relating the stress and the electric displacement in the direct effect. Therefore the inverse effect can be written as follows:

$$S = dE \tag{1.8}$$

where S is the stress and E is the electric displacement

Hence, piezoelectricity couples between the mechanical and electrical constants. The mechanical variables can either be the stress or strain, while the electrical constants can either be the electrical displacement or electrical field;

$$d = (\frac{\partial D}{\partial T})_E = (\frac{\partial S}{\partial E})_T \tag{1.9}$$

This coefficient exhibits in two different forms. One corresponds to the direct effect while the other corresponds to independent variables. The strain induced in the material is not only determined by the stress, but also the electrical condition. An electrically clamped state is defined when the polarization is constant, while an electrically free state is when the surrounding medium has infinite dielectric susceptibility. The full tensor notation can be written as:

$$S_{jk} = d_{ijk} E_i, \qquad (1.10)$$

in which i, j and k, range from 1 to 3. The piezoelectric coefficient d_{ijk} is a third rank tensor with 27 components. As d_{ijk} has symmetry in j and k, this reduces the effective number to 18. If the material has a higher symmetry, the number of dependent elements will be further decreased.

2. Experimental Process

2.1 Introduction

In this thesis, AlN and ZnO piezoelectric thin films were deposited by radio frequency (rf) magnetron sputtering [62,63] and molecular beam epitaxy (MBE) techniques [64,65]. For applications of piezoelectric materials in SAW devices, the growth orientation of the thin film should match the propagation direction of the SAW in order to obtain the maximum signal transfer [66,67]. One of the loss mechanisms in a SAW device is the scattering of the signal. If multiple orientations are found in a piezoelectric thin film, signals will propagate in its favored direction as a result of the acoustic wave scattering [68]. Better orientation of the thin films leads to a stronger SAW response, lowering the propagation losses. In order to obtain a highly textured and oriented piezoelectric thin film, it should be epitaxially grown on the substrate [69-78]. The selection of the substrate is one of the most important parameters to get high quality thin films. This factor is not only important to the SAW devices but also important for all other thin film based devices [79-88]. The rough areas on the surface of the thin film also function as scattering centers, increasing the propagation loss to the device. Therefore, the device performance of SAW devices depend on crystalinity and surface morphology.

Epitaxial piezoelectric thin films are generally deposited by sputtering and chemical vapor deposition (CVD) growth technique. The CVD growth technique is more

suited for mass production and offers excellent controllability. The drawback of CVD growth technique is to raise environmental pollution. In addition, it was shown that there is a high probability of obtaining rough surface of the as-deposited piezoelectric thin films, leading to difficulty in fabricating micropattern interdigited transducer. Therefore, sputtering technique was mainly used to deposit piezoelectric thin films in our studies.

Al_2O_3 (0001) and Al_2O_3 (1120) are commonly used as substrates for the growth of high frequency SAW devices because they are closely lattice matched with ZnO and AlN thin films [89-98]. For example, the lattice mismatch between AlN and Silicon (Si) is 18% [92] but that between AlN and Al_2O_3 is 13.3% [92]. It is well known that large lattice mismatch leads to a poor film quality as well as internal stress [99]. The internal stress can also vary the elastic constant of the piezoelectric material. Therefore, Al_2O_3 substrates were used in our studies in order to minimize the adverse effects caused by large lattice mismatch.

2.2 Growth of AlN and ZnO thin films on sapphire by rf magnetron sputtering and MBE techniques

2.2.1 AlN and ZnO deposition by rf magnetron sputtering technique

2.2.1.1 Principle of rf magnetron sputtering

Radio frequency (rf) magnetron sputtering is one of the most commonly used methods for the deposition of thin films. This method was first described 150 year ago. To start the sputtering process, the plasma was initiated by applying a large voltage across a gap containing a low-pressure gas. Once the plasma was formed, ions in the plasma were accelerated towards the negatively charged cathode. When they deposited on the surface, they released secondary electrons, which accelerated away from the cathode. They may collide with neutral species while crossing from cathode to anode. If the energy transfer was less than the ionization potential of the gaseous species, the atom could be excited to an energetic state. The atom decayed from this excited state through an optical transition, providing the characteristic glow. If the energy transfer was high enough, the atom would be ionized and accelerated towards the cathode. The bombardment of the cathode by the ion stream was the main process of sputtering. While an ion was accelerated by the electric field, it bombarded the surface of the target material on the cathode. Ions with optimal

energies started to deposit on the substrate surface without bound off or implantation. If the energy of the deposited atom was high, the surface mobility of the atoms would also be high. In this case, the atoms could move around on the substrate surface and merge into islands. These islands would eventually join together to form a smooth film. A zone model was developed by Movchan and Demchishin [99] to describe the morphology of the deposited film. Figure 2.1 shows the regions of a film morphology as a function of substrate temperature. The substrate temperature was normalized to the melting point of the film. At low substrate temperature, the film became an amorphous, highly porous solid with a low mass density. This is the zone A of the diagram. It was caused by the low adatom mobility of the growing film. When the chamber pressure was lowered or the substrate temperature was raised, the deposition process entered the "T" zone. Films deposited in this region were highly specular and had very small grains. Increasing the temperature further caused the grain size to increase. Zone B had tall narrow columnar grains that grow vertically from the surface. The grains end in facets. Eventually, the film had large 3-D grains in Zone C. The surfaces of the film in the second and third zone were moderately rough and the film appeared "milky". In order to get a smooth film surface, the substrate temperature was adjusted to allow film growth in zone T region.

Zone model described above showed that, an optimal substrate temperature were provide enough kinetic energy to enhance the surface morphology. The deposition rate could be controlled by sputtering pressure, ratio of gas mixture and the target-to-

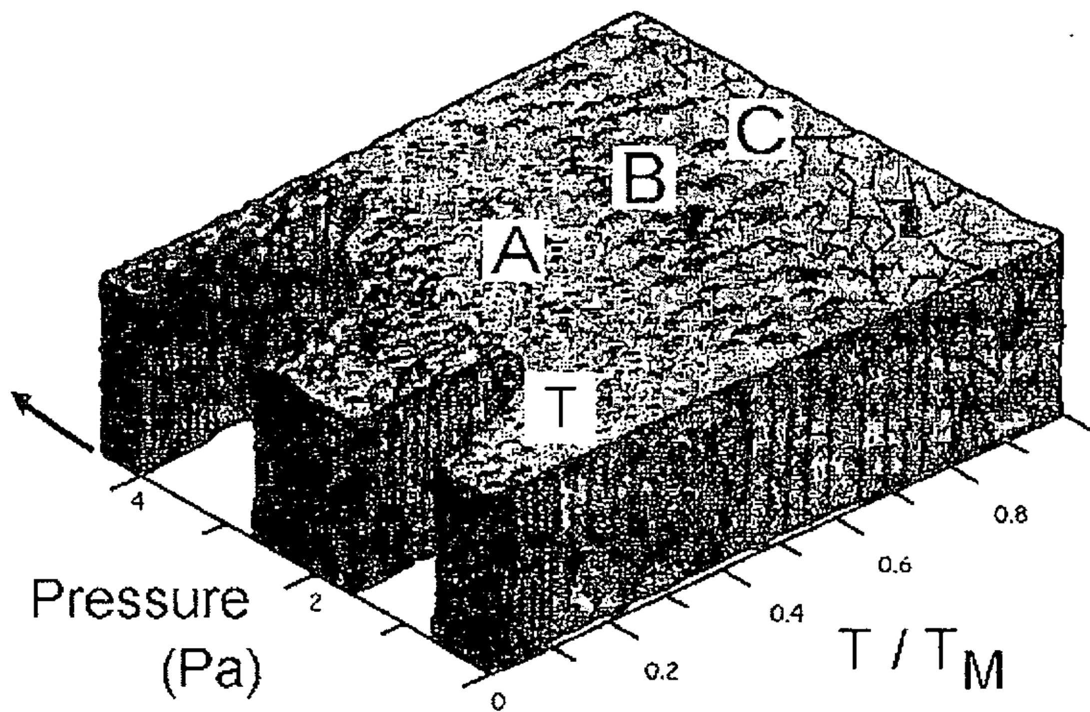

Fig. 2.1 A schematic diagram of zone model of film deposition

substrate distance. Sputtering pressure was a parameter indicating the total number of molecules in the vacuum chamber during the sputtering procedure. As more excited molecules or atoms freely moved in the vacuum, the sputtering process became faster but the mean free path of the molecules was shortened. Since the probability of collision between molecules was higher, the kinetic energy of sputtered atoms decreased and some even failed to reach the substrate. Thus, the rate of deposition decreased with an increase in the sputtering pressure. Furthermore, the optimization of the quality of the thin films could also be accomplished by controlling the energy of the atoms because the highly energetic atoms bombarding substrate surface would roughen the surface of the deposited film. Thus, to improve the crystal of the thin films it was necessary to prevent the bombardment damage to the crystal structure.

The mixture of argon and nitrogen or oxygen (when sputtering AlN and ZnO using nitrogen and oxygen respectively) maintained the stoichiometry of the sputtered films. The argon gas was used to increase the sputtering yield and to enhance the deposition rate. In addition, it provided an easy way to control the flux on the film surface. In other words, varying the composition of the gas mixture could control both film stoichiometry and crystallinity. In the growth of AlN thin films, the variation of the gas ratio of between N_2 and Ar was one of the parameters used to control stoichiometry and the crystallinity due to the composition change of the film. In conclusion, all the factors listed had strong influence on the crystallinity of the film. These parameters factors must thus be systemically optimized

2.2.1.2 Samples preparation

In this thesis, single side polished Al_2O_3 (0001) wafers were used as substrates for the deposition of the piezoelectric AlN and ZnO thin films. First, the substrates were degreased with acetone followed by iso-propanol. Following the degreasing procedure, surface damage due to polishing and contaminants were removed using an etching solution of 3:1 hot H_2SO_4:H_3PO_4. The substrates were dipped in this solution for 15 minutes at 150°C. This was followed by rinsing in deionized (DI) water for 5 minutes and blown dry with filtered N_2 gas.

After the standard cleaning process, the substrates were loaded in the sputtering chamber. In this experiment, an ANELVA SPF-332H rf planar magnetron sputtering system was used to deposit AlN and ZnO piezoelectric thin films. Ceramic targets, ZnO and AlN of 99.5% purity, were used, which were water cooled on the backside during sputtering. The distance between the target and the substrate was about 50 mm. The chamber was baked to outgas and then evacuated by diffusion pump to below 4×10^{-7} torr. The substrate temperature was varied in the range of 50-200°C. The target was pre-sputtered for about 10 mins before deposition on the substrate, and also gaseous mixture was injected into the chamber during the pre-sputtering process. The pre-sputtering process was carried out for cleaning of the sputtering target and reaching the equilibrium states of the plasma. For sputtering nitride or oxide compound, nitrogen gas or oxygen gas was added and mixed with argon gas to balance the stiochiometery of the sputtered thin films. Different ratios of the gases

were used to optimize the film quality. During sputtering, the substrate was rotated at a 3 rpm improve the thickness uniformity of the thin film. The duration of the sputtering process was experimentally determined in order to obtain the required thickness of the piezoelectric thin films. Table 2.1 is the summary of the deposition conditions for ZnO and Table 2.2 is the summary of the deposition conditions for AlN.

In order to optimize the sputtering conditions in obtaining good thin film quality, different parameters were varied during the sputtering process such as the ratio of the gaseous mixture, sputtering pressure, substrate temperature and sputtering power.

Substrate temperature	Room temperature -200°C
Ar/O_2 ratio	0-1
Gas pressure	0.3-1.5 Pa
RF Power	50-150 W
Target ZnO ceramic	99.9 % purity
Base pressure	4×10^{-5} Pa
Target to substrate distance	5 cm

Table 2.1 Variation of sputtering conditions for ZnO

Substrate temperature	200-400°C
Ar/N_2 ratio	0-1
Gas pressure	0.3-1.5 Pa
RF Power	200-350 W
Target AlN ceramic	99.9 % purity
Base pressure	4×10^{-5} Pa
Target to substrate distance	5 cm

Table 2.2 Variation of sputtering conditions for AlN

2.2.2 AlN thin films deposition by MBE technique

2.2.2.1 Principle of MBE growth

MBE is a versatile technique for growing thin epitaxial semiconductor, metal or insulator films. In this process, the molecular or atomic beams of the constituent elements react and deposit on a substrate surface. The substrate is maintained at an elevated temperature under ultrahigh vacuum condition. The composition of the epilayer and its doping level depend on the relative arrival rates of the constituent elements and the dopants, which in turn depends on the evaporation rates of the appropriate sources. The growth rate is about 1 monolayer per second, which is low enough to ensure sufficient surface migration of the impinging species on the growing surface so that the surface of the grown film will be smooth. A simple mechanical shutter placed in front of the beam sources can be used to start or to stop the deposition and doping of the film. The major difference between MBE and other vacuum deposition techniques is that beam fluxes and growth conditions in MBE can be more precisely controlled. MBE growth is carried out under conditions far from thermodynamic equilibrium and is governed mainly by the kinetics of surface processes occurring when the impinging beams react with the outermost atomic layers of the substrate crystal. This is different from other epitaxial growth techniques such as the liquid or vapor phase epitaxy, which proceeds at conditions near thermodynamic equilibrium and are most frequently controlled by diffusion processes occurring in the crystallizing phase surrounding the substrate.

2.2.2.2 Samples preparation

In this thesis, single side polished sapphire were used as substrates. The sapphire substrates were cleaned before transferring to the MBE growth chamber. The detailed cleaning procedures have been described clearly in section 2.2.1.2. After loading to the MBE growth chamber, the substrate was thermally cleaned at 850°C and out-gassed for 30 minutes. The substrate temperature was then decreased to about 800°C for the deposition of the AlN thin film. The Al cell temperature was varied with fixed nitrogen flux and fixed rf power. The summary of the AlN deposition conditions by MBE is shown in the following Table 2.3.

Substrate Temperature	800 °C
rf Power	350 W
Nitrogen flow	1 sccm
Temperature of Al cell	1120 to 1135 °C
Base pressure	2×10^{-10} torr

Table 2.3 Summary of growing conditions of AlN by MBE

2.3 Thin film characterization

The characterization techniques for the AlN and ZnO thin films include X-ray diffraction (XRD), atomic force microscopy (AFM) and scanning electronic microscopy (SEM).

2.3.1 X-ray diffraction (XRD)

X-ray diffraction is a powerful analytical method for determining the structural properties of materials, such as crystal structure, orientation and lattice parameters, film texture, thickness, grains size, stress and etc. [100-101]. This is achieved by using the method in a variety of modes. The most widely used are as follows. The first type of scanning is $\omega - 2\theta$ scan, in which the incident angle ω and the reflected angle θ of the scanning beam are equal. The x-ray source and the x-ray detector are coupled during the scan. From the XRD diffractogram, one can readily extract the lattice parameter, film texture, grain size etc. The rocking curve is another common type of scan to examine the orientation and the texture of thin films. The sample is rotated or rocked through an angular range, bringing the plane in and out of the Bragg condition. The width of the measured peak, normally measured in terms of the FWHM value contains information on the amount by which the measured plane is off from the surface normal, sometimes referred to as the 'degree of orientation' of the specimen. This method also enables accurate determination of very small deviations in d-spacing due to strain effects, etc. and is widely used to compare the

crystallinity of thin films. The third scan type is the ϕ scan. This scan is performed by studying two crystallographic planes, one from the substrate and one from the film which are not parallel to the sample surface. The incident X-ray is locked at an angle ω defined by the chosen plane and the detector is locked at the diffraction angle 2θ for the same plane. The ϕ-scan is then performed by rotating the sample around its normal axis, while the intensity of the plane is simultaneously recorded. The in-plane orientation relationship can be determined by comparing the positions of the resulting peaks from the two ϕ-scans.

2.3.2 Atomic force microscopy (AFM)

Atomic force microscopy (AFM) probes the surface with a sharp tip of a few microns long, often less than 100nm in diameter [102]. The tip is mounted on a flexible cantilever that is 100 to 200 μm long. Forces between the tip and the sample surface cause the cantilever to bend and a laser diode reflects the signal back to a photodetector CCD array which is used to sense movement. Precise control of the tip movement over the surface to be scanned is achieved by the use of piezoelectric ceramics. Atomic force microscopy has become a very powerful analytical technique in materials science since this measurement can provide information on surface morphology on a nanometer scale without any vacuum isolation.

2.3.3 Scanning electron microscopy (SEM)

Secondary electron microscopy (SEM) is used to examine the physical features with dimensions from several microns down to a few nanometers [103]. Secondary electrons emitted or scattered from the surface are detected through synchronization with the raster. The orientation of surface features influences the number of electrons that reach the secondary electron detector, which creates variations in the image contrast that represents the secondary electron detector, and also in the image contrast that represents the sample's surface topography. The secondary electron image resolution for an ideal sample is about 3 nm making it suitable for topographical and morphological analysis of materials. Hence, this method provides high-resolution imaging of fine surface morphology.

2.4 SAW filters fabrication and characterization

2.4.1 SAW filters fabrication

After the thin film was grown, interdigital transducer IDT electrodes were fabricated on the thin film using the liftoff method. As ZnO thin films can be etched by an acidic solution [104], thus liftoff method was used to prevent the acidic solution from coming into contact with the ZnO thin film. Although AlN film is stable in an acidic environment, liftoff technique was also used to fabricate IDT electrodes on AlN such that the same fabrication process was used for both AlN and ZnO based devices. In this experiment, a simple SAW filter was used to examine the electroacoustic effect of the thin film.

Firstly, the samples were soaked in acetone followed by isopropanol. The samples were then rinsed in DI water and blown dry with filtered N_2 gas, followed by baking in an oven at temperature below 100°C. After cooling, AZ3100 photoresist was then spun on the samples at 7000 rpm for 15 s. The samples were then exposed to UV source (320 nm) with a Karl Suss MA6 mask aligner that enables to fabricate a minimum linewidth of 1 μm. The exposure time was approximately 150 s and the light intensity was about 3.0 mW / cm^2. After UV exposure, the sample was then dipped into the developer for about 15 s followed by DI water rinse and dried with filtered N_2 gas. Electron beam (e-beam) evaporation was used to deposit Al IDTs of

250 nm thickness on the samples. The e-beam evaporation system was evacuated by a turbo molecular pump and achieved a base pressure of 9×10^{-3} mbar. Finally, the pattern of IDTs was formed by liftoff technique, which is shown in Fig. 2.2.

A schematic diagram of the SAW device with IDT electrode is shown in Fig. 2.3, in which d is the linewidth of each transducer, d_1 is the minimum separation of the input and output IDT, d_2 is the center to center separation between two IDTs and w is the overlapping of the transducer

The acoustic wavelength is defined as,

$$\lambda = 4 \times d \qquad (2.1)$$

where λ is the acoustic wavelength and d is the linewidth of the IDT electrode. The parameters of a simple SAW filter are summarized in table 2.4.

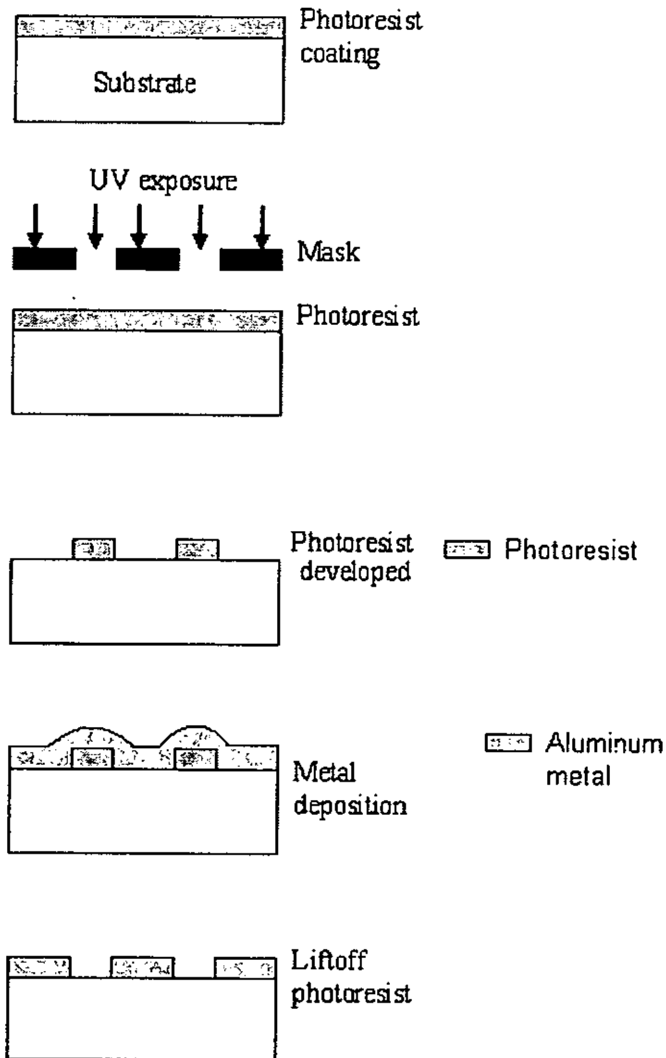

Fig. 2.2 Fabrication of IDT using liftoff process

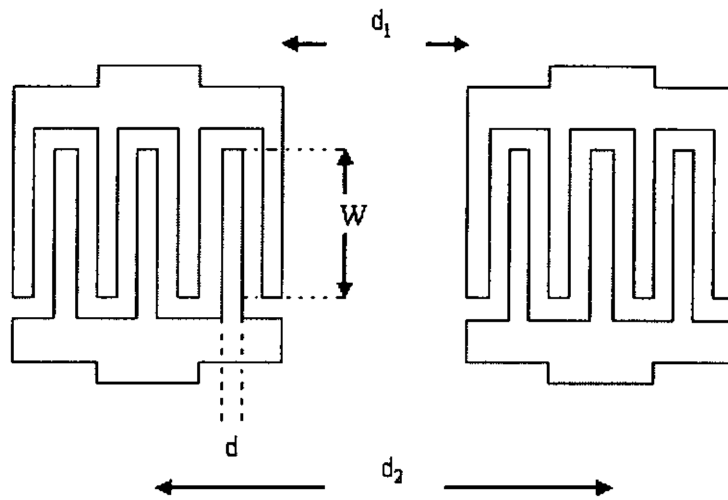

Fig. 2.3 Schematic diagram of a SAW filter

d (μm)	w (μm)	d_1 (μm)	d_2 (μm)	Number of electrode
1	900	500	2000	100
2	950	550	2000	200
4	950	550	2000	200

Table 2.4 Parameters of the designed SAW filter

2.4.2 SAW filters measurements

2.4.2.1 Frequency response and insertion loss

In this thesis, the frequency response and insertion loss of the SAW filter were measured by the direct probing method. The measurement setup is shown in the Fig. 2.4. Casade air coplanar mirco-probes were used to excite the SAW from the input port of the IDT and signals were received from the output port of the IDT. The advantages of using the on-wafer probing method are easy impedance matching, high accuracy, low insertion loss and low noise. Frequency response measured the operating frequency of the device which excited the piezoelectric thin films with the use of the IDT electrodes. Electromechanical coupling coefficient K^2, insertion loss and phase velocity were also measured, which is a measure of the efficiency of converting electric energy to mechanical energy. The K^2 was obtained by measuring the conductance and suspectance of the device and then calculated using an equivalent circuit suggested by W. R. Smith [105] as shown in the Fig. 2.5. The admittance of the IDT had two parts: the ordinary capacitive part, which had nothing to do with SAW, and the acoustic admittance.

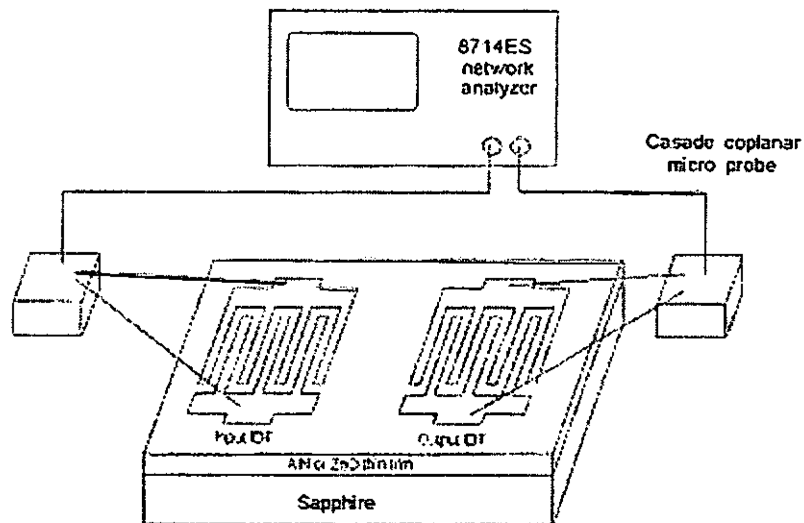

Fig. 2.4 The measurement setup of the frequency response and insertion loss.

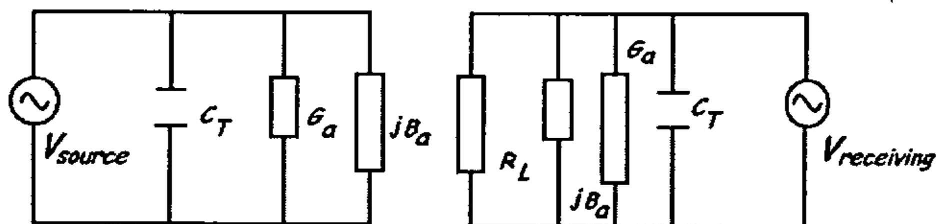

Fig. 2.5 A equivalent circuit of a SAW filter

The circuit elements as shown in Fig.2.5, are given by the expression below:

$$Y_a(f) = G_a(f) + j[\omega C_T + B_a(f)] \tag{2.2}$$

where $G_a(f)$ is the radiation admittance, $B_a(f)$ is the radiation conductance and C_T is the static capacitance of an IDT electrode. $G_a(f)$ and $B_a(f)$ can be calculated by the following equations,

$$G_a(f) = \hat{G}_a(\sin x / x)^2 \tag{2.3}$$

$$B_a(f) = \hat{G}_a[(\sin 2x - 2x) / 2x^2] \tag{2.4}$$

in which $\hat{G}_a(f)$ is the unit vector of $G_a(f)$ and x is the frequency change. In this equivalent circuit, $\hat{G}_a(f)$ can be expressed by,

$$\hat{G}_a(f) = (4/\pi)K^2\omega_O C_S N^2 \tag{2.5}$$

in which ω_o is the centre frequency, C_S is the static capacitance of each pair of electrode and N is the number of electrode part in the IDT. When the operation frequency occurs at $\omega = \omega_0$, we have $x = 0$, and the equation (2.3) and (2.4) becomes,

$$G_a(\omega_o) = \hat{G}_a \text{ and}$$

$$B_a(\omega_o) = 0$$

then, equation (2.2) becomes,

$$Y = (4/\pi)K^2 N\omega_o C_T + j\omega_o C_T = \hat{G}_a + j\omega_o C_T \tag{2.6}$$

$$K^2 = \frac{\pi G_a}{4NB_a} \tag{2.7}$$

The second method is to measure the difference of the phase velocity with and without a metal thin film on the piezoelectric thin film in between the propagation path of SAW filter, this difference can be expressed as

$$K^2 = \frac{2\Delta v}{v} \tag{2.8}$$

The additional of a metal film on the piezoelectric thin film is to provide a time delay in the wave propagation. In the transmission line model, the relationship between the acoustic wave v_o, the inductance L, the acoustic impedance Z_o and the capacitor C, not C_o are,

$$L = \frac{Z_O}{v_O}, \tag{2.9}$$

$$C = \frac{1}{Z_O v_O}, \quad \text{and} \tag{2.10}$$

$$v_O = \frac{1}{\sqrt{LC}}. \tag{2.11}$$

When a metal plate is deposited on the thin film surface, the accumulation of charge will be such that the total electric potential Φ_s and longitudinal electric field E_x are zero. The vertical component E_y still exists, so that the field distribution can be modeled as a parallel-plate capacitor as shown in Fig. 2.6. Using the transmission line model, the deposition of a conductive metal thin film is equivalent to adding a capacitor to the circuit. Since the net stress acting on the film surface is also zero, as observed from the above relation, the acoustic velocity of the surface wave propagation under the conductive metal film decreases.

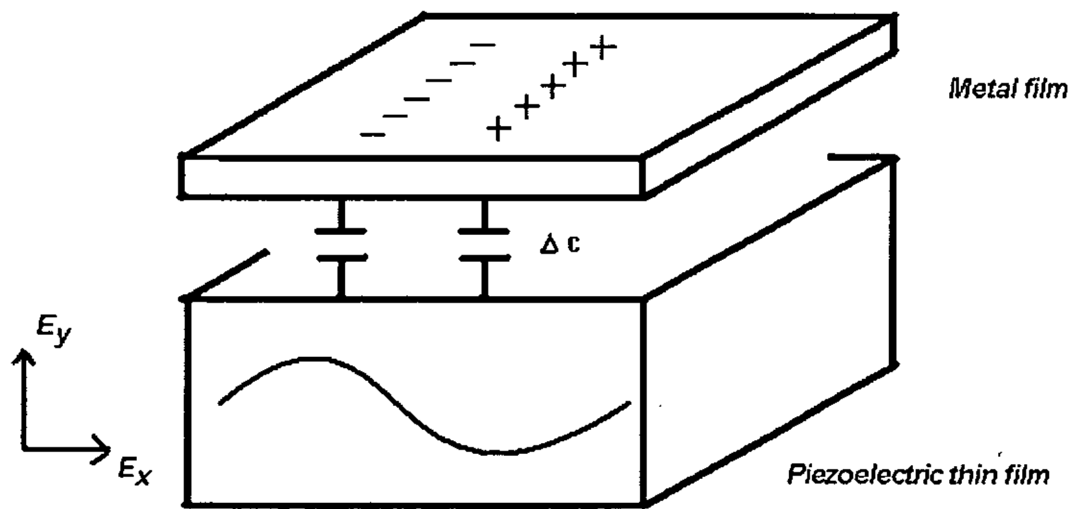

Fig. 2.6 Thin metal film on the top of the piezoelectric substrate

2.4.2.2 Phase noise measurement

Phase noise is commonly found in SAW device. In much of the prior researches conducted, 1/f noise distribution can be found in any electronic device, such as carbon resistors [106-111], vacuum tubes [112] and semiconductors [113-120]. In semiconductors, much of 1/f noise has been attributed to surface effects [120], so it is not too surprising to find that the surface acoustic wave device is a source of 1/f phase noise. 1/f noise has been observed in quartz SAW filters [121-125] and resonators [126-133]. Since SAW resonators are used as the feedback elements in oscillation circuit [134-143], its noise performance is necessary to be investigated. The causes of 1/f phase noise are not very well understood. Some researchers believe that the quantum 1/f effect [144-149] was due to the quantum fluctuation present in the quantum mechanical notion of physical cross section σ and physical process Γ, caused by the reaction of the electromagnetic field on the electric or dielectric dipole that emitted it, rather than the scattering of individual carriers. Another group suggested the structure of the delay line is a source of phase noise in SAW devices [150]. The researchers tried to find out the relationship between the length of the delay line and noise level has still yet to be found. T. E. Parker et al. also proved the delay dependence of the phase noise of SAW devices. They reported that the noise source is due to the bulk effect, rather than the surface effect [151,152]. In addition, defects in thin films are another possible noise source and the device performance is directly proportional to the material quality. Therefore, material quality is thus suggested to be a factor in influencing the noise level of SAW device,

however, the detailed mechanism has yet to be determined.

For phase noise measurement, the most common parameter used to characterize the phase noise of the device is the power spectral density of phase fluctuation, $S_{\varphi}(f)$, which can be defined as the Fourier transform of the autocorrelation function $R_{\varphi}(\tau)$. The power law model is frequently used for describing phase noise. It assumes that $S_{\varphi}(f)$ is equal to the sum of the terms, each of which varies as an integer power of frequency.

$$S_{\varphi}(f) = A(\frac{1}{f^4}) + B(\frac{1}{f^3}) + C(\frac{1}{f^2}) + D(\frac{1}{f}) + E(\frac{1}{f^0}) \qquad (2.12)$$

where A, B, C, D and E are the constant. In each term, it corresponds to a noise process. For the first term, $1/f^4$ is due to the random walk noise, $1/f^3$ is due to flicker frequency modulation of the frequency, $1/f^2$ is due to white phase modulation of the frequency modulation, $1/f$ is due to the flicker phase modulation of the frequency and $1/f_0$ is due to the white phase modulation of the frequency

In industrial standards, single sideband (SSB) signal $\mathcal{L}(f)$ is the most essential parameter in measuring the phase noise either oscillator or resonator. Actually the SSB can be converted back to the power spectral density. When the phase noise of the device is going to be measured, a pair of sideband comes out and the experiment

data is taken and analyzed. The result is so called double sideband signal to noise ratio, otherwise filtering one sideband and continues the experiment the results called single sideband signal to noise ratio. Consider one sideband the noise process N(v) around the carrier, for the root means square (rms) voltage of carrier frequency $\sqrt{R_O P_C}$, taking a frequency f away from the carrier in the bandwidth B, the rms voltage is $\sqrt{R_O NB}$ and causing a phase modulation $\tan^{-1}\varphi_{rms} = \sqrt{\frac{NB}{2P_C}}$, in this stage the variation induced by amplitude is insensitive since $\mathcal{L}(f)$ is almost always measured by means of a phase to voltage converter. Under the assumption of low noise to carrier ratio, that modulation angle becomes $\varphi_{rms} = \sqrt{\frac{NB}{2P_C}}$. Hence the spectrum density is $S_\varphi(f) = \frac{N(\upsilon + f)}{P_C}$. The physical dimension of $S_\varphi(f)$ is rad^2 / Hz. The quantity used to describe the power spectral density thereby obtained is

$$\mathcal{L}(f) = \frac{N(\upsilon + f)}{2P_C} = \frac{1}{2} S_\varphi(f) \tag{2.13}$$

The physical dimension of $\mathcal{L}(f)$ is Hz^{-1}; the unit of angle, rad, has already be omitted. $\mathcal{L}(f)$ is usually expressed in dBc / Hz, where dBc means noise per unit carrier power. That means the power density in one sideband per 1 Hz bandwidth at an offset frequency f away from the carrier frequency under the input signal power.

As mentioned above, the source of the phase noise in SAW devices has yet to be found and thus no physics-based model exists for phase noise in the SAW devices. It is common practice to utilize the noise model of an oscillator for simulating phase noise in SAW oscillators [151]. The first model involving the phase noise of a quartz oscillator has been proposed by D. B. Leeson *et al* [153]. The schematic diagram of the model is shown in the Fig. 2.7, which is heuristic description of the expected spectrum of a feedback oscillator in terms of known oscillator parameters. This phase noise model contains two parts, open loop and closed loop model. For the open loop model, the phase noise is measured from the amplifier output with a known amplification factor and the noise figures, connecting with the device under test that is surface acoustic wave delay line. For the closed loop model, converting the above open loop circuit into an oscillator by closing the loop, and the power spectral density of the phase noise takes on a different shape compared with the open loop case. Two different testing circuits result in different shapes of the spectral density of the device. For open loop circuit, the power spectral density of phase fluctuation is divided into two parts which is

$$\mathcal{L}(f) = \frac{\alpha}{2\pi f_m} + \frac{GFkT}{P_o} \tag{2.14}$$

where F is the amplifier noise figure, kT is the thermal energy, α is a constant, P_O is the input power and G is the voltage gain. The phase noise power spectral density appearing at the output of the open loop configuration will be independent of f_m for values of $f_m > f_\alpha$, and will have a value here of approximately $\frac{GFkT}{P_O}$. This is the

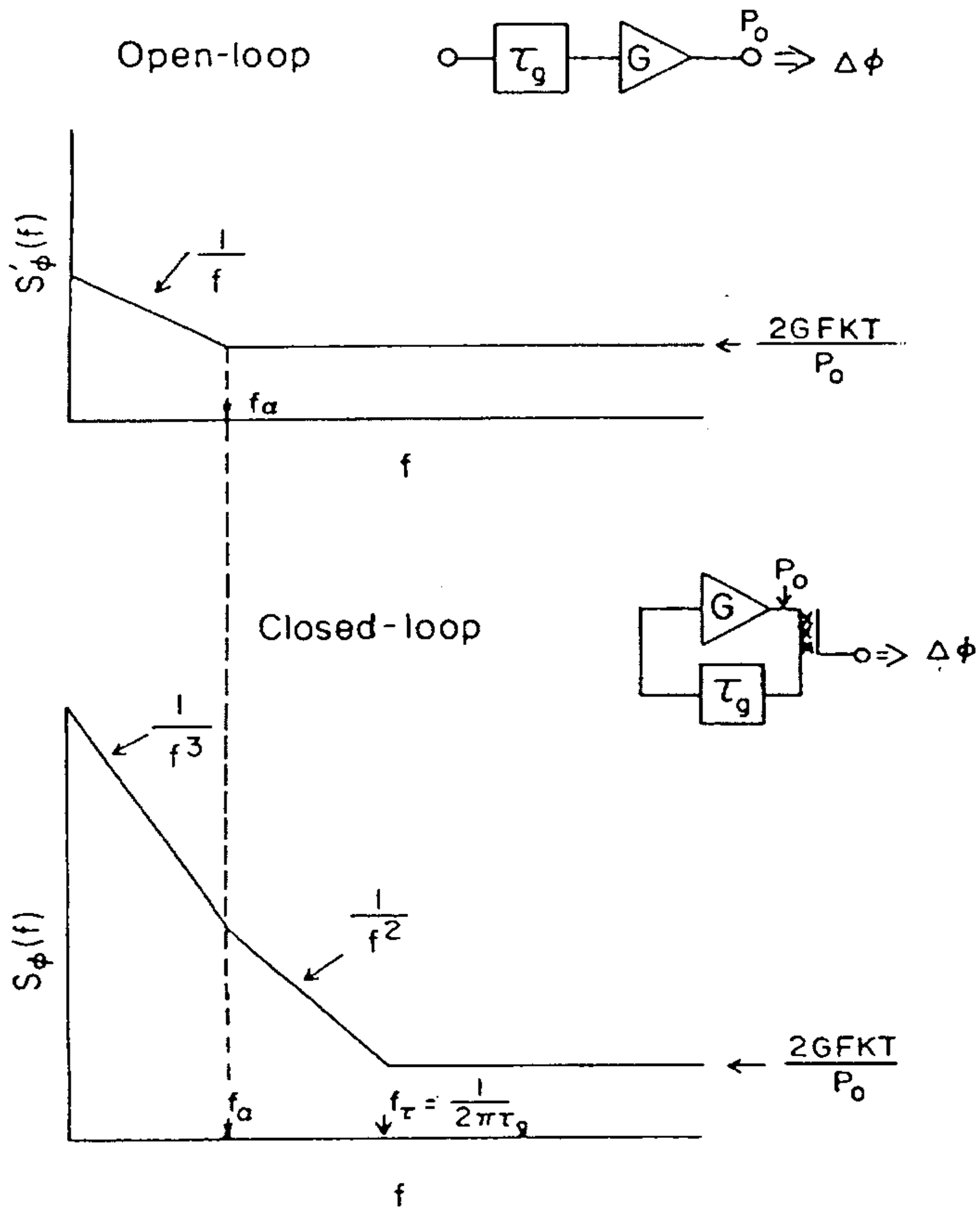

Fig. 2.7 The schematic diagram of Leeson's model

thermal noise floor that can be calculated theoretically. The flicker noise parameter α and the flicker frequency f_α are extracted from the experimental results.

The experimental setup for detecting phase noise in SAW is well established. The direct phase noise measurement setup includes a HP 8565B signal generator, a power splitter, a low loss noise mixer, a phase shifter, a PAR113 low noise amplifier and a HP3651A dynamic signal analyzer as shown in the Fig. 2.8. The signal from the clean source HP 8565B is splited into two paths. Half of the signal is passed through the SAW device and mixed with the remaining half of the signal, which connected with the phase shifter. The output of the mixer is amplified using a low noise amplifier to enhance the output voltage. The phase shifter is adjusted such that the two signals at the mixer are in quadrature, causing the mixer output (for dc and low frequencies) to be proportional to the phase difference between the two signals.

The output voltage of the mixer can be converted back to the phase fluctuation of the SAW filters. While the mixer is used as a phase detector, fundamental and harmonics signals are obtained

$$r(t) = \sqrt{2R_O P_C}\cos(2\pi\upsilon_c t) \tag{2.15}$$

$$s(t) = \sqrt{2R_O P_C}\left[1 + \alpha(t)\right]\cos(2\pi\upsilon_c t + \varphi(t)) \tag{2.16}$$

where *r(t)* and *s(t)* are the reference and modulated frequency respectively, R_0 is the

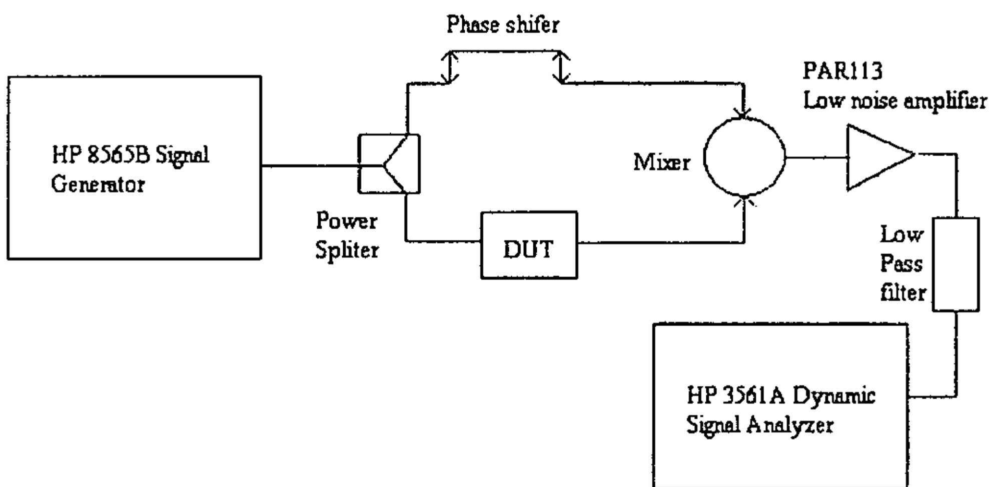

Fig. 2.8 Phase noise measurement setup

internal resistance, P_C is the power of the frequency, α is the amplitude modulation coefficient, υ_C is the centre frequency of the SAW filter and φ is the phase fluctuation of the frequency. And a low-pass filter is used to filter out the harmonic part of the output signal since the mixer acts a multiplier that it added up two input signals and different two input signals. For this experiment, two input frequencies are nearly the same and thus it likes a harmonic of the original signal and the output signal can be expressed as,

$$V_{OUT} = [r(t)s(t)] * H_{filter}(t) = R_O P_C (1 + \alpha(t)\sin[\varphi(t)]) \tag{2.17}$$

where $H_{filter}(t)$ is he Fourier transform function of a low pass filter. For detector operation, the mixer is set in saturated region that both power level of the reference and modulated signal entered into the mixer is the maximum withstand of the mixer such that the output signal can independent of the input power. The amplitude noise can be neglected, thus

$$S_V(f) = K_d S_\varphi(f), \tag{2.18}$$

where K_d is the phase detector scale factor, $S_\varphi(f)$ is the power spectral density of phase fluctuation of the SAW device and $S_V(f)$ is the power spectral density of voltage fluctuation of the SAW device.

3. Experimental results

3.1 Experimental results of AlN and ZnO SAW filters deposition on sapphire grown by rf magnetron sputtering technique

3.1.1 Characterization of AlN and ZnO thin films deposition on sapphire grown by rf sputtering technique

For any thin film application, the quality of the thin film must be characterized and optimized. In this thesis, the piezoelectric AlN and ZnO thin films, grown by rf sputtering technique, were optimized and characterized before device fabrication. Different sputtering parameters resulted in different crystal structure and surface morphology. The crystallinity and the surface roughness of both AlN and ZnO thin films were characterized by the XRD, SEM and AFM measurement then a systematic study on the performance of the SAW filters was conducted to examine the relationship between the material quality and device performance. For further demonstration of the relationship of the material quality and SAW filter performance, we have investigated the device performance of SAW filters fabricated on MBE-grown AlN films and the results are reported in this chapter

The XRD measurements on AlN and ZnO thin films deposited on sapphires by

sputtering under different parameters were first discussed to show the effect of the sputtering parameters on the film quality. This study enabled us to optimize the condition of rf magnetron sputtering for application in SAW filters. In the Fig. 3.1, when the sputtering power 100W was used, the FWHM of the AlN thin films was shown to be the highest value of the FWHM. When the power increased, the FWHM decreased indicating that the both crystallinity and surface morphology of the AlN thin films were improved.

After the sputtering power was varied, the sputtering pressure during the sputtering process was then varied systematically as shown in Fig. 3.2 with sputtering pressure varying from 0.1 Pa. to 1.5 Pa. It was found that the minimum value of FWHM was 0.5 P.a. sputtering pressure.

The gas composition in the plasma was also one of the parameters that need to be optimized. In general a mixture of N_2 and Ar is used for the sputtering the films. In Fig. 3.3, different percentage of nitrogen (N_2) gas was used for deposition process. It was found that this factor has strong influence on the optimal crystal structure of the AlN thin films.. In the Fig. 3.3, the gas ratio of N_2 gas was about 50%, leading to the lowering of the FWHM value.

The fourth parameter was the temperature of the substrate during the deposition process. From Fig. 3.4, when the substrate temperature was increased, the value of

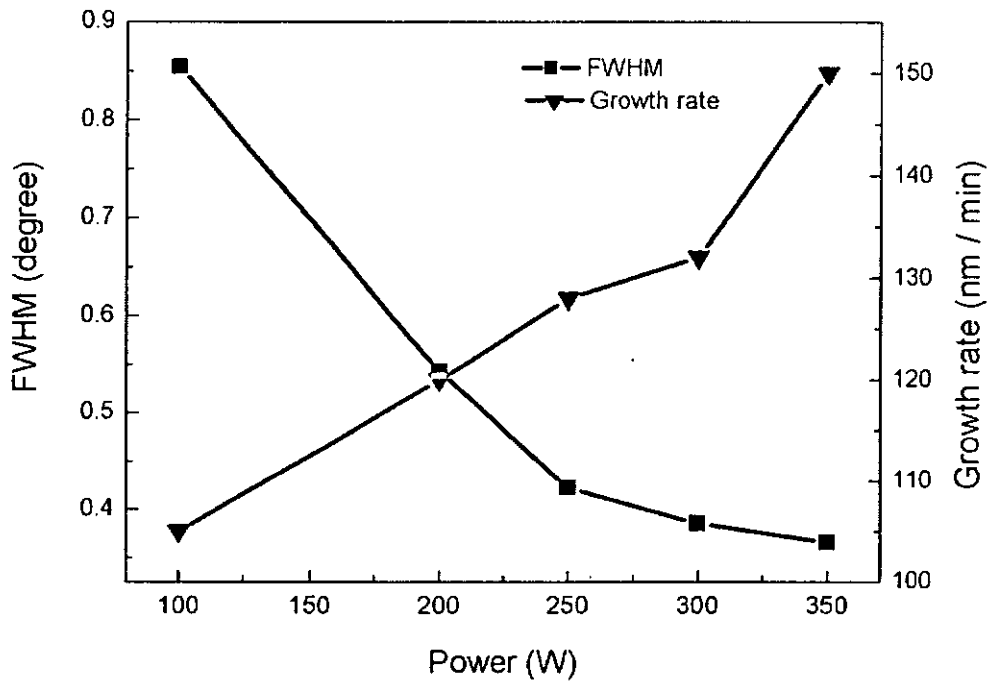

Fig. 3.1 Influence of different sputtering powers to the FWHM and growth rates on the sputtering AlN grown with 0.5Pa., 400°C and 50% N_2.

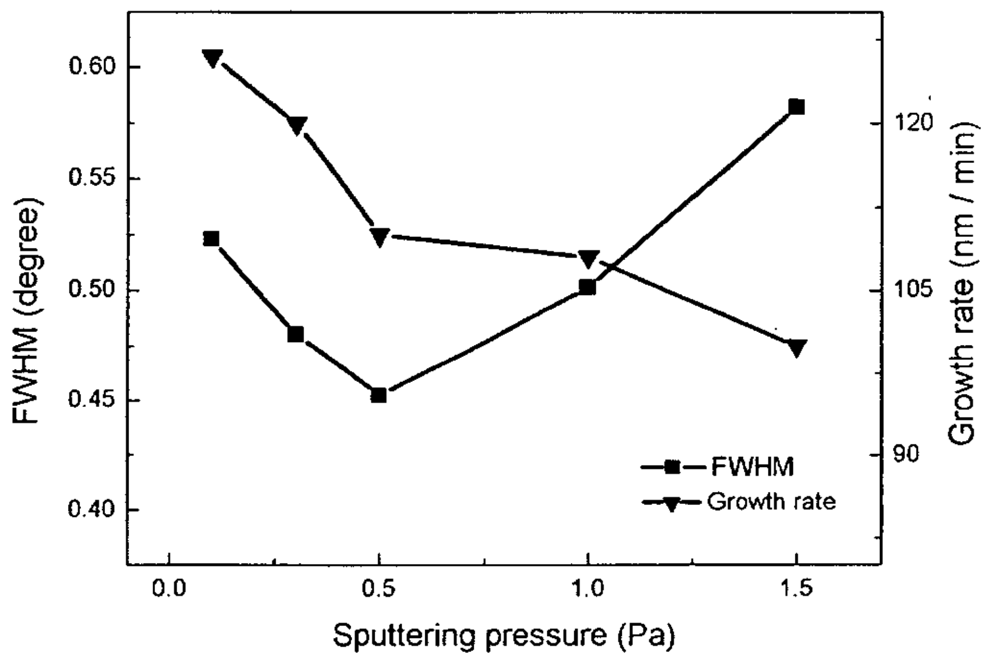

Fig. 3.2 Influence of different sputtering pressures to the FWHM and growth rates on the sputtering AlN grown with 350W, 400°C and 50% N_2.

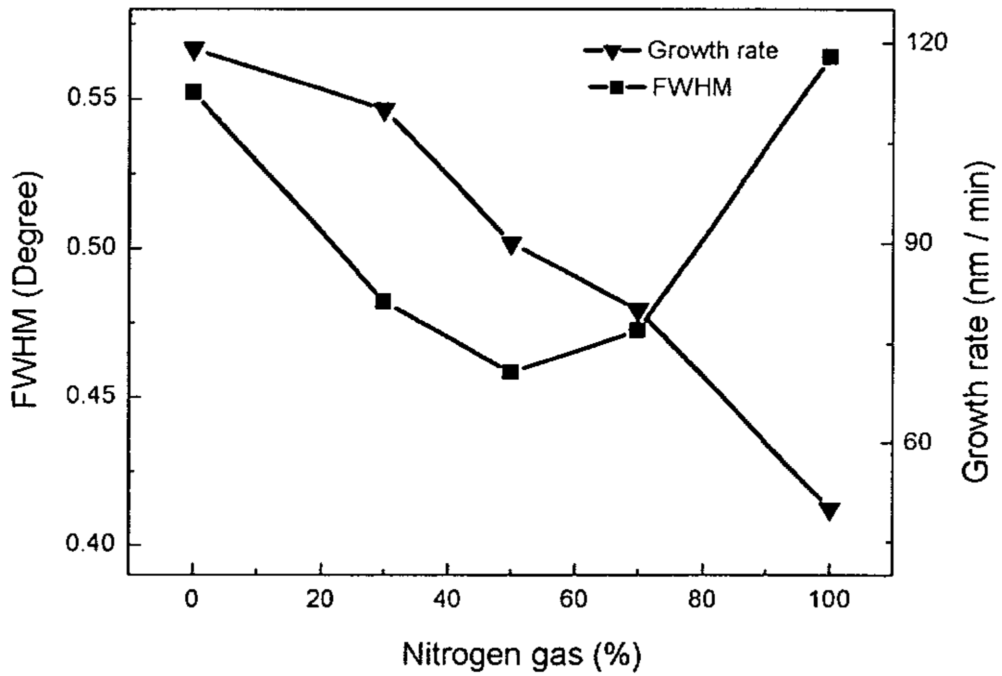

Fig. 3.3 Influence of different gas ratios to the FWHM and growth rates on the sputtering AlN grown with 0.5Pa., 400°C and 350W.

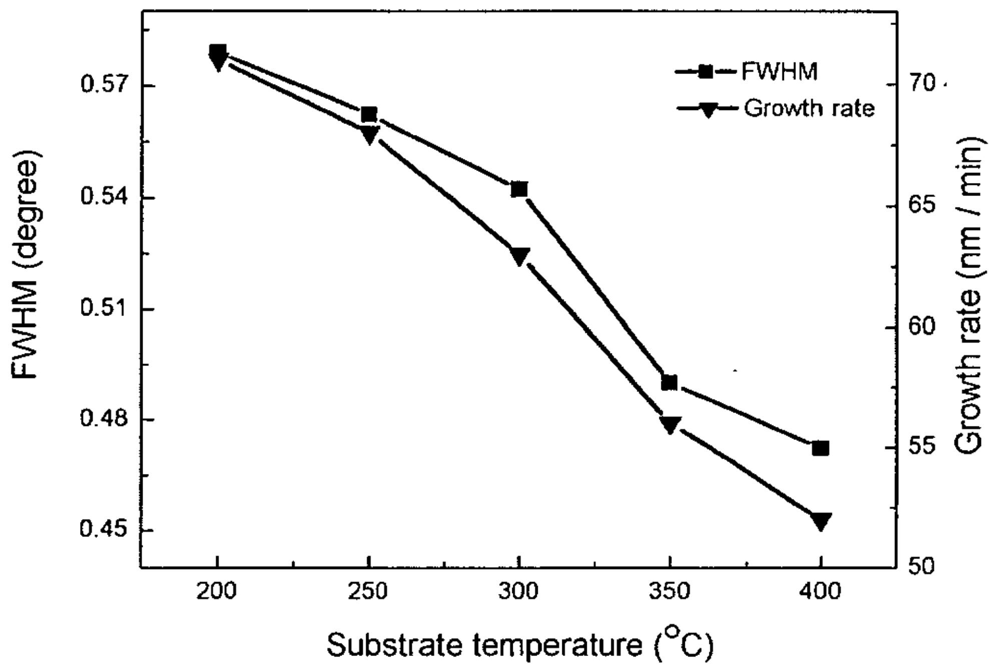

Fig. 3.4 Influence of different substrate temperatures to the FWHM and growth rates on the sputtering AlN grown with 0.5Pa., 50% N_2 and 350W.

the FWHM and the growth rate were both decreased. When the temperature was raised to 400°C, the FWHM of the AlN thin film was the minimum indicating the optimal substrate temperature for the AlN film growth. It is believed that the elevated substrate temperature provided the thermal energy required for re-arrangement of the adsorbed atoms leading to the improved crystallinity of the films. Using the optimized conditions, an AlN film was grown.

The c-axis orientation (002) and the rocking curve of AlN thin film grown on (0001) sapphire are shown in the Fig. 3.5 and Fig. 3.6. At the same time, the XRD results shows that the sputtering power was attributed to the quality of the thin films since the change of FWHM due to the variation of sputtering power was larger than the change due to the variation of N_2, the sputtering pressure and the substrate temperature. The FWHM of the optimized AlN film was 0.35°, this figure was shown that the AlN thin film was optimized by systematically varying the sputtering conditions.

The XRD measurement results of the ZnO thin films grown by rf magnetron sputtering technique are presented. The sputtering parameters were also varied systematically to optimize the growth conditions of the ZnO thin films. Firstly, from the XRD results, with the sputtering power varying from 50W to 150W in Fig. 3.7, there was a minimum value when the sputtering power was at 100W. The sputtering pressure is plotted against the FWHM of XRD of ZnO films as shown in Fig. 3.8. The growth rate of sputtering pressure was decreased and a minimum value of

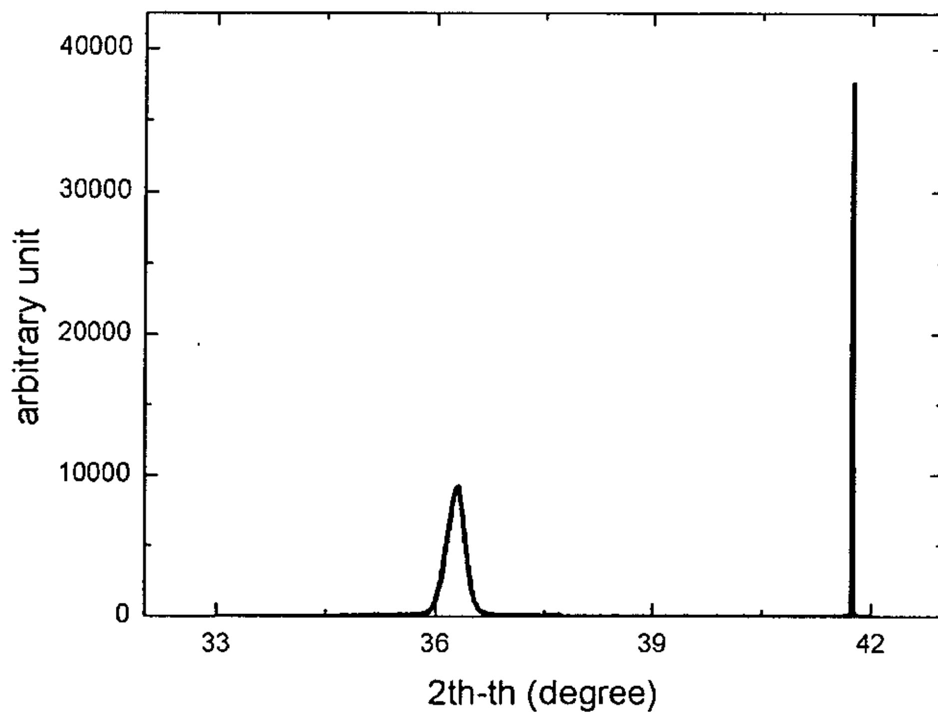

Fig 3.5 The 2th-th scanning of AlN / sapphire grown at 0.5Pa., 50% N_2, 400°C and 350W.

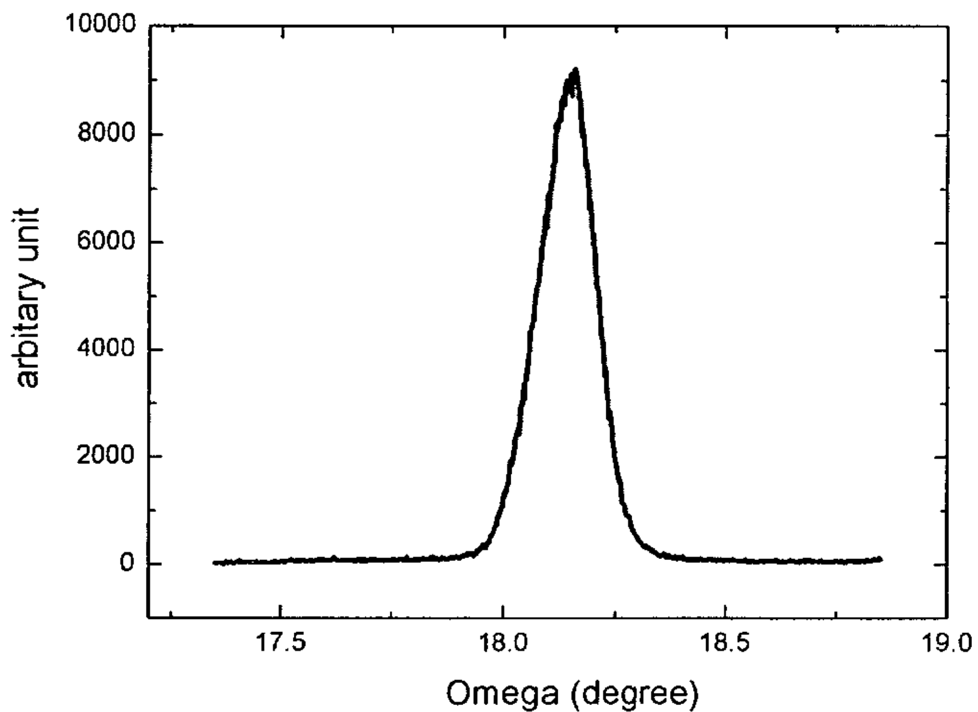

Fig 3.6 The rocking curve of AlN / sapphire grown at 0.5Pa., 50% N_2, 400°C and 350W.

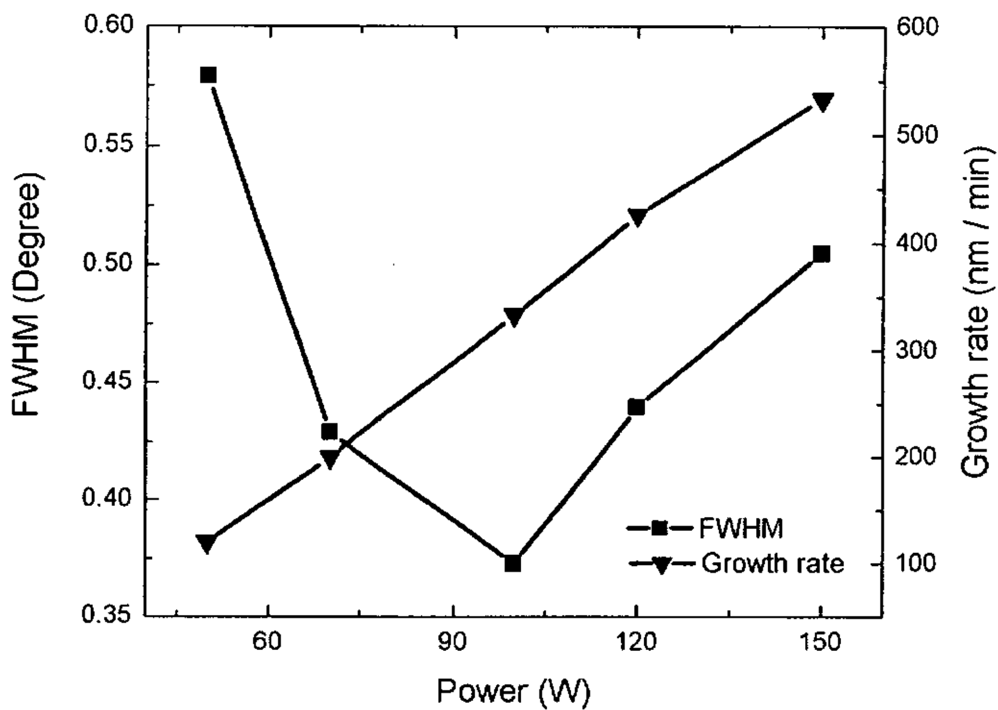

Fig. 3.7 Influence of different sputtering powers to the FWHM and growth rates on the sputtering ZnO grown with 1.5Pa. , 100°C and 50% O_2.

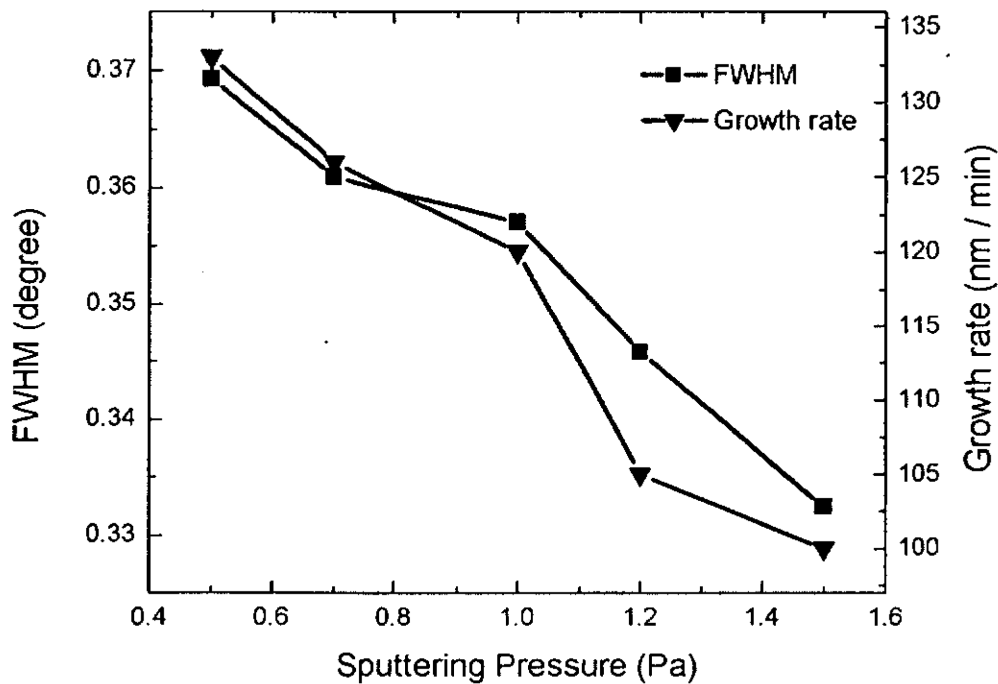

Fig. 3.8 Influence of different sputtering pressures to the FWHM and growth rates on the sputtering ZnO grown with 100W, 100°C and 50% O_2.

FWHM was at 1.5Pa. It is suggested that the increase in the sputtering pressure resulted with high probability of collision among the energetic atoms, the mean free path of the atoms would be shortened such that deposition rate would be lower.

Thirdly, the oxygen concentration was related to the stiochiometery and the crystal structure of the ZnO thin film. It is believed that some of the oxygen atoms in the sputtered ZnO molecules were lost during the bombardment with energetic atoms inside the plasma, the injection of the oxygen gas in the plasma was used to balance the loss of oxygen atom during the sputtering process. From Fig. 3.9, the growth rate of the ZnO thin films was decreased when the O_2 partial pressure was increased because the argon atom inside the plasma was decreased. This was because the mass of argon atom was much higher than the oxygen atom, the sputtering rate due to argon atom was higher than that of oxygen atom and thus the decrease in the partial pressure of argon will lead to a decrease in the growth rate of ZnO.

In Fig. 3.10, the minimum value of the FWHM of ZnO film was at a substrate temperature of about 100°C. The growth rate was decreased as the substrate temperature was increased up to 200°C because of the sorption of the ZnO atoms. The c-axis orientation (002) and the rocking curve of the ZnO thin film grown on (0001) sapphire using the optimized growth conditions are shown in the Figs. 3.11 and 3.12. From the results, it was found that the variation of the FWHM due to the variation of the sputtering power for both AlN and ZnO thin films was about 0.45° that the variation of the FWHM due to the other parameters was about 0.2°.

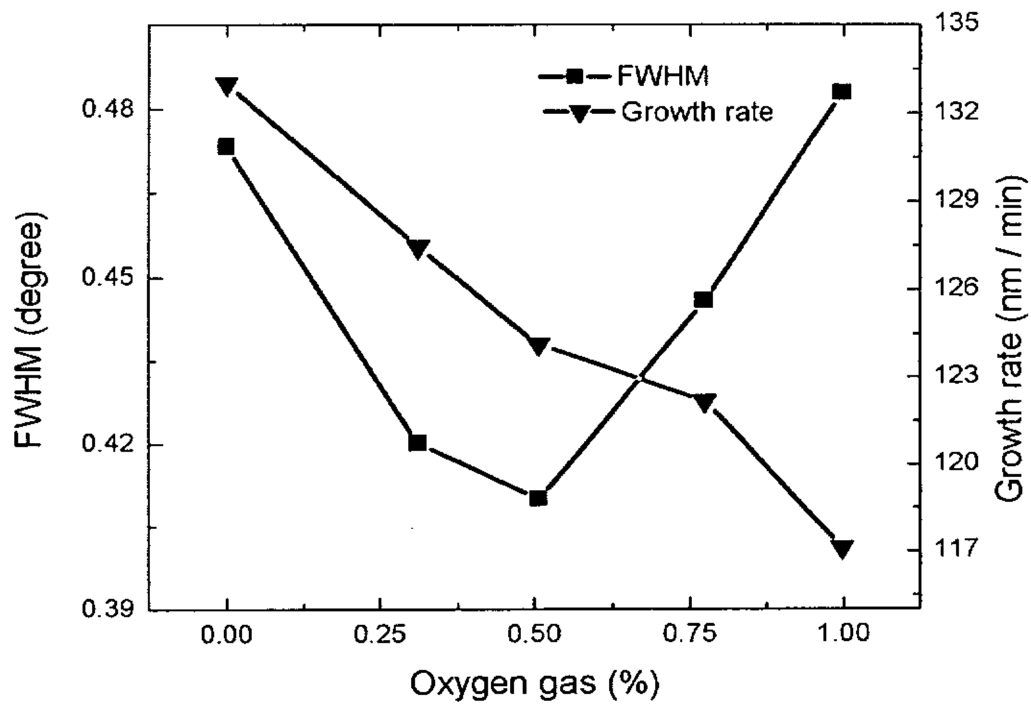

Fig. 3.9 Influence of different gas ratios to the FWHM and growth rates on the sputtering ZnO grown with 1.5Pa., 100°C and 100W.

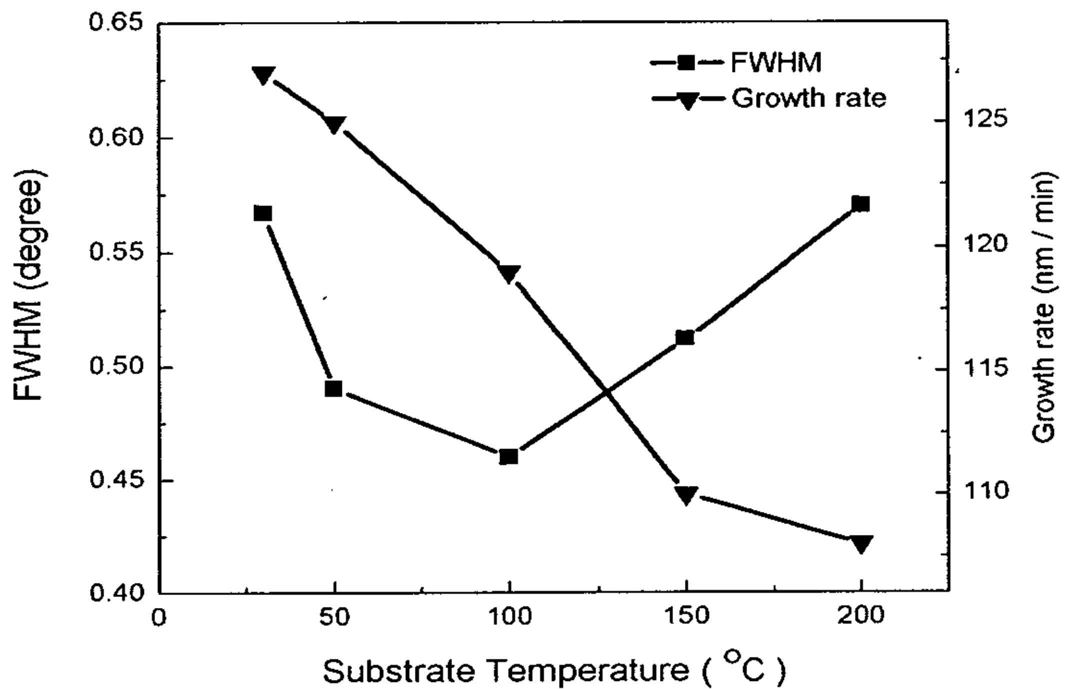

Fig. 3.10 Influence of different substrate temperatures to the FWHM and growth rates on the sputtering ZnO grown with 1.5Pa., 50% O_2 and 100W.

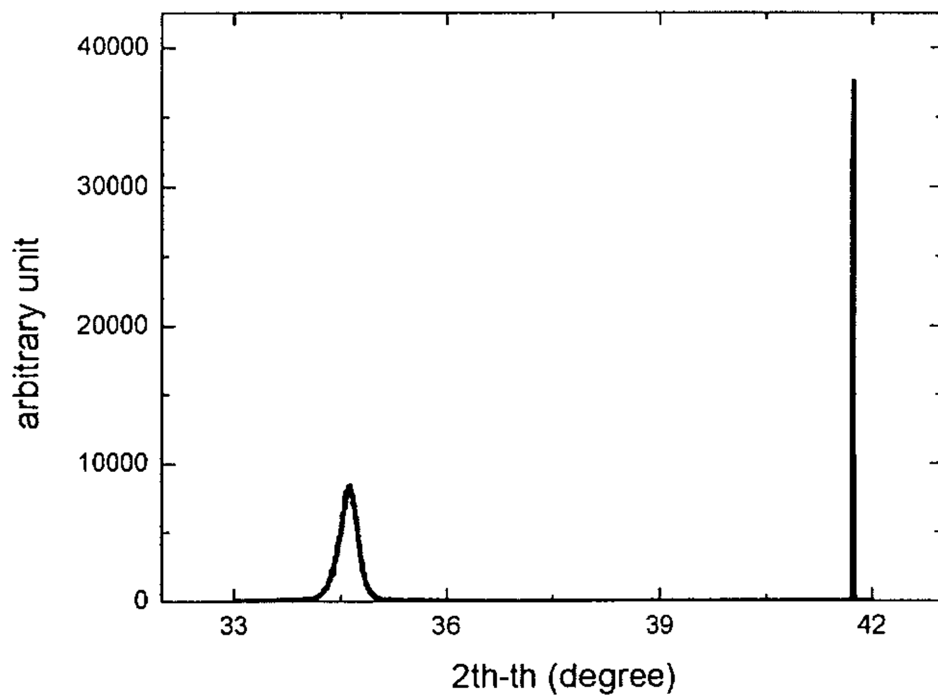

Fig. 3.11 The 2th-th scanning of ZnO / sapphire grown at 1.5Pa. , 50% O_2, 100°C and 100W.

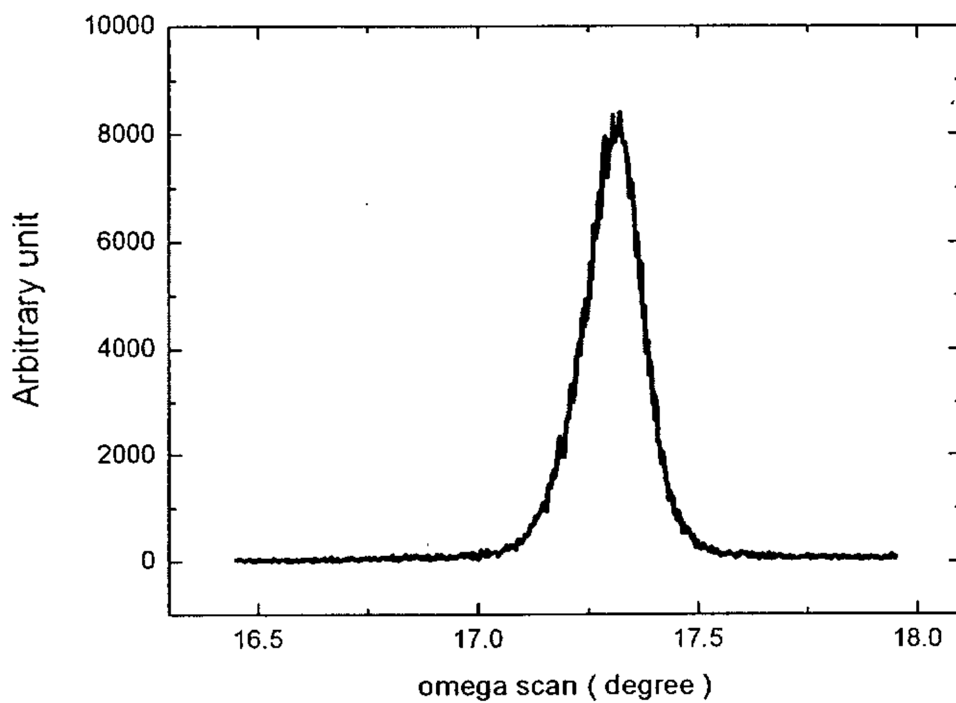

Fig. 3.12 The rocking curve scanning of ZnO / sapphire grown at 1.5Pa, 50% O_2, 100°C and 100W.

Therefore, the sputtering power had a strong effect on the quality of both AlN and ZnO thin films grown on sapphire substrate.

In order to observe whether columnar structure was present in both AlN and ZnO films, these two films were grown with their optimal condition and were examined using SEM. The columnar structure of the sputtered AlN and ZnO thin films are shown in Fig. 3.13 (a) and (b) respectively. In the SEM pictures, grains and grains boundaries of AlN and ZnO thin film can be found and the columnar structure of the AlN and ZnO thin film is clearly demonstrated. This shows that both AlN and ZnO thin films were grown in the c-axis direction normal to the substrate. In this way the insertion loss could be minimized since the thin film grown in c-axis direction allowed the acoustic velocity propagating in one preferred direction and became less dispersive.

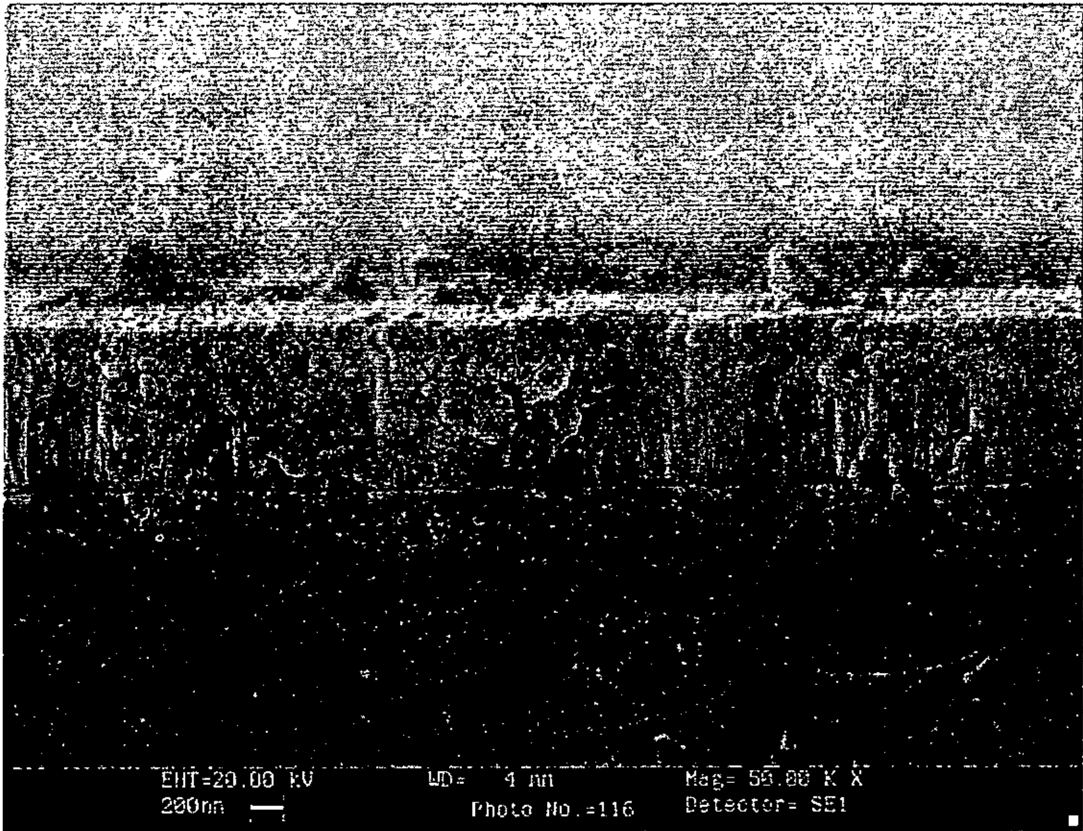

(a)

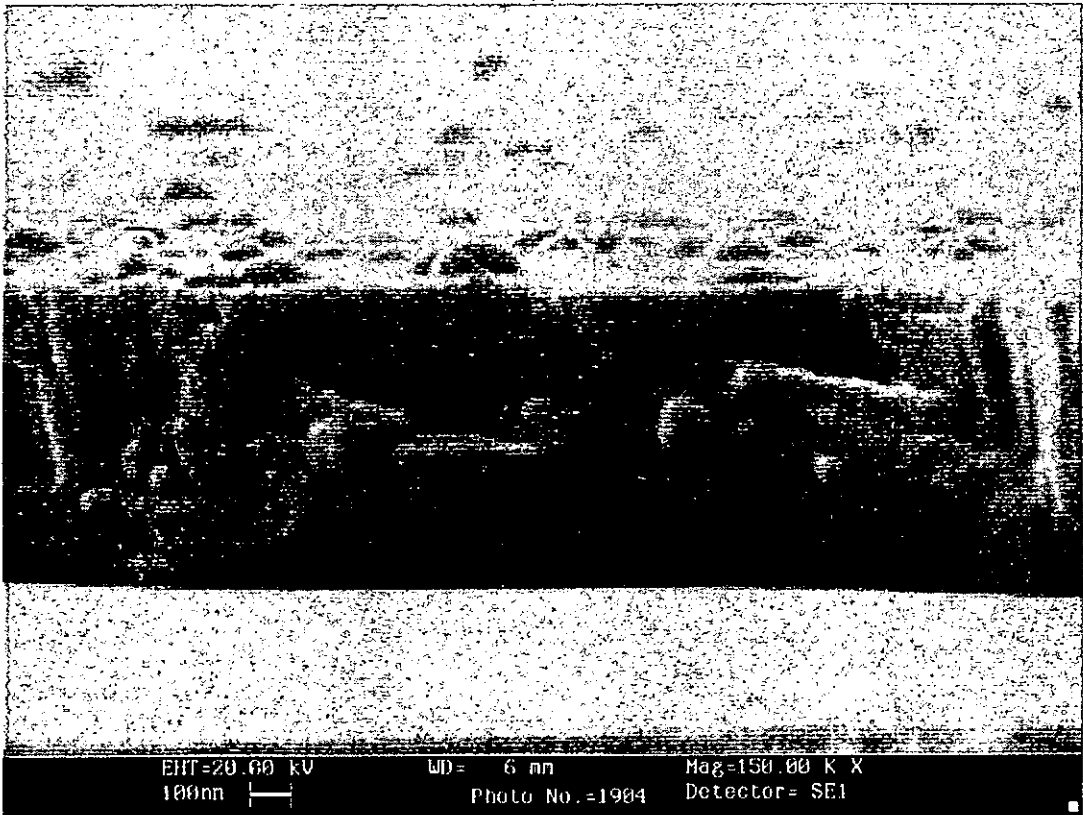

(b)

Fig. 3.13 The SEM picture of the cross-section of both (a) AlN (b) ZnO thin films

To investigate the effect of the sputtering power and substrate temperature on the performance of the SAW filters, AlN and ZnO film grown under different sputtering powers and substrate temperatures under optimized condition were needed to be prepared. In Figs. 3.14 and 3.15 shows the FWHM of the XRD of AlN and ZnO films against different sputtering powers. When the sputtering power increased, the FWHM of the XRD of AlN films was minimum at 350W. And the minimum FWHM value of the XRD of ZnO films appeared at 100W. The same measurement process was also put on the both AlN and ZnO films grown with different substrate temperatures as shown in Figs. 3.16 and 3.17. An optimal value of substrate temperature of AlN and ZnO films is 400°C and 100°C respectively.

The surface morphology of the both AlN and ZnO thin films was characterized by the SEM. In Fig. 3.18, the roughness of the surface of the AlN thin film was varied in different substrate temperatures. The grain size of AlN thin film deposition at 200°C was the largest and the grain size was decreased while the substrate temperature was increased. SEM examined the surface morphology of the ZnO thin film with different substrate temperatures. In Fig. 3.19, the SEM pictures showed that the grain size varied with the substrate temperatures. The grain size was found to increase and maximum 100°C. However, the size decreased again when the temperature was raised to 200°C. This was because at higher substrate temperature the thermal energy facilitated the surface motion of atoms and it also provided the energy required for individual atom to form bonds

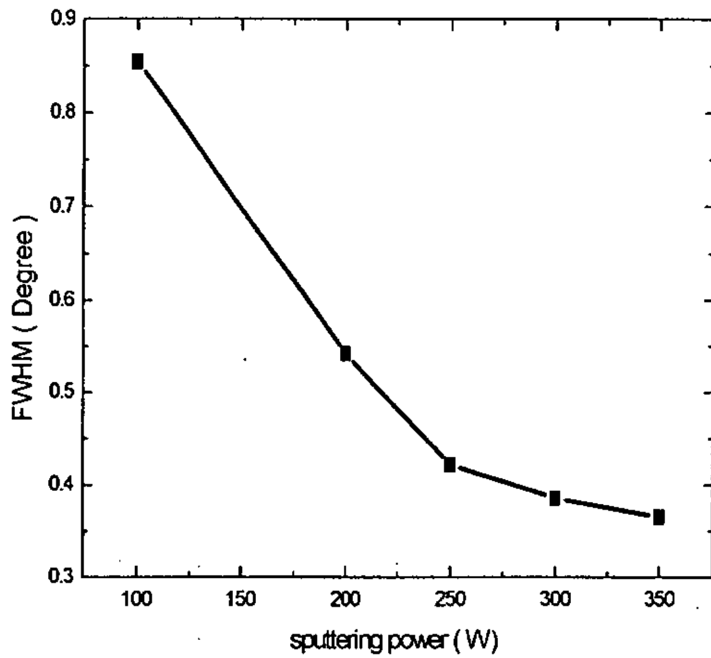

Fig. 3.14 The FWHM of XRD peak from the AlN films grown by different sputtering powers

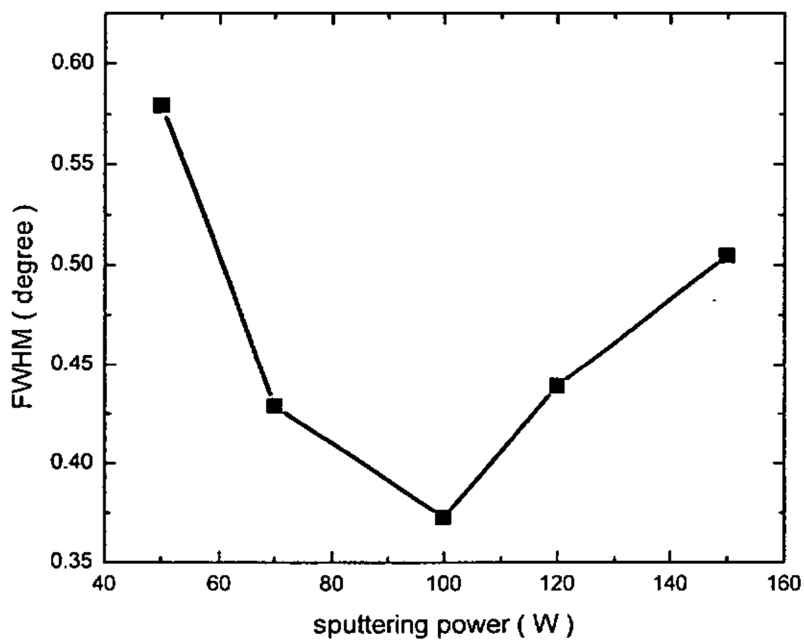

Fig. 3.15 The FWHM of XRD peak from the ZnO films grown by different sputtering powers

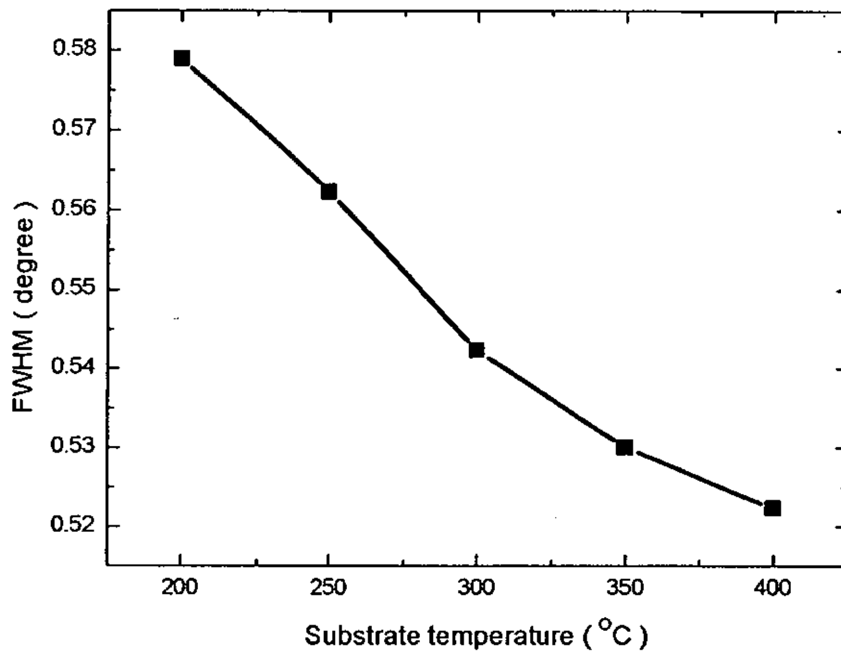

Fig. 3.16 The FWHM of XRD peak from the AlN films grown by different substrate temperatures.

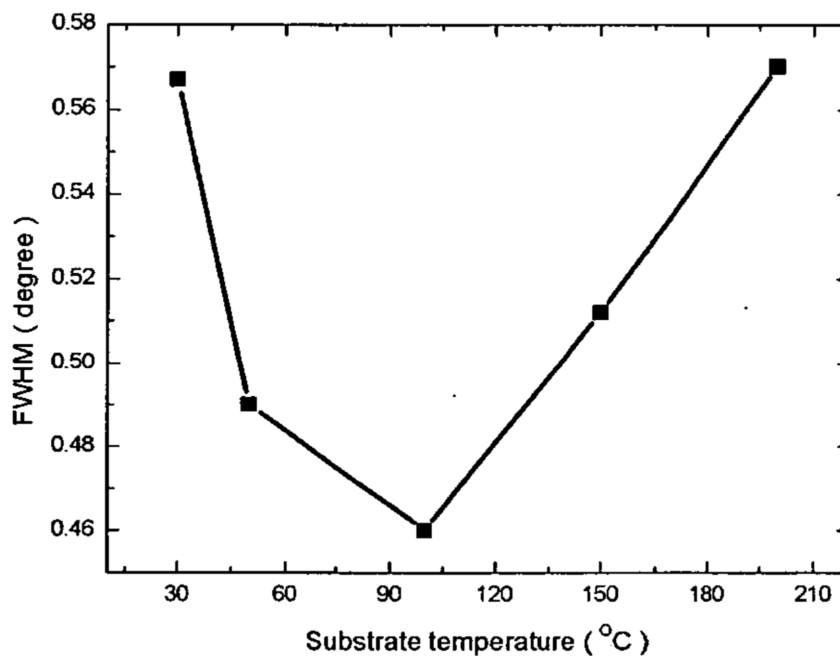

Fig. 3.17 The FWHM of XRD peak from the ZnO films grown by different substrate temperatures.

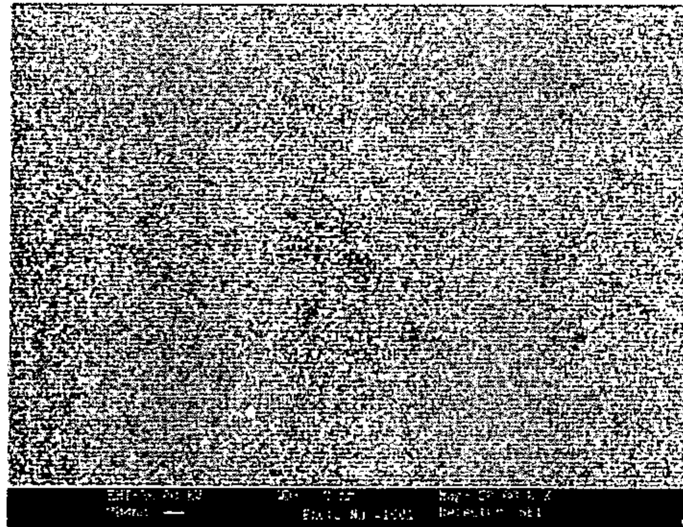

(a) 200°C

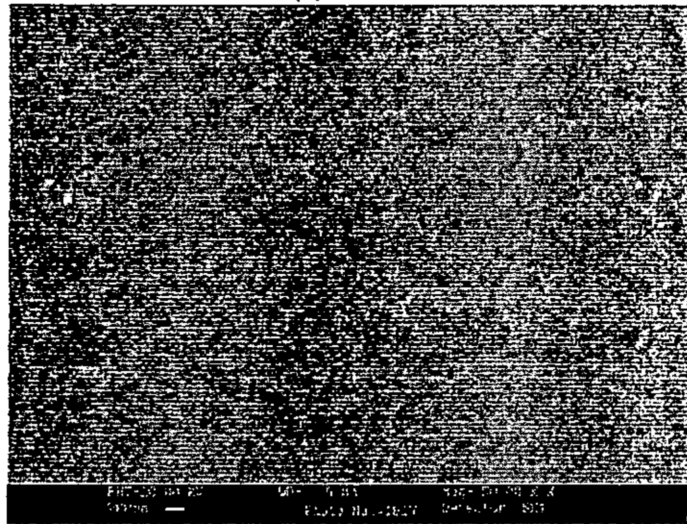

(b) 300°C

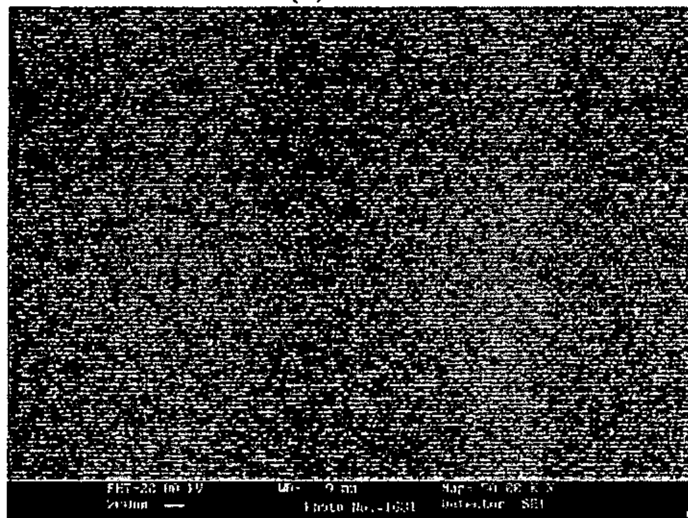

(c) 350°C

Fig. 3.18 The effect of the different substrate temperatures on the surface morphology of AlN / sapphire at (a) 200°C (b) 300°C (c) 400°C

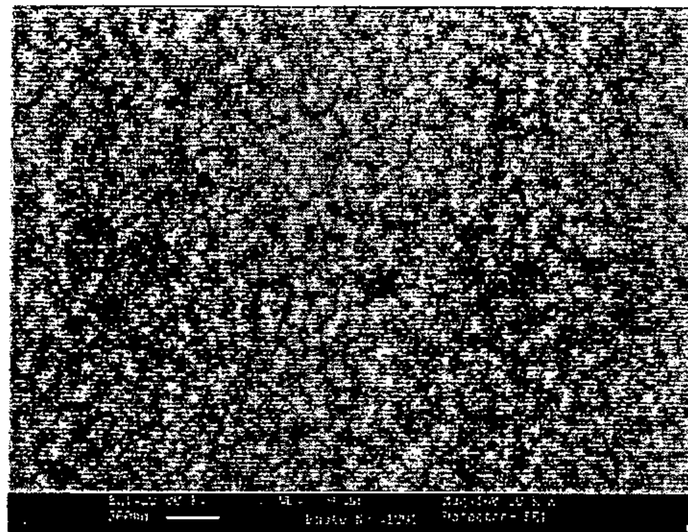

(a)

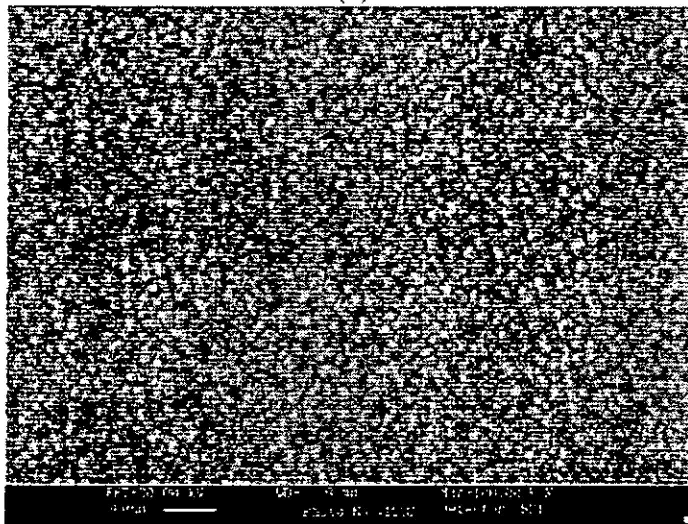

(b)

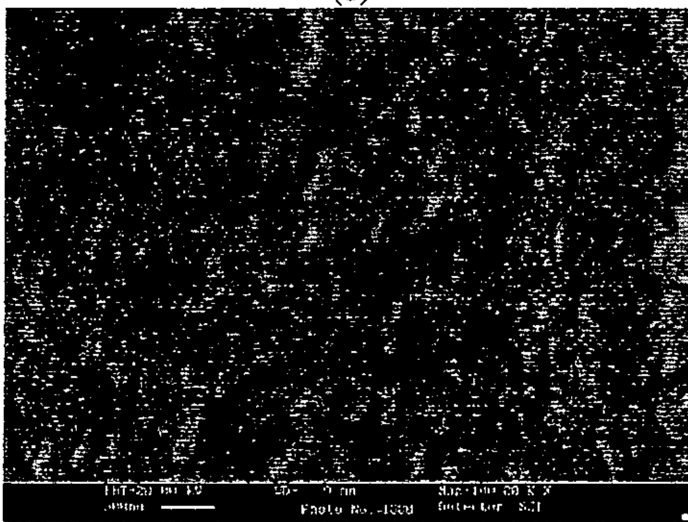

(c)

Fig. 3.19 The effect of the different substrate temperatures on the surface morphology of ZnO / sapphire at (a) 50°C (b) 100°C (c) 200°C

leading to increase in grain size.

Besides using SEM, the surface morphology of both AlN and ZnO thin films grown with different sputtering powers and substrate temperatures were also examined by AFM. In Figs. 3.20 and 3.21, the surface roughness of the AlN thin films is plotted against different sputtering powers and substrate temperature. For AlN films, when the substrate temperature was fixed, the rms roughness was minimum when the sputtering power increased up to 350W. When the sputtering power was fixed, the roughness of the AlN film was at minimum value when the substrate temperature is at 400°C.

For ZnO thin films, the trend was different with that of the AlN thin films. In Figs. 3.22 and 3.23, the surface roughness of the ZnO thin films is plotted against different sputtering powers and substrate temperatures respectively. When the substrate temperature was fixed, the roughness of the ZnO thin films was optimized at the 100W of the sputtering power. When the sputtering power was fixed, the roughness of the ZnO films appeared at 100 °C of the substrate temperature.

The surface morphology of the ZnO thin film grown at 100°C and AlN film grown at 400°C are shown in Figs 3.24 and 3.25. It is also important to note it corresponds to the optimal growth conditions of the AlN and ZnO films based on our investigation of the dependence of FWHM of the XRD measurements on various growth conditions as presented above.

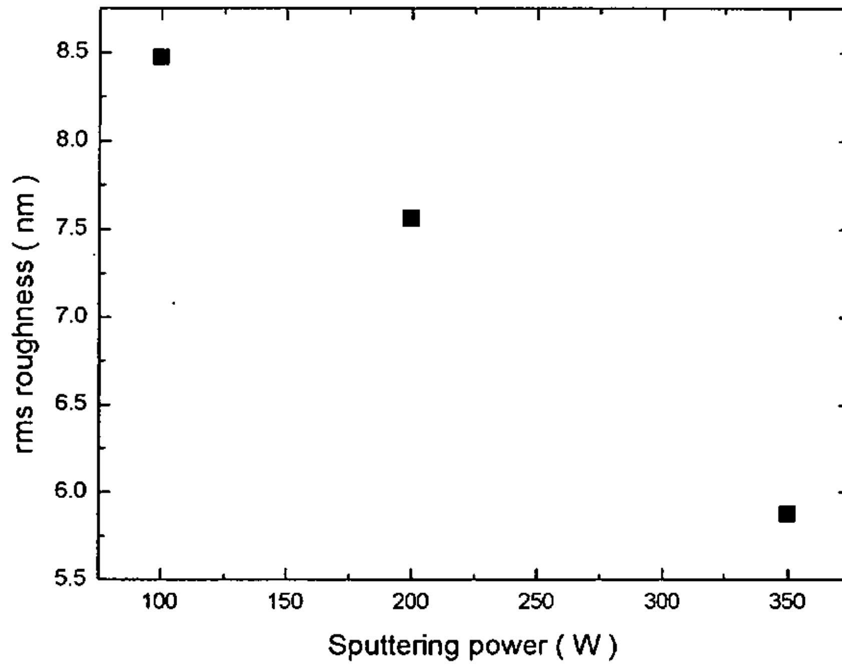

Fig 3.20 The surface morphology of the AlN thin films deposited at different sputtering powers

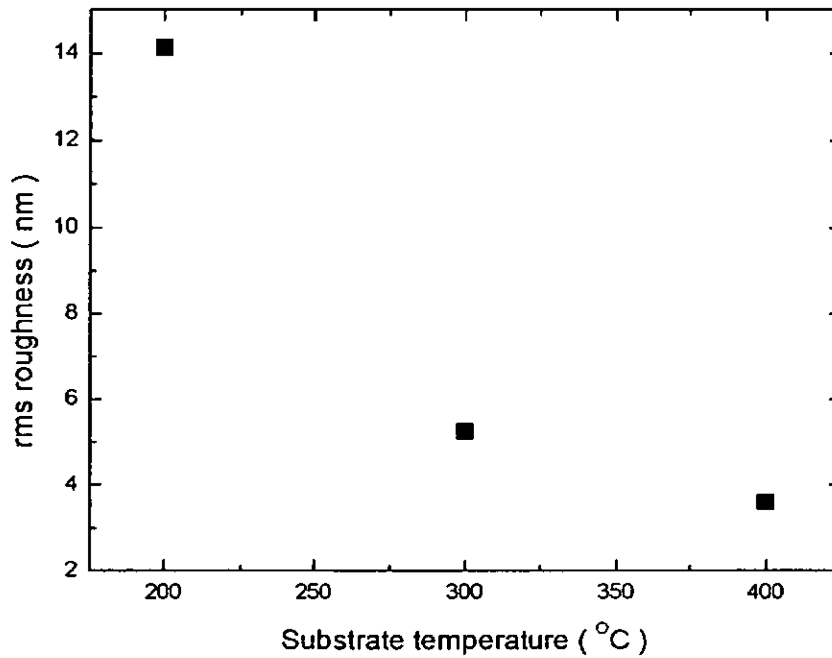

Fig 3.21 The surface morphology of the AlN thin films deposited at different substrate temperatures

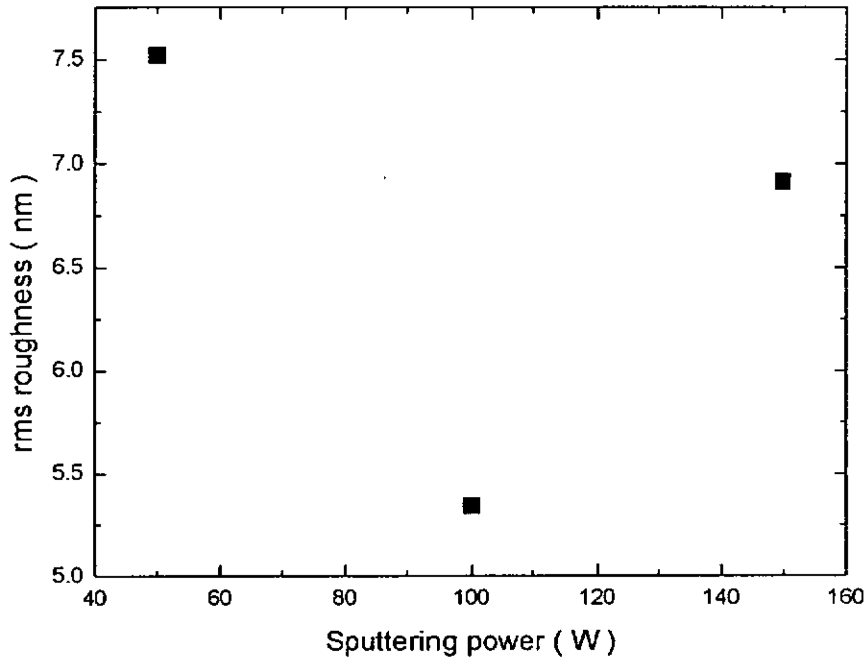

Fig. 3.22 The surface morphology of the ZnO thin films deposited at different sputtering powers

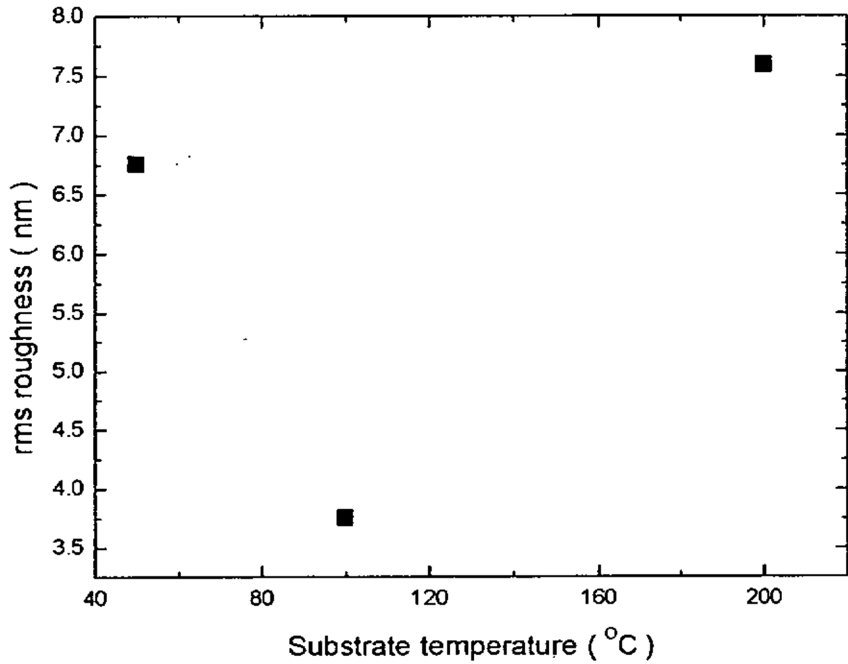

Fig. 3.23 The surface morphology of the ZnO thin films deposited at different substrate temperatures

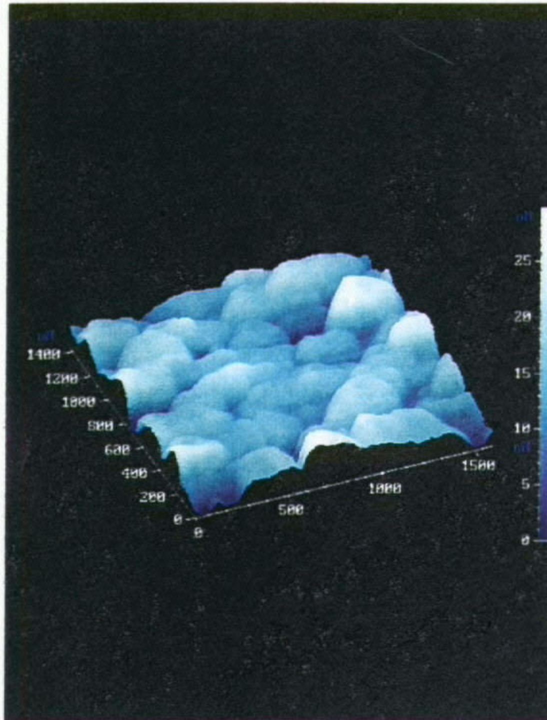

Fig. 3.24 The surface morphology of the AlN thin film grown at 400°C under AFM measurement

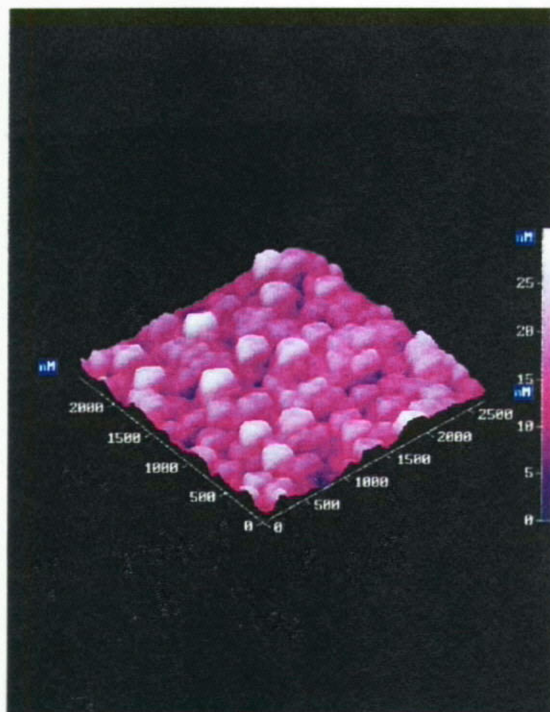

Fig. 3.25 The surface morphology of the ZnO thin film grown at 100°C under AFM .measurement

3.1.2 Characterization of AlN and ZnO SAW filters grown by rf magnetron sputtering technique

The measurement results of AlN and ZnO SAW filters grown by rf sputtering technique are presented in this section. The AlN and ZnO based SAW filter were fabricated and shown in Fig. 3.26. Three classes of the linewidth of the IDT were fabricated: they were in 1 μm, 2 μm and 4 μm and their corresponding acoustic wavelength were 4 μm, 8 μm and 16 μm as the even-transducers length type of IDT was used. For the ease of fabrication and characterization of the SAW filters, 4 μm linewidth of the IDT electrode length was used and the acoustic wavelength was 16 μm. The frequency response of the AlN and ZnO SAW filter grown with the optimized conditions, were measured and shown from the Fig. 3.27 to Fig. 3.28. The summary of the measured SAW velocity of AlN and ZnO SAW filters under different linewidths are shown in the Table 3.1

In order to study the influence of the material quality on the SAW filter performance, SAW filters were fabricated using AlN and ZnO thin films grown by rf magnetron sputtering technique. Different sputtering parameters were used in deposition process. Since the sputtering power and substrate temperature were found to have strong influence on the crystallinity and surface morphology of the AlN and ZnO thin film, for both AlN and ZnO thin films, the samples were grown with systematically varying substrate temperatures of thin films, and all samples were fabricated into SAW filters and examined with 4 different device measurements.

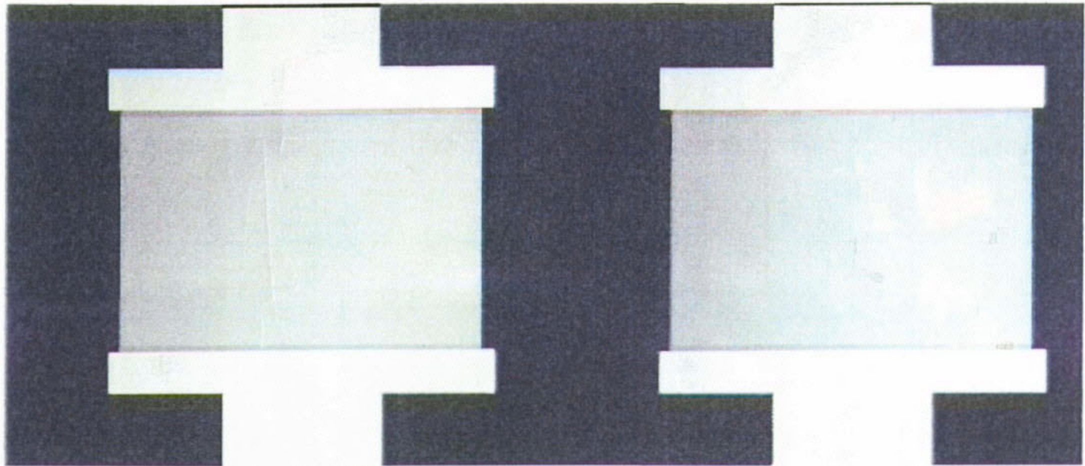

Fig. 3.26 The picture of SAW filter under optical microscope

Fundamental mode	ZnO SAW filter	AlN SAW filter
4 μm (λ = 16 μm)	4848ms^{-1} (303 MHz)	5520ms^{-1} (345 MHz)
2 μm (λ = 8 μm)	4550ms^{-1} (568.75 MHz)	4772ms^{-1} (684 MHz)
1 μm (λ = 4 μm)	4480ms^{-1} (1120 MHz)	5316ms^{-1} (1329 MHz)

Table 3.1 The summary of the operation frequency of both AlN and ZnO SAW filters under different IDT electrode linewidths.

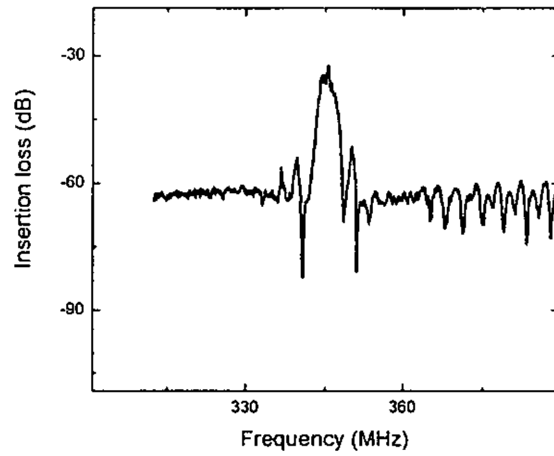

(a)

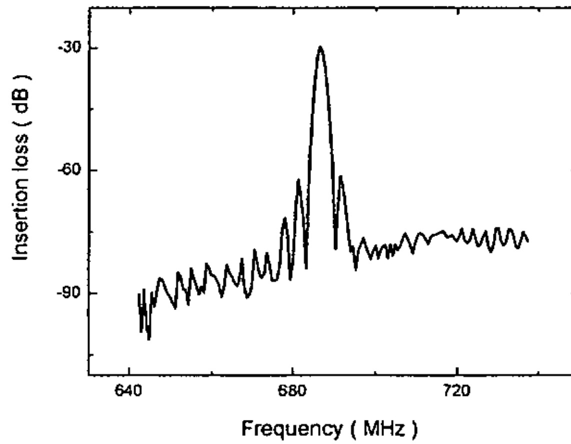

(b)

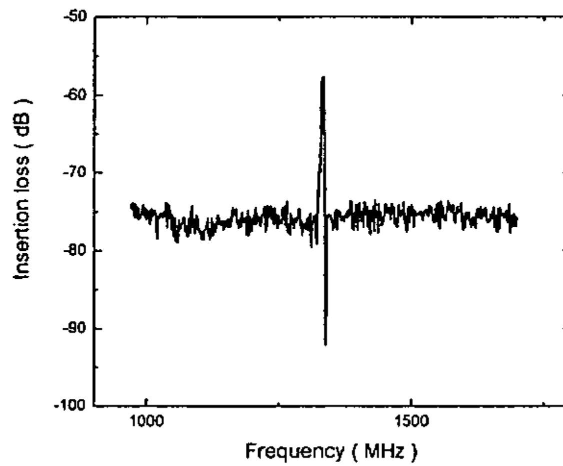

(c)

Fig. 3.27 The frequency response of AlN SAW filters fabricated with various electrode linewidths (a) 4 μm (b) 2μm (c) 1μm

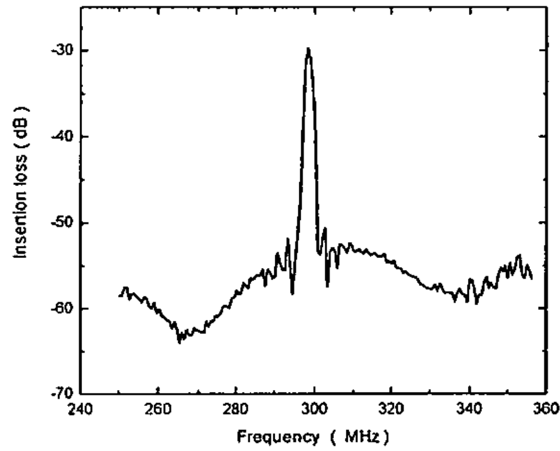

(a)

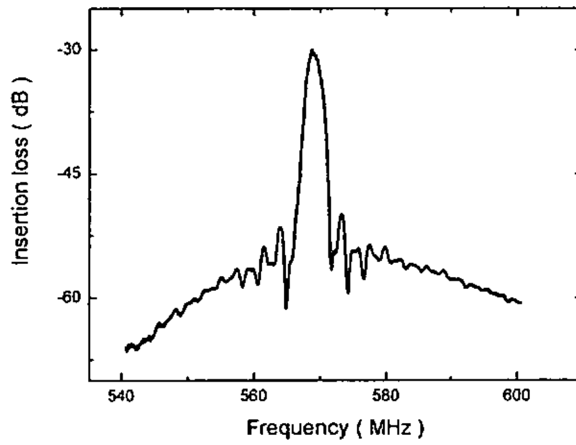

(b)

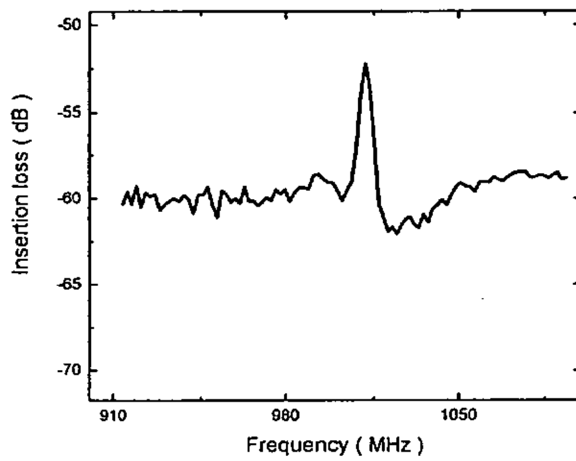

(c)

Fig. 3.28 The frequency response of ZnO SAW filters fabricated with various electrode linewidths (a) 4 μm (b) 2μm (c) 1μm

In frequency response measurement, the AlN and ZnO SAW filters exhibited different trends when the sputtering power and substrate temperature were varied. In Figs. 3.29 and 3.30, for both AlN and ZnO SAW filters, phase velocity of the AlN and ZnO SAW filters was directly related to the sputtering powers and substrate temperatures. For AlN SAW filters, the phase velocity was increased with the sputtering power. For ZnO SAW filters, the maximum value of phase velocity was found to correspond to a sputtering power of 100W. The phase velocity of the AlN SAW filters was about 5520ms^{-1} which was higher than that of ZnO SAW filters (Vp = 4848ms^{-1}) and this showed that AlN SAW filters can be used in high speed devices. From the graphs, the deviation of phase velocity of the AlN and ZnO SAW filters was about 200ms^{-1} in average due to the change of the sputtering power. On top of that, the deviation of phase velocity of the AlN and ZnO SAW filters was about 20ms^{-1} in average due to the change of the substrate temperature. Thus, the phase velocity is more affected by sputtering power rather than substrate temperature.

The K^2 for both AlN and ZnO SAW filters are shown in Figs. 3.31 and 3.32 respectively. The figures demonstrate different sputtering power and substrate temperature effect on K^2 of the AlN and ZnO SAW filters. It indicated that the maximum K^2 values of the AlN SAW filters were found at 350 W and 100 °C. The maximum values of K^2 of the ZnO SAW filters were found at 100 W and 100 °C. From the above data, the maximum value of K^2 of ZnO SAW filters (K^2 = 0.74%) was nearly two times higher than that of AlN SAW filters (K^2 = 0.497%).

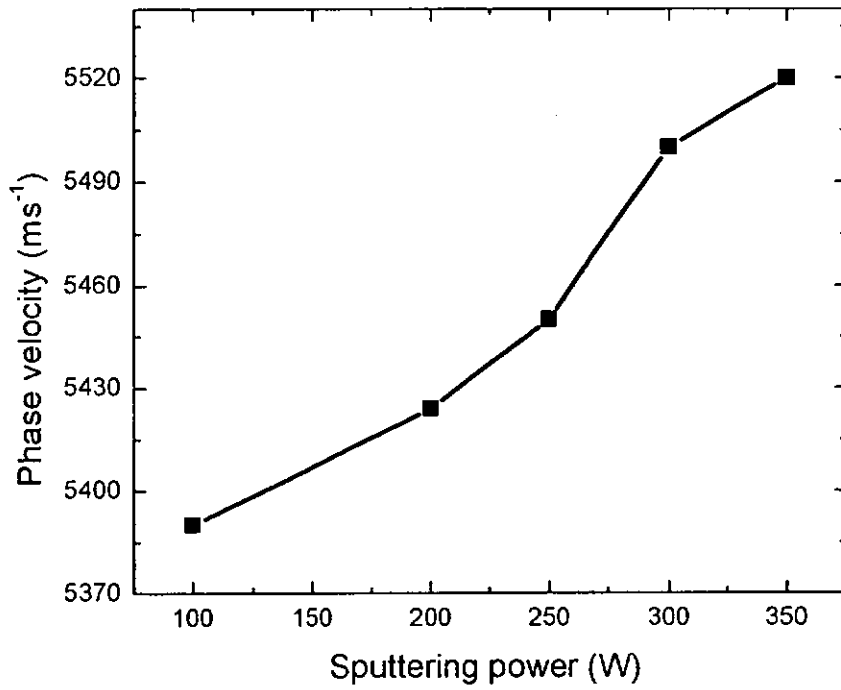

(a)

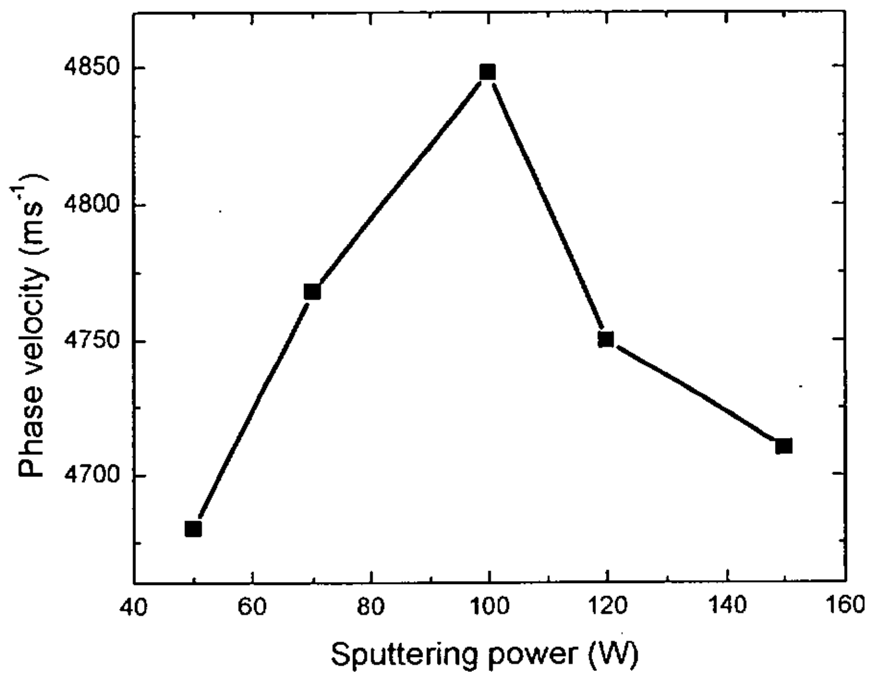

(b)

Fig. 3.29 The phase velocity of SAW filters grown with different sputtering powers (a) AlN SAW filters and (b) ZnO SAW filters

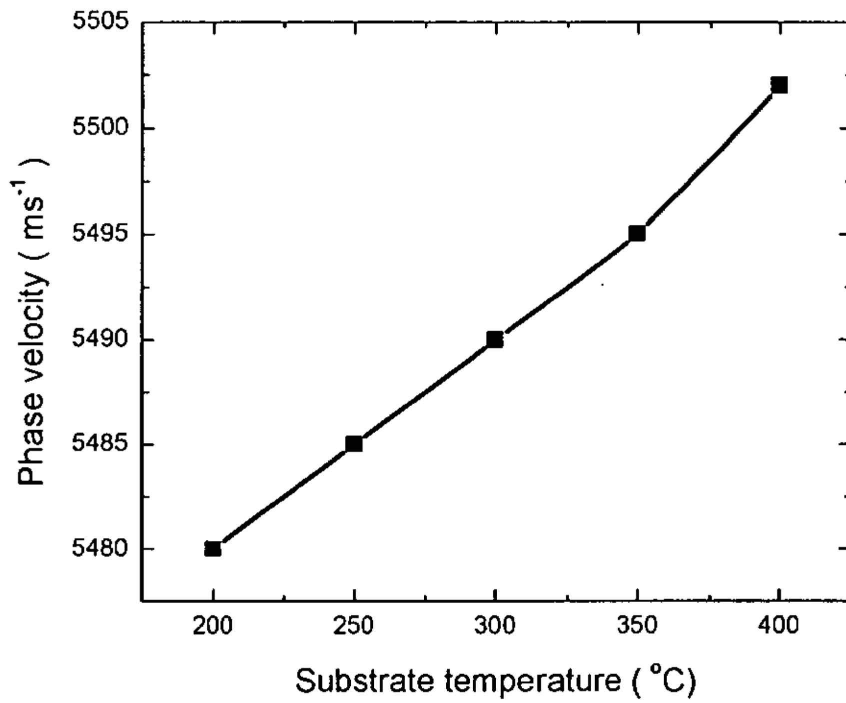

(a)

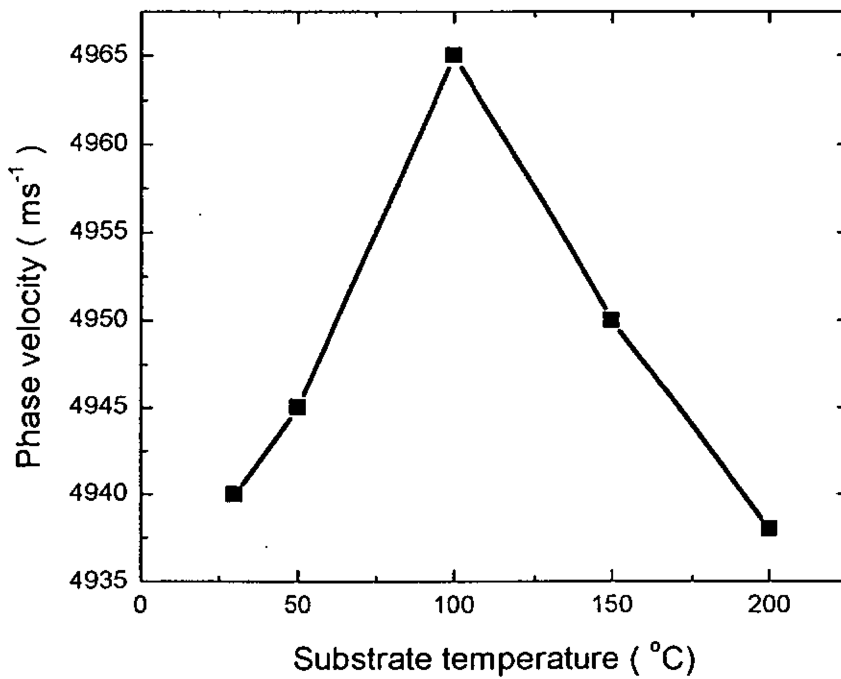

(b)

Fig. 3.30 The phase velocity of SAW filters grown with different substrate temperatures (a) AlN SAW filters and (b) ZnO SAW filters

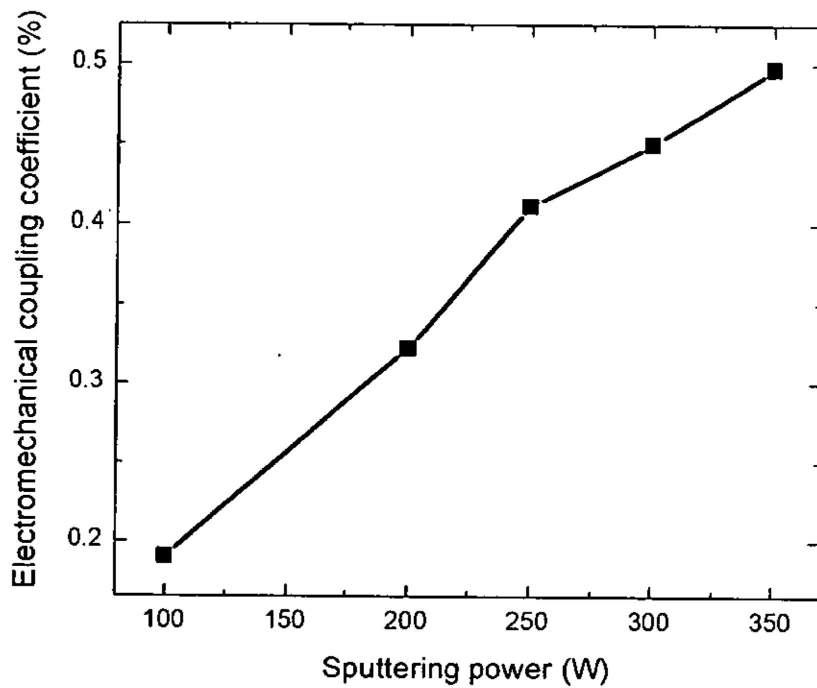

(a)

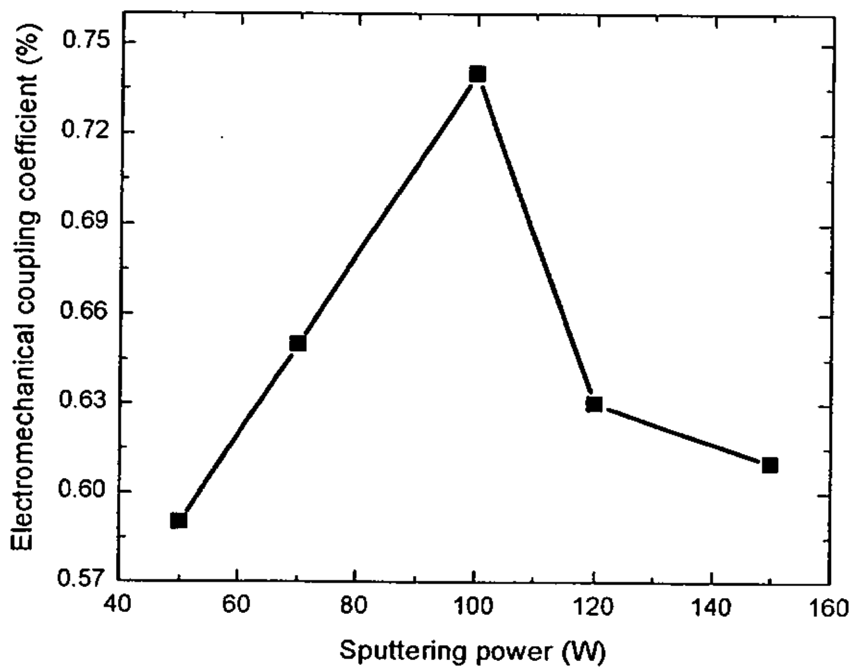

(b)

Fig. 3.31 The electromechanical coupling coefficient of SAW filters grown with different sputtering powers (a) AlN SAW filters and (b) ZnO SAW filters

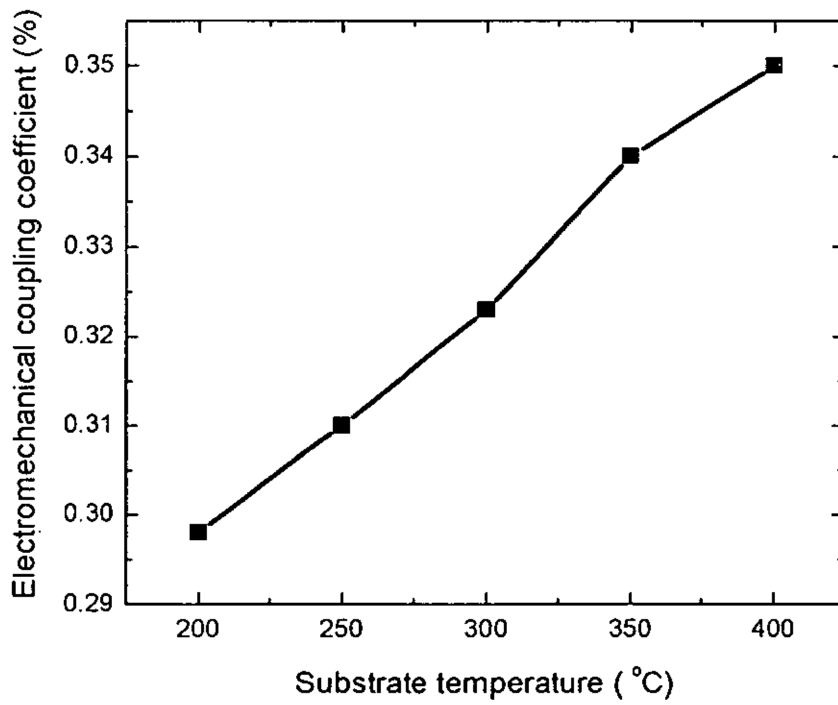

(a)

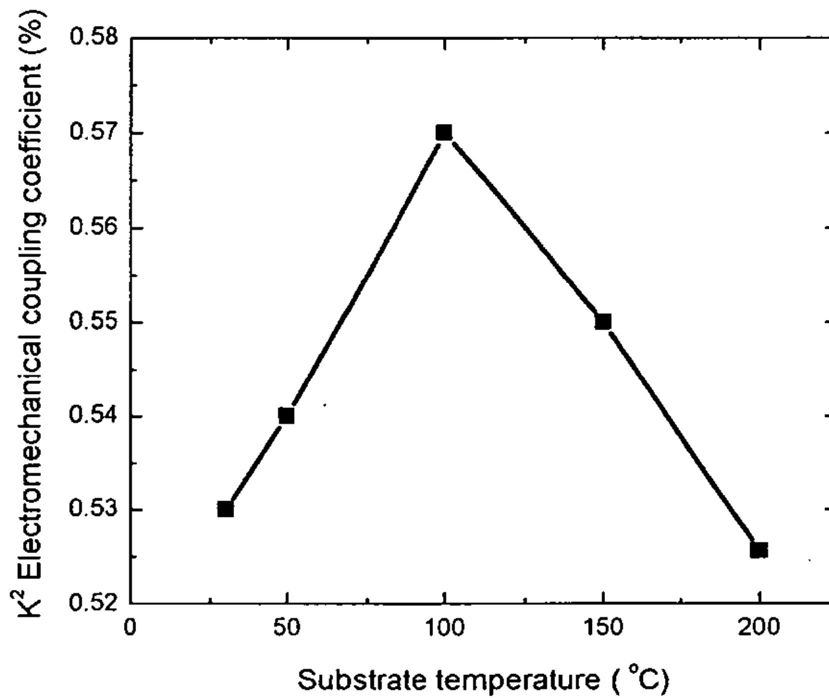

(b)

Fig. 3.32 The electromechanical coupling coefficient of SAW filters grown with different substrate temperatures (a) AlN SAW filters and (b) ZnO SAW filters

The results of the phase noise of both AlN and ZnO SAW filter are presented in the Figs. 3.33 and 3.34. The phase noise of both AlN and ZnO SAW filters were found to vary significantly with the sputtering power. The minimum value of phase noise of AlN SAW filters was about –90 dBc / Hz at 350W and that for 100W for ZnO SAW filters. However, the phase noise due to the substrate temperature is found to be much weaker, for both AlN and ZnO SAW filter. A variation of about 3 dBc / Hz is observed over the entire range. The phase noise of SAW filters was mainly come from the variation of sputtering power.

The final experiment for the examination of SAW filter performance was the study of insertion loss. In Fig. 3.35 and Fig. 3.36, strong dependence on the substrate temperature was observed for both types of SAW filters. The minimum value of the insertion of AlN SAW filter was about -30 dB at 400°C and that of ZnO SAW filter was about -27 dB. However, by varying the sputtering power, the insertion loss varied from -35dB to -36.5dB for ZnO SAW filter and from -42 dB to -44 dB for AlN SAW filter.

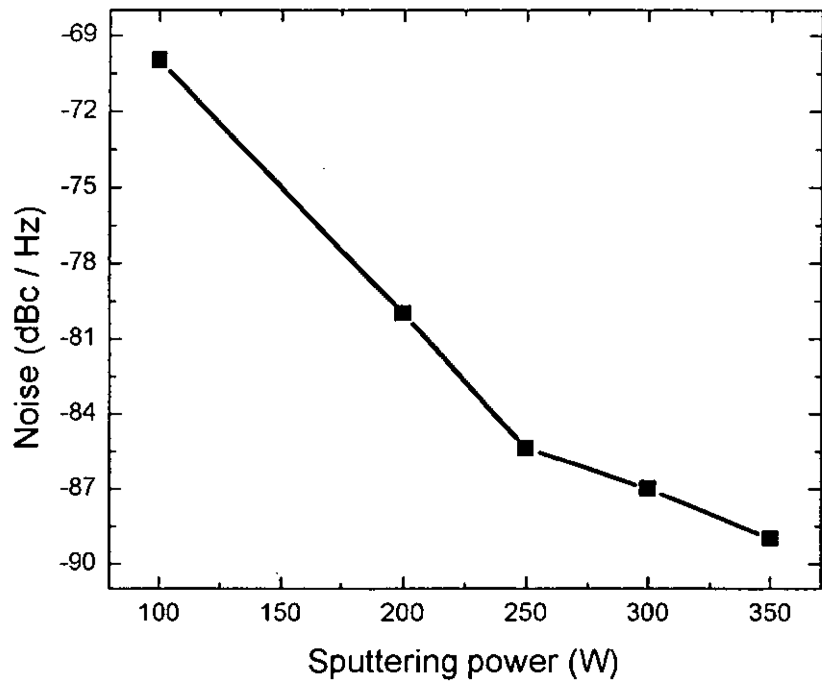

(a)

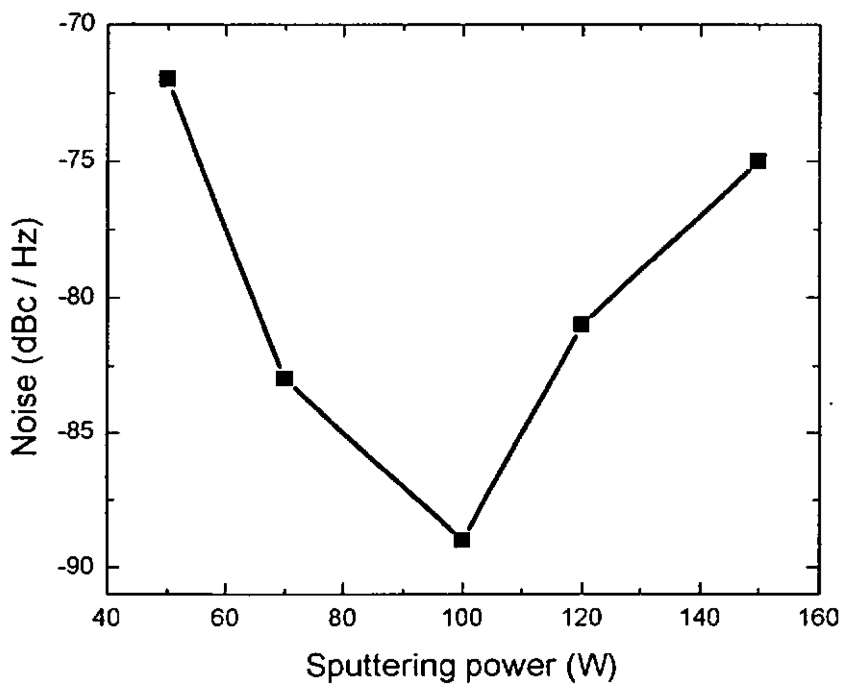

(b)

Fig. 3.33 The phase noise of SAW filters grown with different sputtering powers (a) AlN SAW filters and (b) ZnO SAW filters

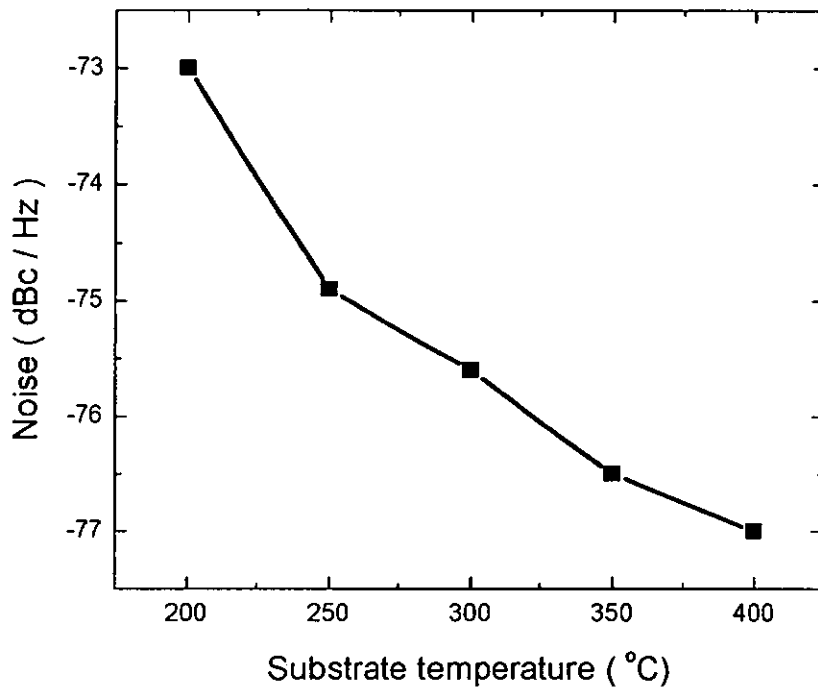

(a)

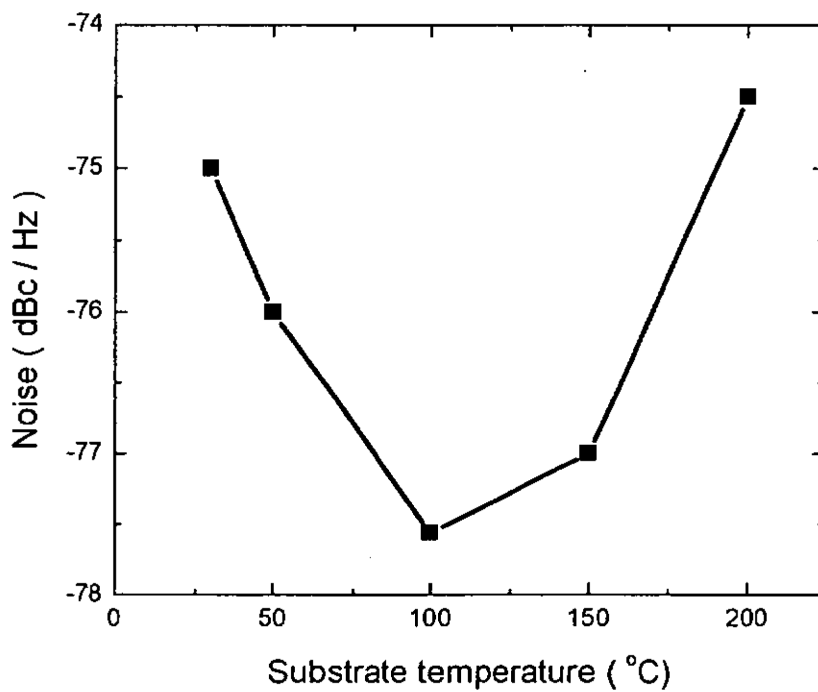

(b)

Fig. 3.34 The phase noise of SAW filters grown with different substrate temperatures (a) AlN SAW filters and (b) ZnO SAW filters

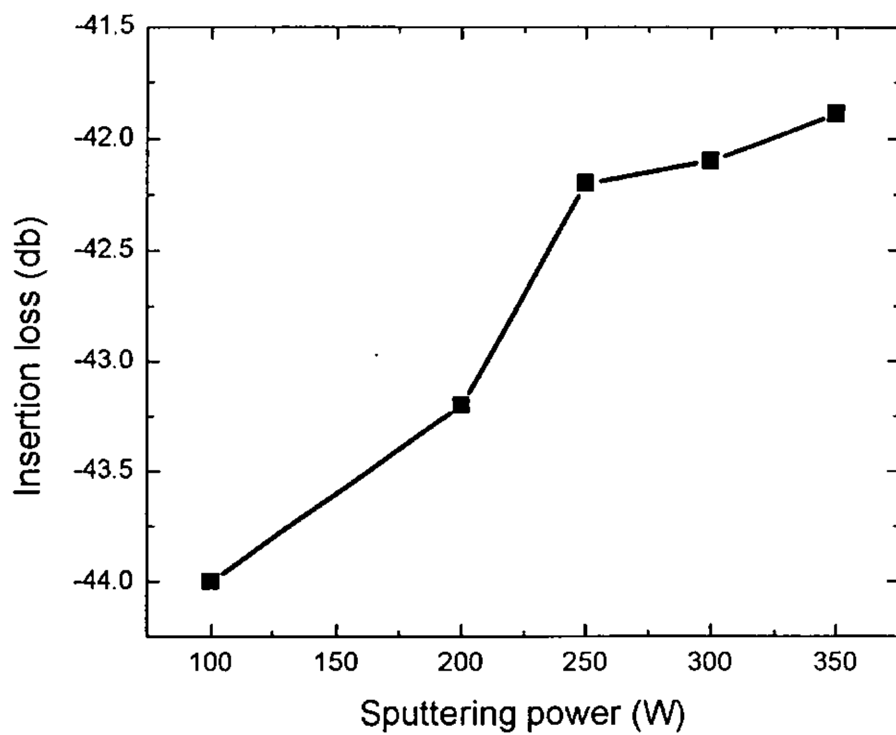

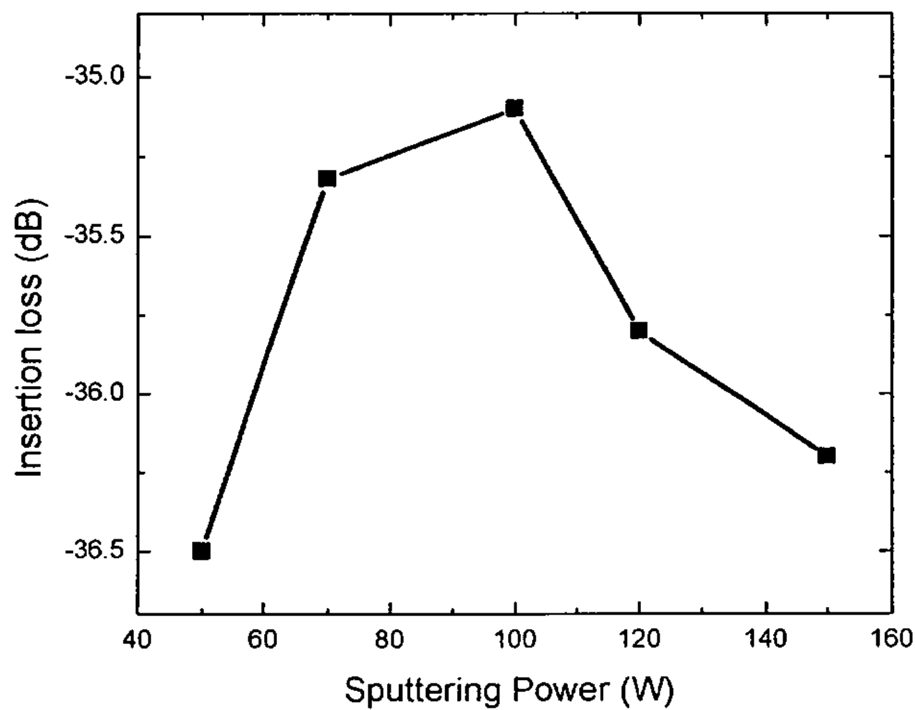

Fig. 3.35 The insertion loss of SAW filters grown with different sputtering powers (a) AlN SAW filters and (b) ZnO SAW filters

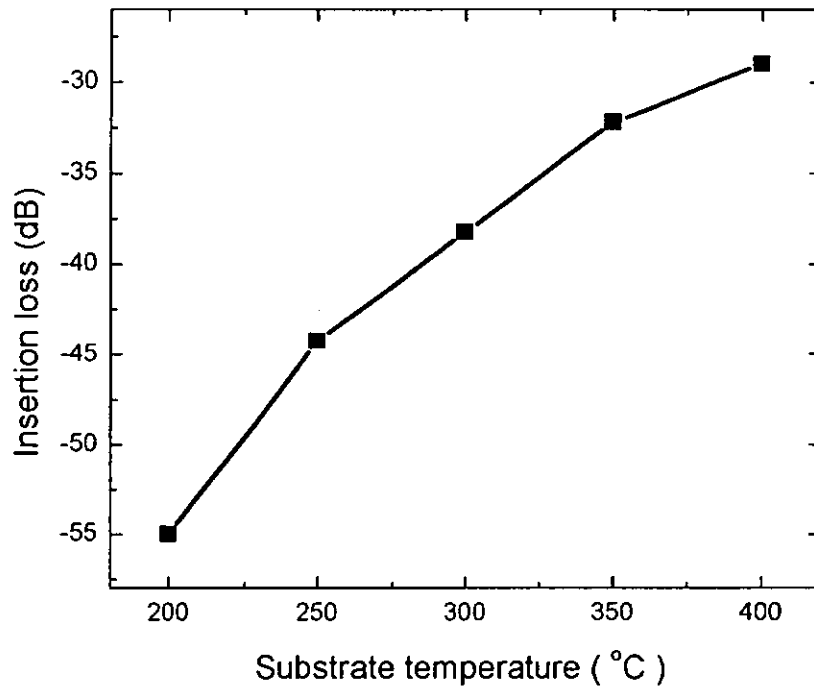

(a)

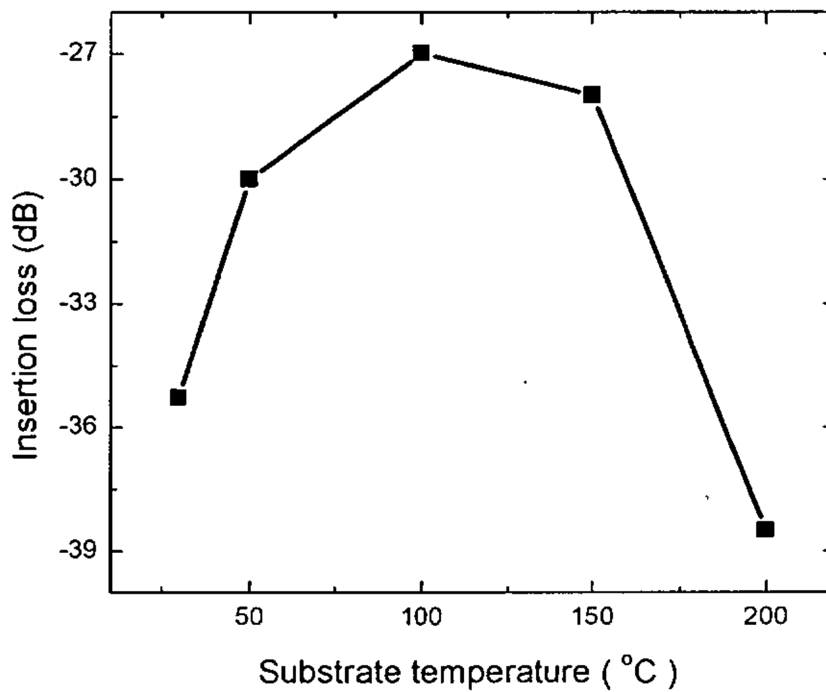

(b)

Fig. 3.36 The insertion loss of SAW filters grown with different substrate temperatures (a) AlN SAW filters and (b) ZnO SAW filters

3.2 Experimental results on AlN SAW filters grown by rf magnetron sputtering and MBE techniques

3.2.1 Characterization of AlN thin films deposition on sapphire grown by MBE technique

In Fig. 3.37, another set of XRD measurement results of the AlN thin film grown on sapphire by MBE system are presented. The temperature of the aluminum cell during the deposition by MBE system was varied under constant substrate temperature and growth chamber pressure. It is known that the temperature of aluminum cell in MBE system controls the aluminum flux is directly related to the composition of the AlN films and affects the texture of the material. The c-axis orientation (002) and the rocking curve of AlN thin film grown on (0001) sapphire are shown in the Figs. 3.38 and 3.39. The results indicate that the quality of the MBE-grown AlN thin film is superior to even the best samples, both AlN and ZnO thin films, grown by the rf sputtering technique.

The surface morphology of the AlN thin film grown by MBE technique is shown and its cross section is indicated in Fig. 3.40. The SEM pictures clearly show that the film has a very smooth surface.

The AFM was also used to measure the surface morphology of AlN thin films grown by MBE technique with different aluminum cell temperatures. The results are also

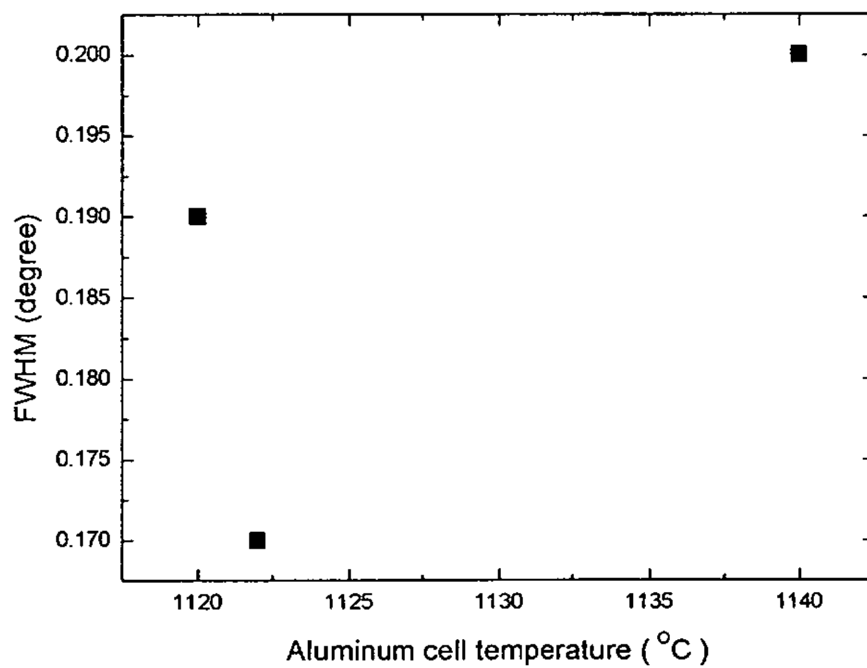

Fig. 3.37 Influence of different aluminum cell temperatures to the FWHM on the AlN thin films grown by MBE.

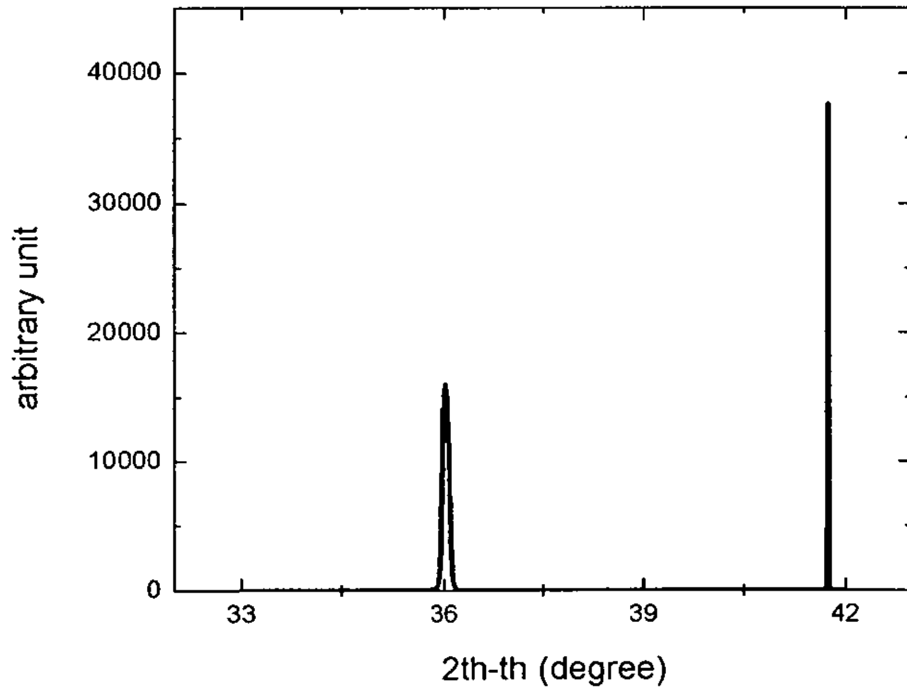

Fig. 3.38 The 2th-th scanning of XRD peak of AlN / sapphire grown by MBE at 1122°C

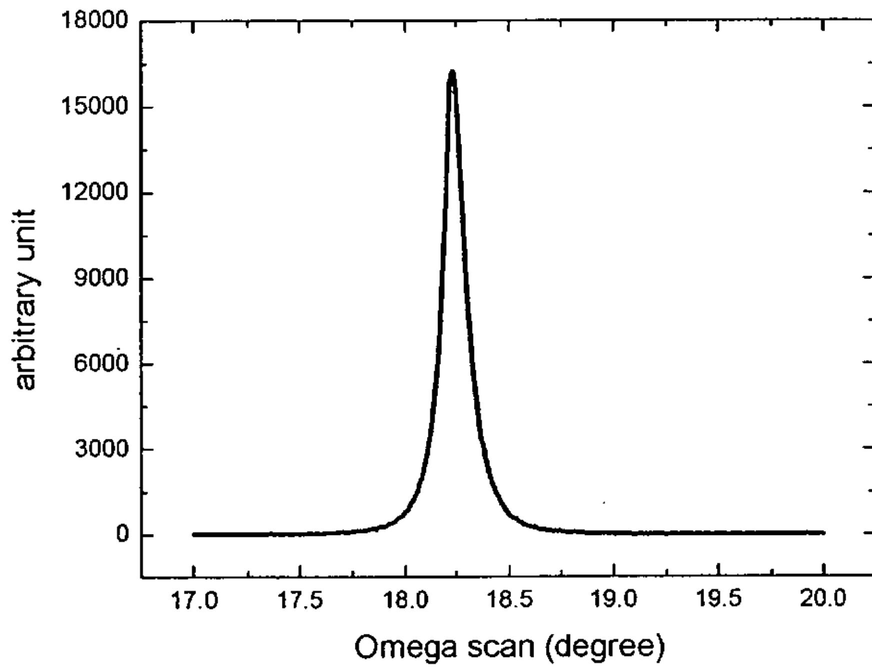

Fig. 3.39 The omega scanning of XRD peak of AlN / sapphire grown by MBE at 1122°C

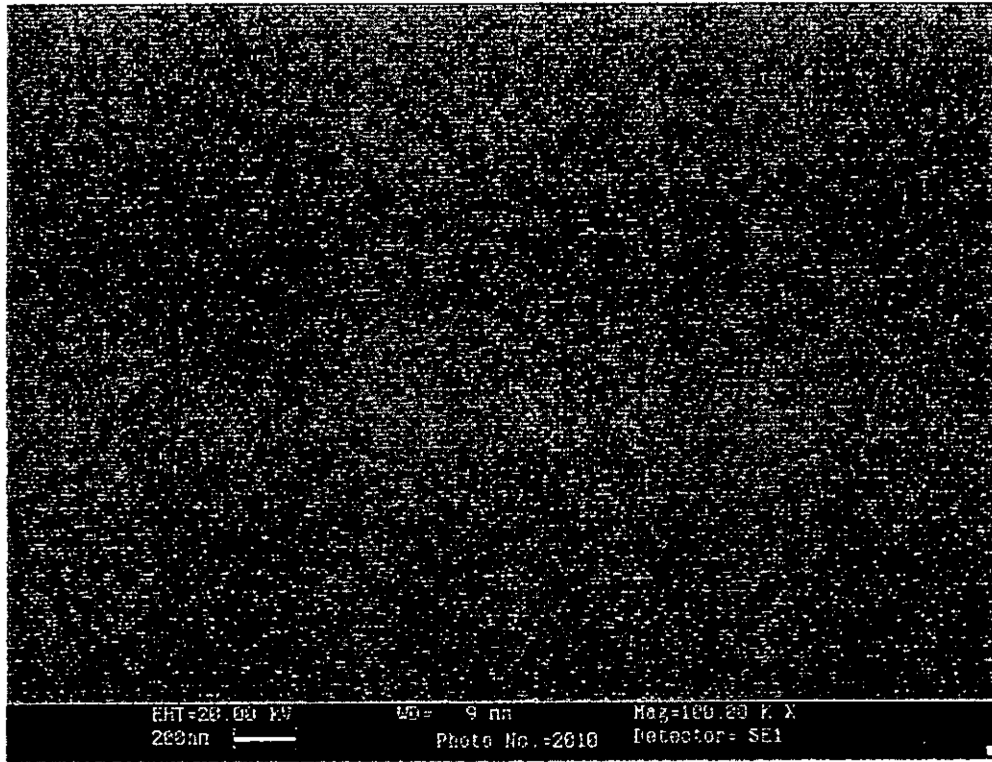

(a)

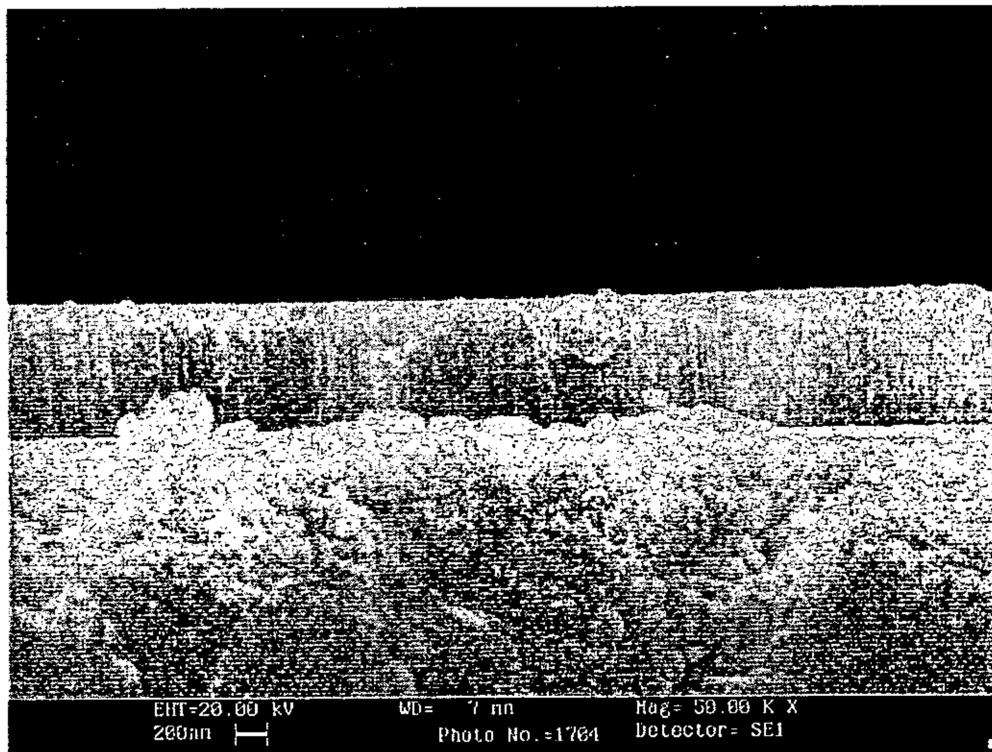

(b)

Fig 3.40 The SEM picture of AlN thin film grown by MBE
(a) surface morphology (b) cross-section

shown from Fig. 3.41 and Fig. 3.42. The lowest r.m.s. roughness of AlN thin film was 0.34 nm at the 1122 °C and it was found that the AlN thin film grown at the 1122 °C Al cell temperature is better than those grown at the other temperatures.

3.2.2 Characterization of AlN SAW filters grown by MBE technique

The measurement results of AlN SAW filters grown by MBE technique are presented in this section. The frequency response of the AlN SAW filters grown by MBE technique is shown in the Fig. 3.43. The maximum value of the phase velocity was achieved in a film grown with an Al cell temperature of 1122 °C as shown in Fig. 3.44. The average value of the phase velocity of the AlN SAW filters grown by MBE technique was about 5568ms^{-1} that the operation frequency was about 347MHz. In the K^2 measurement, the K^2 value was the maximum (0.9%) at 1122°C Al cell temperature showing in the Fig. 3.45. In the Fig. 3.46, the lowest noise level of the samples were grown at the 1122°C and that was -95dBc / Hz. Finally, the insertion loss of the sample grown at 1122°C was also the lowest (-19.5dB) showing in the Fig. 3.47. From the above results, it was shown that the optimal condition for growing AlN was in 1122°C Al cell temperature.

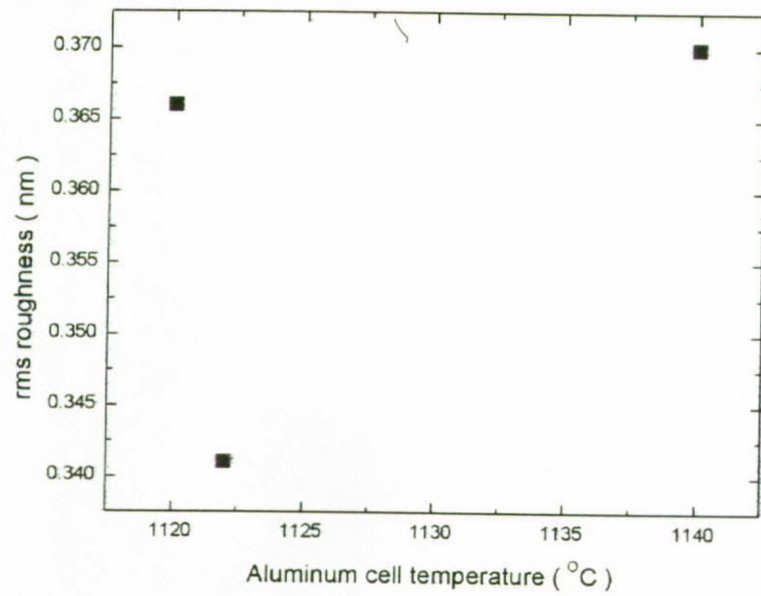

Fig. 3.41 The roughness of AlN thin films grown by MBE at various Al cell temperature

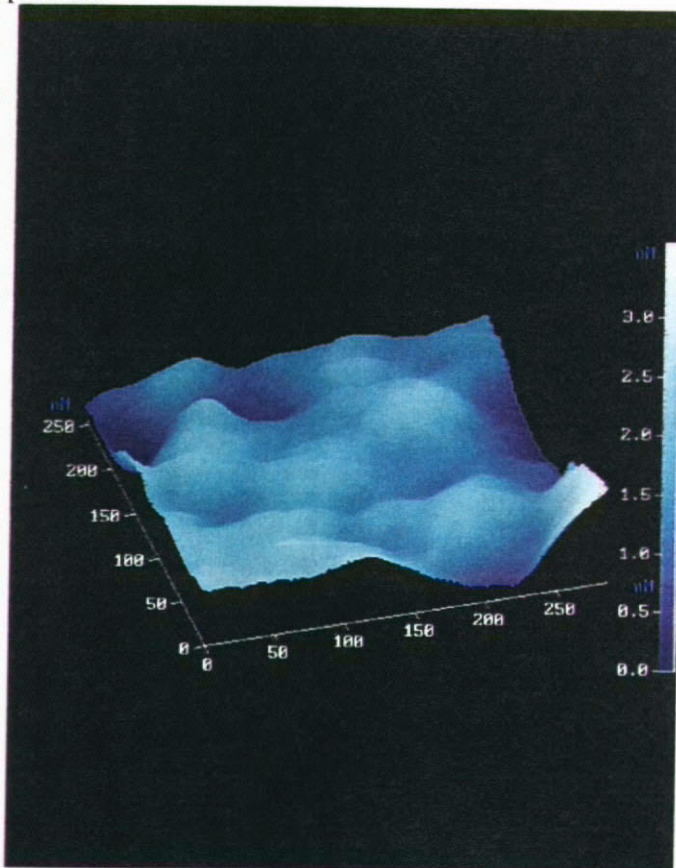

Fig. 3.42 The AFM picture of the surface morphology of AlN thin film grown by MBE at 1125°Ca

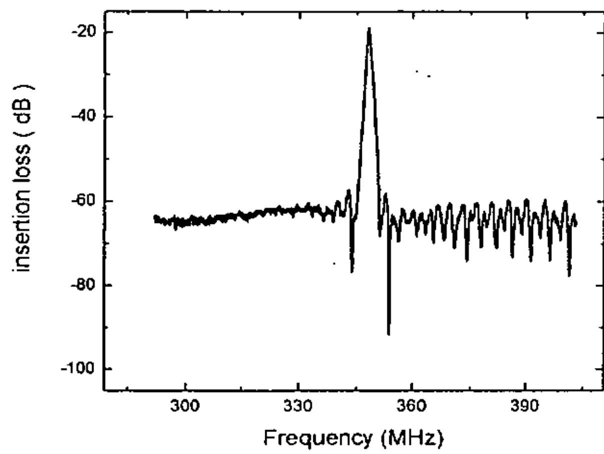

(a)

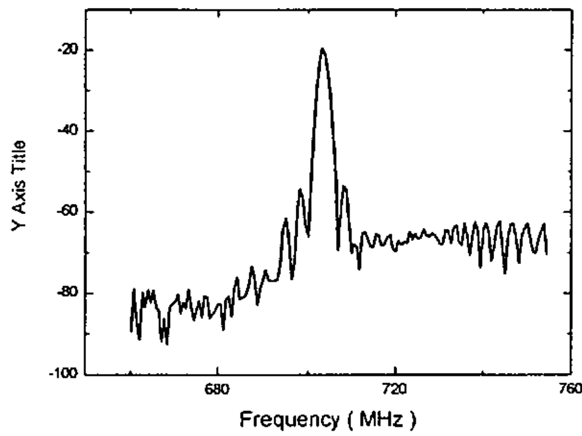

(b)

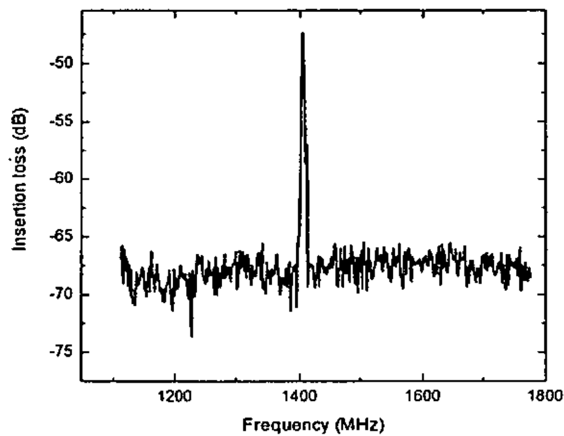

(c)

Fig. 3.43 The frequency response of AlN SAW filters grown by MBE fabricated with various electrode linewidths (a) 4 μm (b) 2μm (c) 1μm

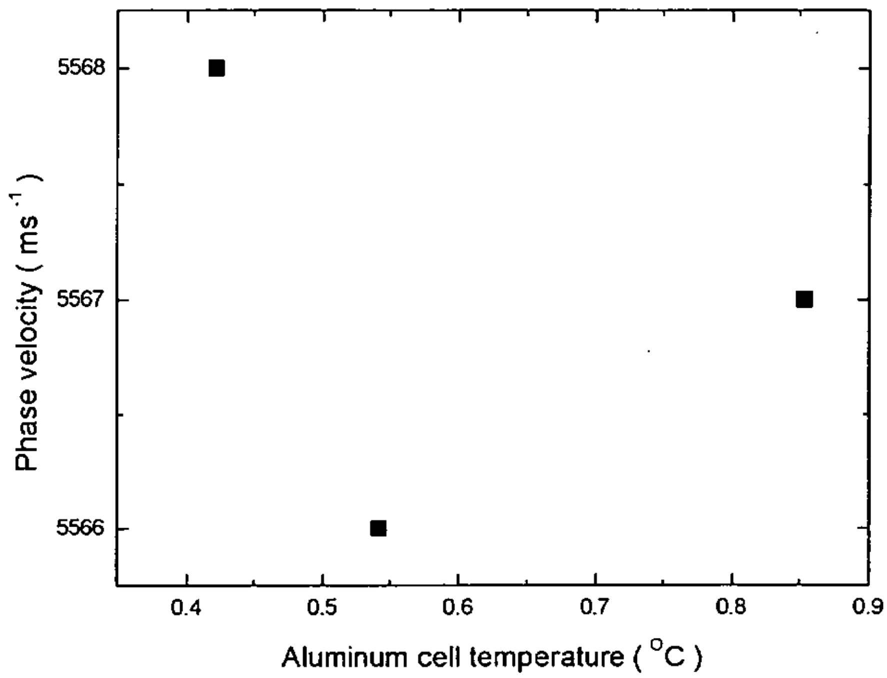

Fig. 3.44 The phase velocity of AlN SAW filters grown by MBE at various Al cell temperatures

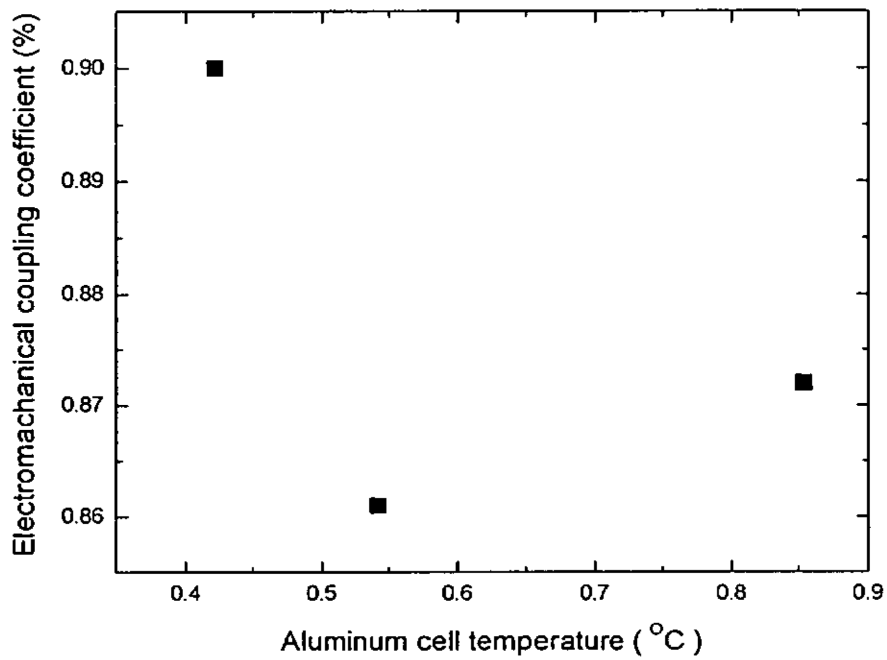

Fig. 3.45 The electromechanical coupling coefficient of AlN SAW filters grown by MBE at various Al cell temperatures

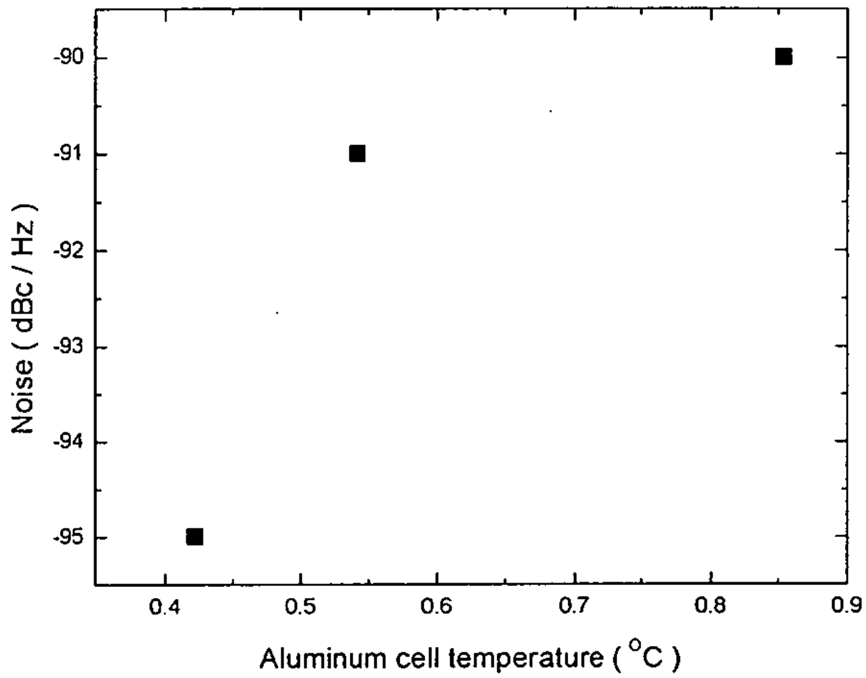

Fig. 3.46 The phase noise of AlN SAW filters grown by MBE at various Al cell temperatures

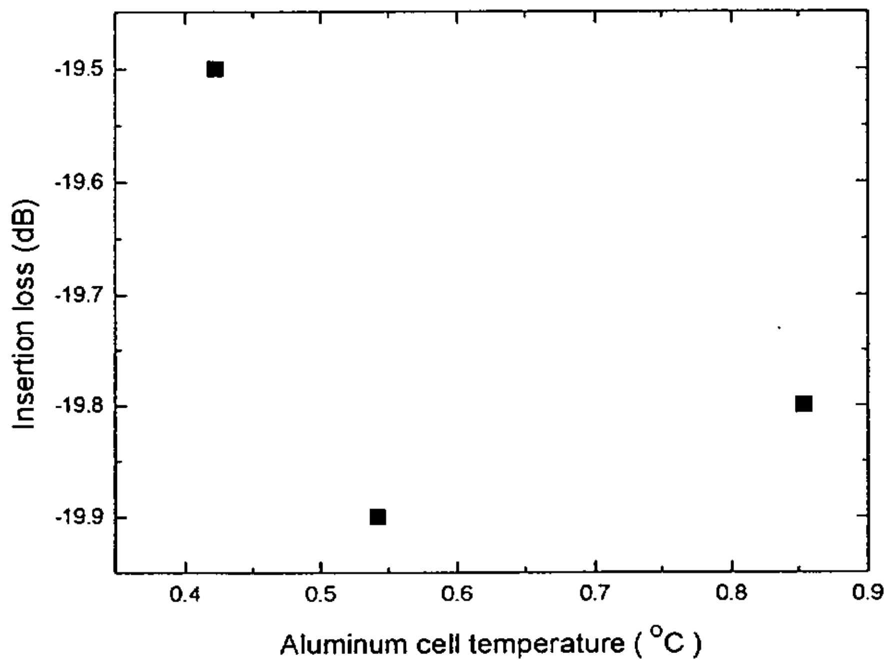

Fig 3.47 The insertion loss of AlN SAW filters grown by MBE at various Al cell temperatures

4. Discussion

4.1 Analysis of AlN and ZnO based SAW filters grown by rf magnetron sputtering technique

4.1.1 Effect of sputtering parameters on the quality of the AlN and ZnO thin films

The crystallinity and the surface morphology of the piezoelectric film were of primary concern for the fabrication of good quality SAW devices. We had systematically optimized the experimental conditions for the deposition of AlN and ZnO films. The sputtering parameter, such as power, gas ratio for plasma and temperature etc were varied systematically to obtain good quality thin films. All the films were grown with 1 μm thickness. In the following paragraphs the mechanisms of how each experimental parameter may affect the film quality will be discussed.

(a) Sputtering power

In our studies, as shown Figs. 3.1 and 3.7, it was observed that the sputtering power had strong influences on the film quality for both AlN and ZnO thin films. For AlN films, it was found that as the sputtering power increase, the intensity of the XRD signal increased, coupled with a monotonically decreasing FWHM of the main peak.

This shows that the crystalinity of the AlN films improved with increasing sputtering power. As for the growth of ZnO films, a minimum in the FWHM for the XRD signal was observed at a sputtering power of about 100 W. It was suggested by B. A. Movchan *et. al.* [99] that the kinetic energy supplied to the depositing atoms strongly affects the mechanism of the film growth since this provides the energy required for the atoms to embed themselves in the crystal structure and to diffuse in the horizontal direction. The experimental results obtained from the AlN film growth clearly demonstrate systematic improvements in the FWHM value of the XRD signal with the sputtering power. This was because the higher the sputtering power, the higher would be the kinetic energy of the sputtered AlN molecules, leading to improve crystallinity of the film. However, incident species with excessive kinetic energy may lead to the generation of crystalline defects. Thus, an optimal power exists for each material that depends on the physical properties such as the bond strength of the material. It is interesting to note that for ZnO film growth, when the sputtering power increased beyond 100W degradation in the FWHM value of the XRD signal was observed. Also, the film was found to exhibit cloudy color instead of usual clear color. This was most likely due to the degradation of the crystallinity of the film arising from the use of increased sputtering power. It was also observed that the growth rates of the films exhibit strong dependencies on the sputtering power.

To explain the experimental results, we noted that the deposition of the films was really a competition of two parallel processes – deposition and re-sputtering. In the

low energy range, the sputtered species would embed themselves and diffuse out horizontally once they reached the substrate leading to the deposition of the material. However, if the kinetic energy of the sputtered species exceeded a certain limit the momentum transferred from the sputtered species to the surface atoms might become so large that it might lead to the ejection of the atoms on the film surface. This is commonly known as the "re-sputtering" condition. This will generally lead to the reduction in the growth rate as observed in the AlN growth. It may also couple with the increased surface roughness in the film that was observed in the case of ZnO growth.

(b) Sputtering pressure

The effect of the sputtering pressure on both AlN and ZnO films is shown in the Figs. 3.2 and 3.8, and the optimal pressure for the growth of AlN and ZnO thin films were systematically determined. The FWHM of the XRD for the AlN thin films was decreased with increasing sputtering pressure and the FWHM of the XRD for the ZnO thin films minimized in 0.5 Pa. During the sputtering process, when the sputtering pressure increased, the number of sputtered molecules increased and enhanced the deposition rate initially. As the number of molecules continued to increase, the collisions among molecules also increased and the mean free path of molecules will be reduced. The average energy of the molecules would be decrease. Some of the molecules might be deflected by the collision and might never reach the target. Thus the deposition rate would be decrease with further increase in the

sputtering pressure.

(c) Substrate temperature

This parameter also strongly affected the surface roughness of the sputtered thin film. In Figs. 3.4 and 3.10., it showed that the substrate temperature enhanced the thin film quality and also the surface roughness by the gain in additional energy for the surface atoms to enable them to diffuse in the horizontal direction. There were some differences between AlN and ZnO. For AlN, the increase of substrate temperature until 400°C is needed to improve the film quality. For ZnO, it was believed that substrate temperature of 100°C was sufficient to result in improved crystallinity. At substrate temperature above 100°C, the deposition rate of ZnO films decreased due to re-evaporation of the material leading to the degradation of the film quality.

(d) Sputtering gas ratio

Ceramics targets were used for rf magnetron sputtering of the materials. During the sputtering processes, argon gas was used for the plasmas gas. The composition of sputtered molecules lost in balance and the stoichiometry of the thin film was changed as a result. The solution is to add some other gas in the plasma to improve the stoichiometry by recovering the balance in the plasma reaction and during the deposition on the substrate surface. This is demonstrated in the following experiment, in which nitrogen and oxygen gases were introduced in the plasma,

during the sputtering process of aluminum nitride and zinc oxide, respectively. The Figs. 3.3 and 3.9 show that the effect of introducing the compensation gas in the sputtering process. The quality of AlN and ZnO was improved after introducing the respective gases during the sputtering processes. The reduction in the FWHM of the XRD of the thin films was obtained as the partial pressure of the gas compensating gases increased as shown in Fig. 3.4. The excess compensating gas also affected the influence to the composition of the sputtered films. Therefore the experiment result was appeared with a minimum value in FWHM with a specific ratio of gas in the plasma. The optimial partial pressures for the compensating gases corresponded to the condition for minimum FWHM.

Figs. 3.13, 3.18 and 3.19 illustrated the experimental results of SEM and AFM of AlN and ZnO thin films under such optimal growth conditions. From the SEM picture of the cross-section and the surface morphology of AlN and ZnO films, c-axis columnar growth and large grain size were observed in both thin films.

In conclusion, we have determined the optimal conditions for the growth of AlN and ZnO thin film as shown in the following table.

Substrate temperature	100 °C
Ar/O_2 ratio	1
Sputtering pressure	1.0 Pa
RF Power	100 W
Base pressure	4×10^{-5} Pa
Target to substrate distance	5 cm

Table 4.1 Optimal sputtering conditions for ZnO

Substrate temperature	400 °C
Ar/N_2 ratio	1
Based pressure	4×10^{-5} Pa
RF Power	350 W
Target to substrate distance	5 cm
Sputtering pressure	1.0 Pa

Table 4.2 Optimal sputtering conditions for AlN

Pao Yue-kong Library
PolyU • Hong Kong

4.1.2 The relationship between substrate roughness, crystallinity and AlN and ZnO SAW filters performance

In this section, we focus on the effects of the sputtering power and the substrate temperature on device performance. These two parameters are much closely related to the material quality. For thin film devices, it is believed that the material quality is closely related to the device performance. For example, high defect density was shown to be the main cause for the increase in the noise level of device. Material defects also affected the optical properties such as the yellow emission in GaN-based LEDs. Different material qualities of AlN and ZnO based SAW filters were measured. The measurements included the frequency response, electromechanical coupling coefficient (K^2) and phase noise measurement. Frequency response measurement can exam three parameters: insertion loss, phase velocity (V_p) and K^2. The phase velocity can be calculated by the operation frequency of the SAW filter. The summary of the phase velocities for the sputtered AlN and ZnO SAW filters are shown in the Table 3.1. For the AlN / sapphire SAW filters, typical reported value of the phase velocity is around 5400 ms^{-1} to 5900 ms^{-1}. For ZnO / sapphire SAW filters, the phase velocity is about 3900 ms^{-1} to 4500 ms^{-1}. The acoustic velocities obtained from the AlN and ZnO SAW filters are similar to the values reported by others.

To determine how the material quality and the surface morphology of AlN and ZnO thin films affect the performance of the SAW filters, we first determined the factors affecting the phase velocity. In our experiments, the units of two sputtering

parameters – sputtering power and substrate temperature were Watt and Degree Celsius respectively, which were hard to compare and analyze. Since our samples were varied by one parameter each time, it is more convenience to unify them into FWHM of XRD of AlN and ZnO films. Fig. 4.1 is summarized for both AlN and ZnO SAW filters. The variation of the phase velocity due to the sputtering power was larger than that due to substrate temperature. From our experiment results that both sputtering power and substrate temperature affected the crystallinity of the thin films. It showed that there is a rapid decrease in the phase velocity with the material quality. The deviation of the phase velocity of the AlN SAW filters due to the variation of the material quality was about 130 ms^{-1} leading to the shift of the operation frequency of the AlN SAW filters shifting by 8.125 MHz. However, the deviation of the phase velocity and the operation frequency for the AlN SAW filters due to the variation of the substrate temperature was about 22 ms^{-1} and 1.375 MHz respectively. For the ZnO SAW filters, the deviation of phase velocity due to the variation of the material quality was about 168 ms^{-1} leading the operation frequency shifting about 10.5 MHz. And shifting of the phase velocity and the operation frequency due to the surface morphology was only about 27 ms^{-1} and 1.6875 MHz. It can be concluded that, at the optimal condition, the sputtering power is strongly affects the phase velocity more than the substrate temperature. The bigger the difference in the material quality, the larger the deviation in the phase velocity.

The electromechanical coupling coefficient of the AlN and ZnO SAW filter with different material quality and surface morphology was also examined. Fig. 4.2 was

a summary of the experimental results of K^2 of AlN and ZnO SAW filters. It is shown that the values of K^2 of both AlN and ZnO SAW filter were decreased while the values of the FWHM both AlN and ZnO SAW filter were increased. For AlN SAW filter, the deviation of K^2 caused by the sputtering power was about 6 times larger than that caused by substrate temperature. For ZnO SAW filter, the deviation of K^2 caused by sputtering power was about 3 times larger than that caused by the substrate temperature. It can be concluded that the sputtering power is the most important factor to the K^2 of both AlN and ZnO SAW filter. It is suggested that the sputtering power directly affected the piezoelectric constant of the thin film materials [62- 65].

Phase noise of the SAW filter is another indicator to examine the device performance. Just like the above experiment, the influence of sputtering power and substrate temperature to the phase noise were investigated. In the Fig. 4.3, the result of phase noise of the AlN and ZnO SAW filters caused by the sputtering power and substrate temperature were shown. The phase noise of AlN SAW filters due to the variation of the sputtering power and substrate temperature changed from -89 dBc / Hz to -70 dBc / Hz that the total change was about 19.6 dBc / Hz. This was much larger than the change in the phase noise due to the variation of the substrate temperature changing from –77 dBc / Hz to -73 dBc / Hz. The similar phenomenon was found on the ZnO SAW filters. The phase noise of ZnO SAW filters due to the variation of the sputtering power changed from -89 dBc / Hz to -72 dBc / Hz whereas the phase noise due to the variation of the sputtering power and

substrate temperature was changed from -77 dBc / Hz to -74 dBc / Hz. Both the phase noise of AlN and ZnO SAW filters were mostly affected by the material quality since the average changes due to the variation of the sputtering power was about 17 dBc / Hz but the average changes due to the variation of the substrate temperature was about 3 dBc / Hz. The phase noise of SAW filters can be correlated with the material quality. Some report derived that the source of the phase noise in SAW device came from the bulk material. T.E. Parker *et al.* [152] found that the phase noise was inversely proportional to the device size in quartz SAW oscillators and SAW filters. It is stated that the shorter the device, the higher the device noise. T. E. Parker *et al.*[152] suggested that the source of noises was came from the bulk effect, rather than surface effect.

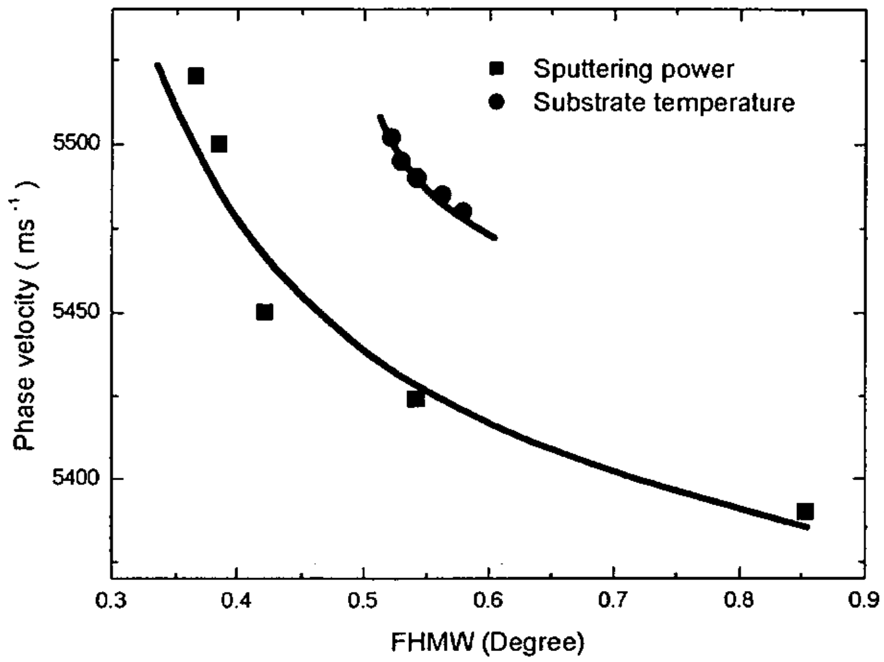

(a)

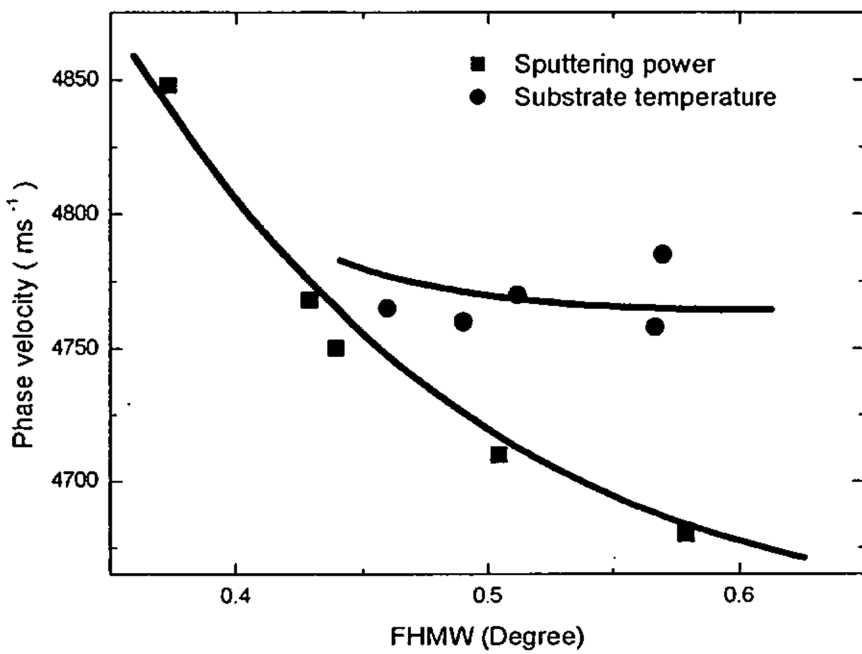

(b)

Fig. 4.1 The phase velocity of SAW filter grown at different conditions (a) AlN (b) ZnO

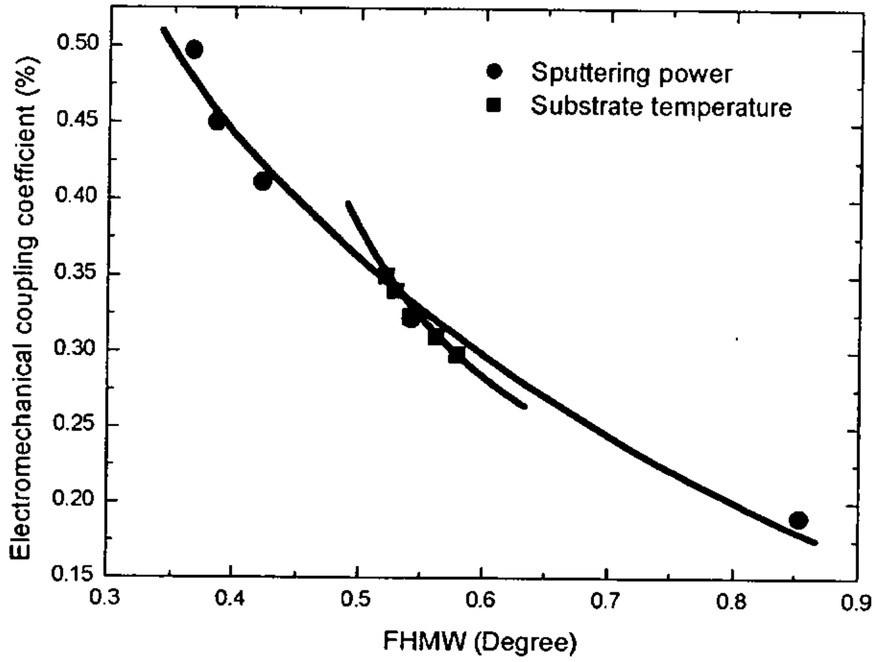

(a)

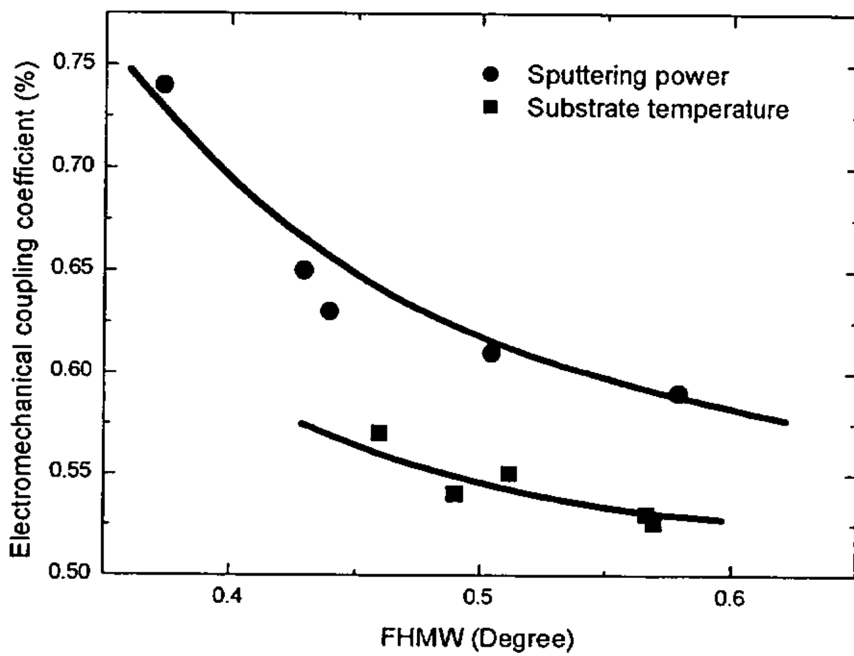

(b)

Fig. 4.2 The K^2 of SAW filter grown at different conditions
(a) AlN (b) ZnO

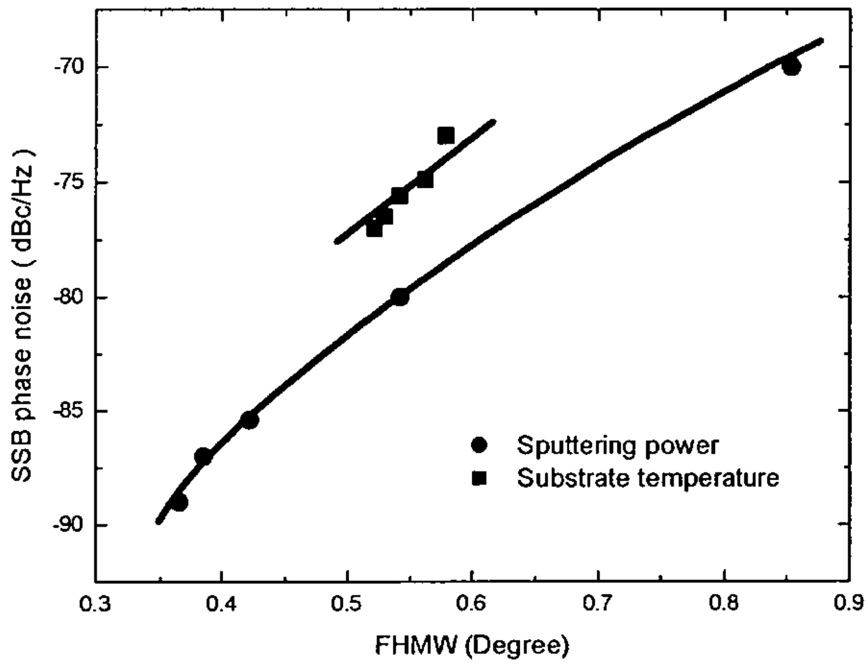

(a)

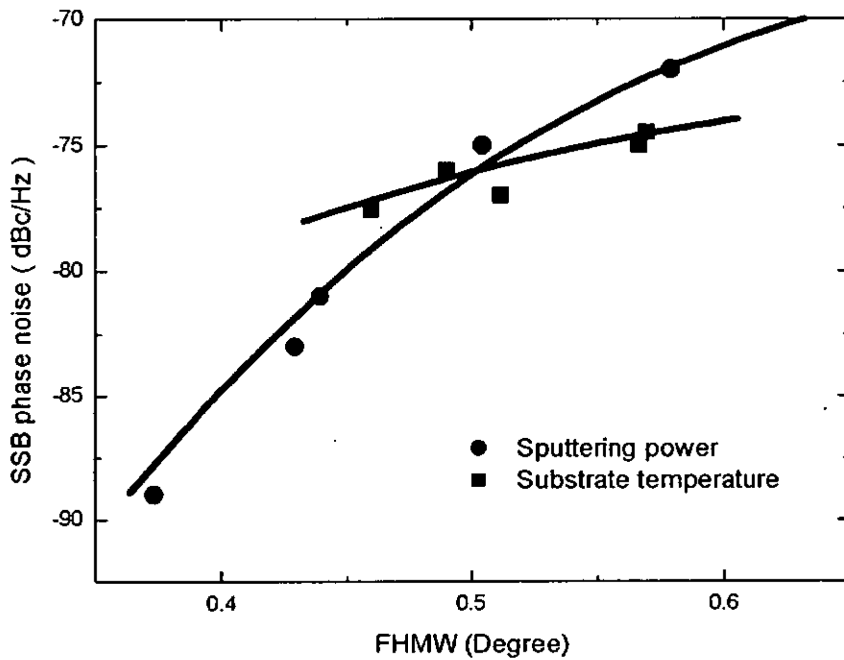

(b)

Fig. 4.3 The phase noise of SAW filter grown at different conditions (a) AlN (b) ZnO

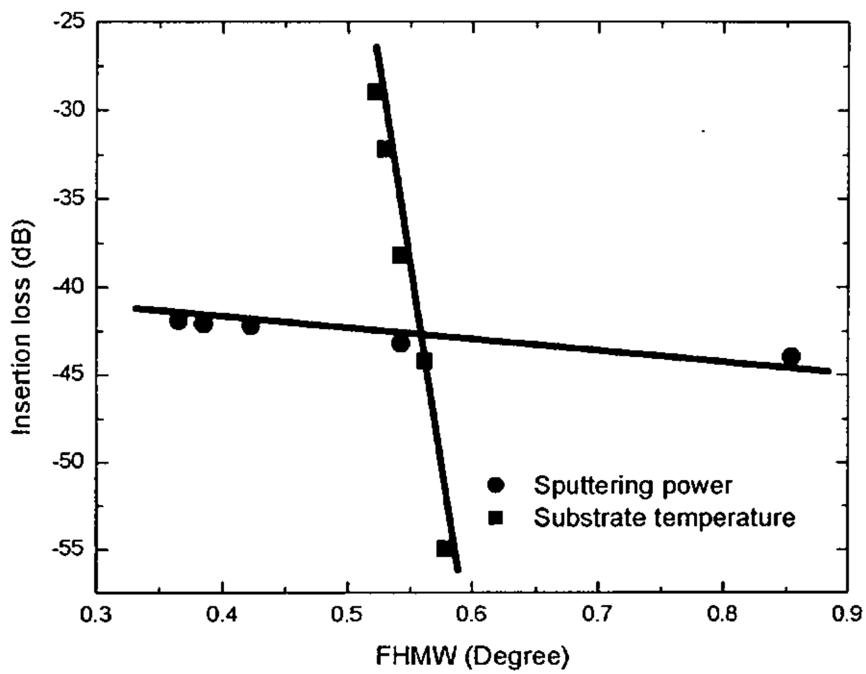

(a)

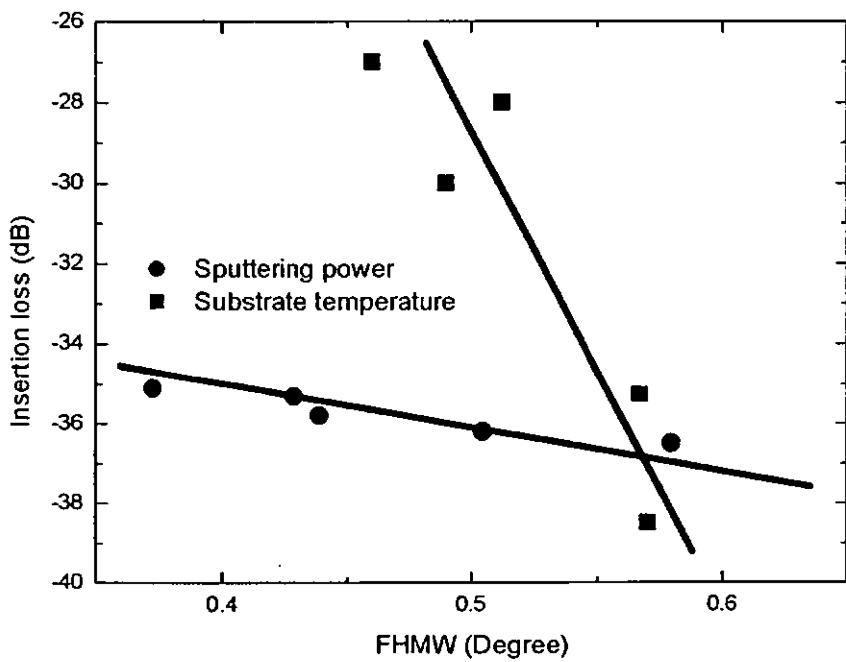

(b)

Fig. 4.4 The insertion loss of SAW filter grown at different conditions (a) AlN (b) ZnO

4.2 The relationship between AlN SAW filters grown by rf sputtering and MBE techniques

4.2.1 Comparison between the material quality of AlN thin films deposition by rf sputtering and MBE techniques

From the above experiments, the crystallinity and surface morphology are the essential parameter affecting the device performance. The following discussion is about the material quality with two different growth techniques. It is known that the overall material quality (crystallinity and surface morphology) deposited by sputtering is inferior to MBE or MOCVD grown materials. MBE technique utilizes evaporation deposition in a ultra high vacuum environment so that the high crystalline structure of thin film can be achieved. In this experiment, a MBE system was used to grow A lN thin film on s apphire and investigate the i nfluence of the further improvement of the cyrstallinity and surface morphology on the device performance..

The comparison of the material quality of AlN thin films grown by rf sputtering and MBE technique was made firstly. In the Fig. 3.13, the FWHM value of AlN thin film grown by MBE technique was about 0.1-0.15 degree. This value was much lower than that of AlN thin film deposition by r f sputtering technique. Also, the XRD intensity of the AlN thin film grown by MBE technique was one order higher than that of the AlN films grown by sputtering technique with the same thickness. It

is shown that the crystallinity of AlN thin film grown by MBE was better than that grown by rf sputtering technique.

The surface morphology of AlN thin films grown by two different methods was also measured. SEM picture of AlN thin film grown by MBE was very smooth and the grains cannot be found in the SEM picture; however, small AlN grains can be found in the SEM picture of AlN thin film grown by rf sputtering technique. The columnar growth of AlN thin film can be found in the cross section SEM picture, whereas, such column growth can not be found in the cross section SEM picture for the sample grown by MBE since the grains of AlN thin film grown by MBE technique was so small over the resolution of the SEM system. Moreover, the roughness of the AlN thin films grown by rf sputtering technique was about twice that was grown by MBE technique. From the above comparison, both material quality and the surface roughness of AlN thin films grown by MBE technique is better than even the best AlN film grown by rf sputtering technique.

4.2.2 Comparison between crystallinity and SAW filters performance grown by rf magnetron sputtering and MBE techniques

From the above analysis, the material quality of the AlN thin film grown by MBE technique was much better than that grown by rf sputtering technique. The discussion on the device performance of the AlN thin film grown by two different methods is the main focus of the section. In Fig. 4.9, the phase velocity of AlN SAW filter grown by MBE technique was measured and plotted against the FWHM of itself. The average value of phase velocity was about 5568ms^{-1} and it was slightly higher while comparing to that of AlN SAW filter grown by rf sputtering technique. From results reported by others, the phase velocity of AlN SAW filters grown by MOCVD technique can be as high as 5900ms^{-1}. That means, the phase velocity was shown to be material quality dependent. The K^2 of AlN SAW filter grown by MBE technique was also measured and plotted against the FWHM of the thin film showing in the Fig. 4.10. The value of K^2 of AlN SAW filter grown by MBE technique was nearly two times higher than that of AlN SAW filter grown by rf sputtering technique, even higher than that of ZnO SAW filter grown by rf sputtering technique. It is suggested that the high crystallinity of a piezoelectric thin film results with a high performance in piezoelectricity. The plot of the phase noise of AlN SAW filter grown by MBE technique against the FWHM of the AlN thin film is shown in the Fig. 4.11. The value was found to be lower about 5 dBc / Hz than that of AlN and ZnO SAW filter grown by rf sputtering technique. The insertion loss of

AlN SAW filter grown by MBE technique was plotted against the FWHM of the AlN thin film in the Fig. 4.12. The insertion loss of AlN SAW filter grown by MBE technique was the lowest in this experiment. This is a strong evidence showing that the further improvement of the quality of the thin film quality and the surface roughness will result with level up all the SAW device performance.

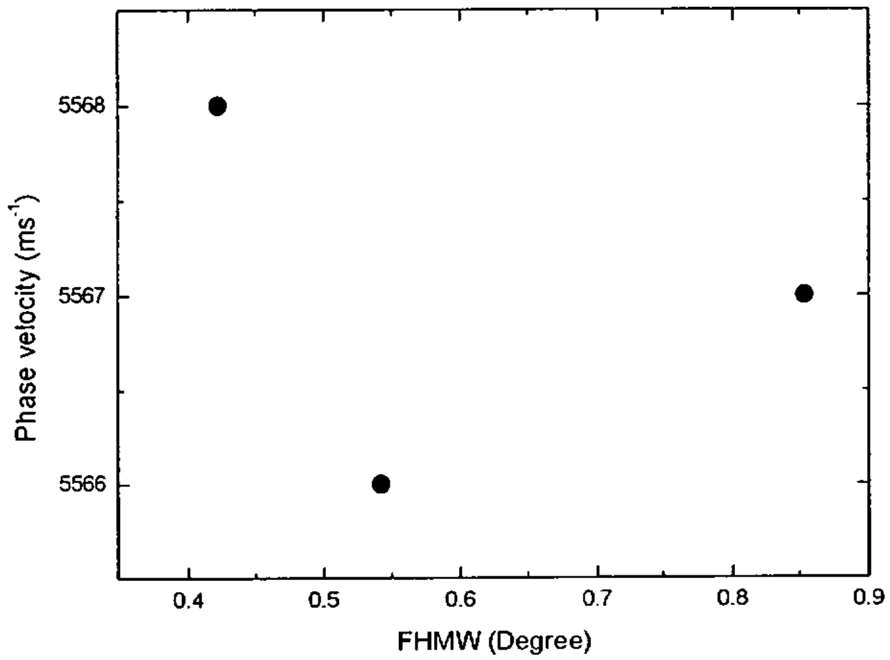

Fig. 4.5 The phase velocity of the AlN SAW filters grown by MBE with different qualities.

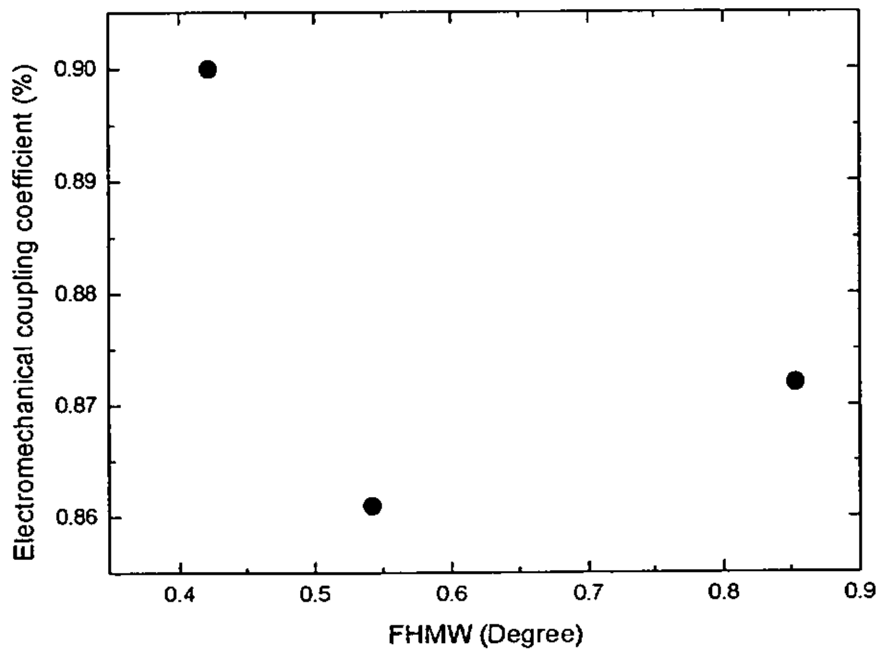

Fig. 4.6 The electromechanical coupling coefficient of the AlN SAW filters grown by MBE with different qualities.

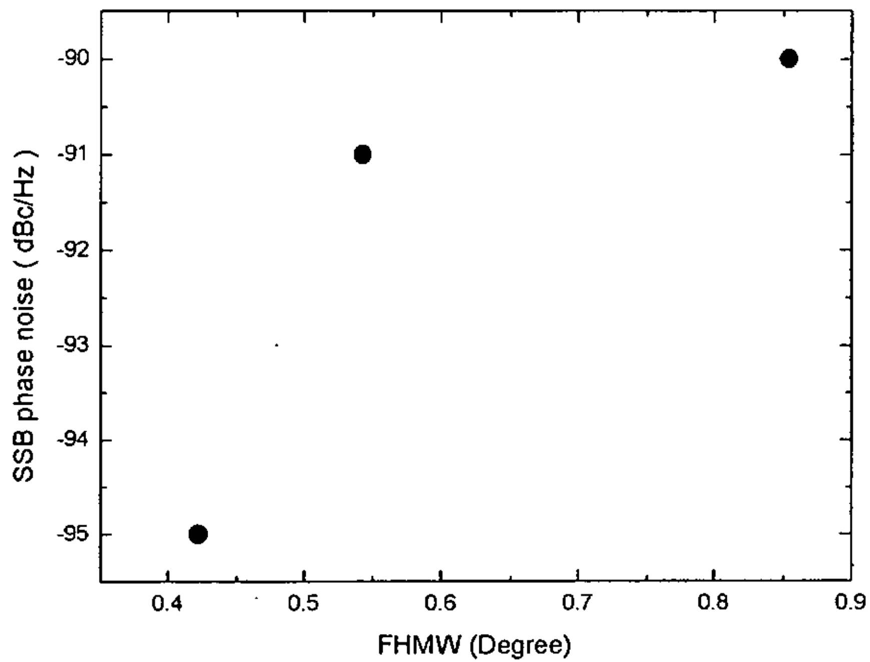

Fig. 4.7 The phase noise of the AlN SAW filters grown by MBE with different qualities.

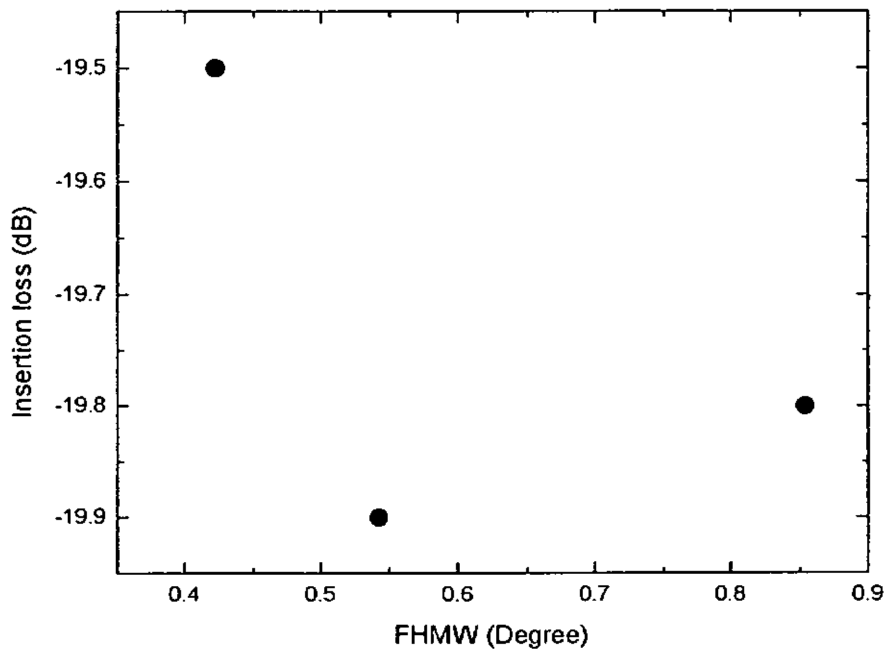

Fig. 4.8 The insertion loss of the AlN SAW filters grown by MBE with different qualities.

5. Conclusion

In this thesis explores the relationship of the influence of the thin film quality on the SAW filters performance. Any device performance can be directly related to the material quality. For this reason, material quality is still an attractive research topic in nowadays. This thesis is divided into two parts. The first part is used to investigate the thin film quality under different deposition parameters. Different deposition results in different thin film quality. The rf magnetron sputtering technique was used to investigate the thin film quality using different sputtering conditions. There were 4 parameters selected to investigate the influence on the AlN and ZnO thin film quality: sputtering power, the composition of gas mixture, substrate temperature and sputtering pressure. SEM, XRD and AFM were used to examine the thin film quality. Amongst those parameters, it was shown that the variation of the sputtering power and the substrate temperature bought about the most influence to the thin film quality and the surface roughness respectively. The optimal conditions for sputtering of AlN was under sputtering power 350W, substrate temperature 400^0C, 50% gas ratio of nitrogen to argon and substrate and the sputtering pressure was 0.5 Pa. For ZnO, the conditions were that the sputtering power 100 W, 1.5 Pa sputtering pressure, 100°C substrate temperature, 50% gas mixture for plasma.

In this thesis, AlN and ZnO thin film were selected for the substrate of the SAW filter according to their own advantages, therefore the influence of the quality of the

AlN and ZnO thin films on the performance of the SAW filter was found out. From the first part of this thesis, the conclusion was drawn that the crystallinity and surface roughness of the thin film were affected by the sputtering power and the substrate temperature. The samples with different crystallinity and roughness were fabricated into SAW filter to be characterized. Four parameters of the SAW filter were measured, and few points can be concluded from the experiment result. Firstly, the phase velocity, K^2 and phase noise of the SAW filter was corresponded with the material quality of thin film. The insertion loss of the SAW filter was linked with the surface roughness of the thin film only. All the measurement results were showed the same trend: the better the quality of the thin film, the better the performance of the device. To further prove this statement, some AlN thin film grown by MBE technique was employed and fabricated into devices. The results of the XRD, SEM and AFM revealed that the material quality of AlN thin film grown by MBE technique was higher than that grown by the rf magnetron sputtering, furthermore, the growing condition of AlN thin film by MBE technique was still not optimized. Amongst the samples, the filter performance of the AlN SAW filter grown by MBE technique was the best and this is a strong evidence proving that there is still room for the improvement of the material.

Reference

1. Lord Rayleigh, 'On waves propagating along the plate surface of an elastic solid", *Proc. London Math. Soc.*, **17**, 4-11, 1885
2. K. Sezawa, 'Dispersion of elastic wave propagated on the surface of stratified bodies and on curved surface', *Bull Earthquake. Res. Intro.*, Tokyo, **3**, 1-18, 27, 1927
3. R. M. White and F. W. Voltmer, "Direct piezoelectric coupling to surface acoustic wave", *Appl. Phys. Lett.*, **7**, 314-316, 1965
4. J. R. Klauder, A. C. Price, S. Darlington and W. J. Albersheim, " The Theory and design of chirp radars", *Bell Syst. Tech. J.*, **39**, 745-808, 1960
5. I. N. Court, "Microwave acoustic devices for pulse compression filters", *IEEE Trans*, **MTT-17**, 968-986, 1969
6. E. A. Ash, R. M. Del la Rue and R. F. Humphryer, "Microsound surface waveguides", *IEEE Trans.*, **MTT -17**, 882-892, 1969
7. E. A. Ash, "Surface wave grating reflectors and resonators', *IEEE Intl Microwave Symp.*, 385-386, 1970
8. J. D. Maines, E. G. S. Daige, A. F. Saunders and A. S. Young, " Simple technique for the accurate determination of delay-time variations in acoustic surface wave structures," *Electronics Lett.*, 5, 678-680, 1970
9. M. Luukkala and G. S. Kino, "Acoustic convolution and correlation and the associated nonlinearity parameters in lithium niobate." *Appl. Phys. Lett.*, 18, 393-394, 1971
10. E. A. Ash and E. G. S. Paige (eds), Rayleigh wave theory and application, Springer, 1985
11. A. J. Bahr (eds), "Special issue on 'microwave acoustics'", *IEEE Trans.*, **MTT-17**, 799-1046, 1969
12. T. M. Reeder (eds), "Special issue on "Special issue on 'microwave acoustic signal processing'", *IEEE Trans.*, **MTT-21**, 161-306, 1973
13. R. C. Williamson and T. W. Britol (eds), "Special issue on 'surface acoustic wave device applications'", *IEEE Trans.*, **SU-28**, 115-234, 1981

14. K. Shibayama and K. Yamanonchi (eds), *Proc. of Intl. Symp. on SAW device for mobile communication*, Sendai, 1992
15. C. K. Campbell, "Applications of surface acoustic and shallow bulk acoustic wave devices'", *Proc. IEEE*, **77**, 1453-1484, 1989
16. C. S. Hartmann, , P. V. Wright, R. J. Kansy and E. M. Garber, "An analysis of SAW interdigital transducers with internal reflections and the application to the design of single phase unidirectional transducer", *Proc. IEEE Ultrason. Symp.*, **19**, 40-45, 1982
17. M. Lewis, "Low loss SAW devices employing single stage fabrication", *Proc. IEEE Ultrason. Symp.*, 104-108, 1983
18. T. Kodama, H. Kawabata, Y. Yasyhara, and H. Sato, "Design of low-loss SAW filters employing distributed acoustic reflection transducers", *Proc. IEEE Ultrason. Symp.*, 59-64, 1986
19. R. H. Tancell, M. B. Schulz, H. H. Barret, L. Daries and M. G Holland, "Dispersive delay lines using ultrasonic surface waves", *Proc. IEEE*, **57**, 1211-1213, 1969
20. R. H. Tancell and M. G Holland, "Acoustic surface wave filters", *Proc. IEEE*, **59**, 393-409, 1971
21. G A. Coquin, and H. F. Tiersten, "Analysis of the excitation and detection of piezoelectric surface waves in quartz by means of surface electrodes", *J. Acoustic Soc. Am.*, **41**, 912-939, 1967
22. S. G Jashi and R. M. White, "Excitation and detection of surface elastic waves in piezoelectric crystals", *J. Acoustic Soc. Am.*, **46**, 17-27, 1969
23. H. Skeie, "Electrical and mechanical loading of a piezoelectric surface supporting surface waves", *J. Acoustic Soc. Am.*, **48**, 1098-1109, 1970
24. W. R. Smith, H. M. Gerard, J. H. Collins, T. M. Reeder and H. J. Shaw, "Design of surface wave delay lines with interdigital transducers", *IEEE Trans.*, **MTT-17**, 856-864, 1969
25. C. S. Hartmann, D. T. Bell and R. C. Rosenfeld, "Impulse model design of acoustic surface wave filters", *IEEE Trans.*, **MTT-21**, 162-175, 1973

26. M. J. Hoskins, H morkoc and B. J. Hunsinger, "Charge transport by surface acoustic waves in GaAs," *Appl. Phys. Lett.*, **41**, 4, 1982
27. M. F. Lewis, "Surface skimming bulk waves", *Proc. IEEE Ultrason. Symp.*, 744-752, 1977
28. T. I. Browing, D. J. Gunton, M. F. Lewis and C. O. Newton, "Bandpass filters employing surface skimming bulk waves", *Proc. IEEE Ultrason. Symp.* , 753-756, 1977
29. B. Auld, J. Gagnepain and M. Tan, "Horizontal shear surface waves on corrugated surfaces", *Electronics Lett.*, **12**, 650-652, 1976
30. A. Renard, J. Henaff and B. A. Auld, "SH surface wave propaagatin on corrugated surfaces of rotated y-cut quartz and berlinite crystals", *Proc. IEEE Ultrason. Symp.*, 996-1001, 1977
31. A. Ballato and T. J. Lukaszek, "Shallow bulk acoustic wave progress and prospects", *IEEE Trans. Microwave Theory & Tech.*, **MTT-27**,1004-1012, 1979
32. K. H. Yen, K. F. Lau and R. G. Kagiwada, "Shallow bulk acoustic wave filters", *Proc. IEEE Ultrason. Symp.*, 680-683, 1978
33. E. G. S. Paige and P. Whittle, " Coupling of surface skimming bulk waves with a multistrip coupler", *Proc. IEEE Ultrason. Symp*, 802-805, 1979
34. W. Tanski, J. Avecedo and T. A. Moore , "A bulk mode suppression technique for surface wave devices", *Proc. IEEE Ultrason. Symp.*, 543-545, 1973
35. K. V. Rousseau, K. H. Yen, K. F. Lau and A. M. Kong, "High Q, single mode S-band SBAW oscillators", *Proc. IEEE Ultrason. Symp.*, **1**, 279-183, 1982
36. D. F. Thompson and B. A. Auld., "Surface transverse wave propagation under metal strip gratings", *Proc. 1986 IEEE Ultrasoinic Symp.*, **1**, 261-266, 1986
37. T. L. Bagwell and R. C. Bray, "Novel surface transverse wave resonators with low loss and high Q", *Proc. IEEE Ultrason. Symp.*, **1**, 319-324, 1987
38. Y. Suzuki, H. Shimuzu, M. Takeuchi, K. Nakamura and A. Yamada, "Some studies on SAW resonators and multipole–mode filters", *Proc. IEEE Ultrason. Symp*, 297-302, 1976
39. E. Akcakaya, "A New analysis of single phase unidirectional transducer",

IEEE Trans. Ultrason. Ferr. Freq. Contr., **34**, 45-32, 1987

40. P. V. Wright, "A new generalized modeling of SAW transducers and gratings", *43rd Annual Symp. on Freq. Control*, 596-605, 1989
41. C. S. Lam, D.P. chen, B. Potter, V. Narayanan and A. Vishwanathan, "A review of the applications of SAW filters in wireless communication:, *Intl Workshop on Ultrasonic Applications*, Nanjing China, 1996
42. J. G. Gualtieri, J. A. Kisinski and A. Ballato, "Piezoelectric materials for SAW application", *IEEE Trans. Ultrason. Ferr. Freq. contr.*, **41**,53-59, 1994
43. T. Shibata, Y. Hori; K. Asai, Y. Nakamura, M. Tanaka, K. Kaigawa, J. Shibata, H. Sakai, "2.4 GHz SAW filters using AlN deposited on off-angle R-plane sapphire substrates by MOCVD", *Proc. IEEE Ultrason. Symp.*, **1**, 287-292, 2002
44. C. Caliendo,G. Saggio, P. Verard and E. Verona," Piezoelectric AlN film for SAW devices applications", *Proc. IEEE Ultrason. Symp.*, **1**,249-252, 1993
45. H. Okano, N. Tanaka and Y. Takahashi, "Preparation of aluminum nitride thin films by reactive sputtering and their applications to Ghz band surface acoustic wave devices ", *Appl. Phys. Lett.*, **64**, 166-168, 1994
46. X. Quyang, Q. Xixin and W. X. Zhang, "The surface acoustic wave velocities and electromechanical coupling coefficients of AlN thin films", *IEEE Proc.*, **1** ,133-135, 1988
47. N. Nakamura and T. Hanaoaka, "Propagation Characteristics of Surface Acoustic Waves in ZnO/$LiNbO_3$ Structures", *Jpn. J. Appl. Phys.*, **321**, 2333-2336, 1993
48. F. S. Hickernell and E. L. Alder, "The experimental and theoretical characterization of SAW modes on ST-X quartz with a zinc oxide thin film layer", *IEEE Intl. Freq. contr. Symp.*, 2333-2336, 1997
49. N. W. Emanetogh, C. Gorla Yliu, S. Liang and Y. Lui, "Epitaxial growth and characterization of high quality ZnO films for surface acoustic wave applications", *Proc. IEEE Ultrason. Symp.*, **1**, 191, 1997

50. I. Yasuhiro, N. Takashi and M. Kenji, "The effects of deposition conditions on the structural properties of ZnO sputtered films on sapphire substrates", *Appl. Surf. Sci.*, **169**, 512-516, 2001
51. H. Hmano, M, Kito, K. Miramatsu and L. Akasaki, "P-Type Conduction in Mg-Doped GaN Treated with Low-Energy Electron Beam Irradiation", *Jpn J. Appl. Phys.*, **28**, L 2112, 1989
52. K. Hirato, H. Fujioka, S. Ito, J. Ohta and M. Oshima," Characteristics of AlN buffer layers for GaAs epitaxial growths on MnZn ferrite substrates", *Thin Solid Films*, **435**, 1, 131-134, 2003
53. S. Strite, M. E. Lin and H. Morkoç, "Progress and prospects for GaN and the III–V nitride semiconductors", *Thin Solid Films,* **231**, 1, 197-210, 1993
54. Wright, A.F., "Elastic properties of zinc-blende and wurtzite AlN, GaN, and InN", *J. Appl. Phys.*, **82**, 6 , 2833-2839, 1997
55. Suzuki, M., Uenoyama T., "Strain effect on electronic and optical properties of GaN/AlGaN quantum-well lasers.", *J. Appl. Phys.,* **80**, 12, 6868-6874, 1996
56. MacMillan, M.F, Devaty, R.P. Choyke, W.J.," Infrared reflectance of thin aluminum nitride films on various substrates", *Appl. Phys. Lett.* **62**, 7, 750-752, 1993
57. K. Tsubouchi, T. Tomioka,T. Sato, C. Endo, N. Mikoshiba, "An asynchronous spread spectrum wireless-modem using a SAW convolver", *Proc. IEEE Ultrason. Symp.*, **1**, 213 -218, 1988
58. V. W. L. Chin, T. L. Tansley, T. Osotchan, "Electron mobilities in gallium, indium, and aluminum nitrides", *J. Appl. Phys.* **75**, 11, 7365-7372, 1994
59. T. Shiosuki, S. Ohnichi, Y. Murakami amd A. Kawabata, *J. Crystal Growth*, **45**, 346, 1978
60. I. Akasaki, M. Hashimoto,"Infrared lattice vibration of vapour-grown AlN. *Solid State Commun.*, **5, 11**, 851-853, 1967
61. G. Carlotti and G. Socino, "Acoustic investigation of the elastic properties of ZnO films", *Appl. phys Lett.*, **51**, 1889, 1987
62. O. Yoshiyuki, T. Haga and Y. ABE, "Crystallographic feature of ZnO single crystals", *Jpn. J. Appl. Phys.,* **36**, L1040-1042, 1997

63. Y. J. Yong and J. Y. lee., "Characteristics of hydrogenated aluminum nitride films prepared by radio frequency reactive sputtering andtheir application to surface acoustic wave devices", *J. Vac. Sci. Technol.*, **A15**, 390-393, 1997

64. A. J. Shuskus, T. M. Reeder and E. L. Paradis, "RF sputtered aluminum nitride films on sapphire", *Appl. Phys. Lett.*, **24**, 155-156, 1974

65. D. G. Ebling, M. Rattunde, L. Steinke, K. W. Benz and A. Winnacker, "MBE of AlN on SiC and influence of structural substrate defects on epitaxial growth", *J Cryst. Growth,* 201-202, 411-414, 1999

66. A. Ohtomo, M. Kawasaki, Y. Sakurai, Y. Yoshida, H. Koinuma, P. Yu, Z. K. Tang, G. K. L. Wong and Y. Segawa Y. F. Chen, P. M. Bagnall, Ziquany Zhu, T. Sekiushi and K. T. Punk., "Room temperature ultraviolet laser emission from ZnO nanocrystal thin films grown by laser MBE", *Matl. Sci. Eng. B,* **54**, 1-2, 24-28 ,1998

67. Y. J. Kim and K.W. Kim, " Characteristics of Epitaxial ZnO Films on Sapphire Substrates Deposited using RF-Magnetron Sputtering", *Jpn. J. Appl. Phys.*, **36**, 2277, 1997

68. A. J. Bahr, R. E. Lee and A. F. Podell," The grating array: A new acoustic surface wave transducer", *Proc. IEEE Ultrason. Symp.*, 194, 1972

69. N. W. Emanietoglu, S. Liang, C. Gorla and Y. Lu, "Epitaxial growth and characterization of high quality ZnO films for surface acoustic wave applications ", *Proc. IEEE Ultrason. Symp.*, 195, 1997

70. K. Kornitzer, K. Thonke, r. Sauer. E. bling, L. Steinke and K. W. beaz, "AlN on sapphire and on SiC: CL and Raman study", *J. Crystal. Growth*, **201**, 441-443, 1999

71. A. Clos, H. Angerer, R. Handschuh, O. Ambacher, M. statmann, *MRS Intl. J. Nitride Semicond. Res.*, B, 43, 1997

72. K. Dovidenko, S. Okyabrsky and J. Norayan, "Aluminum nitride films on different orientations of sapphire and silicon" , *J. Appl. Phys. Lett.*, **79**, 5, 2439, 1996

73. J. E. Northrup and R. Di. Felice, " Atomic structure and stability of AlN (0001) amd (000$\underline{1}$) surfaces", *physical preview B*, **55, 20**, 13878-13883, 1997

74. A. Saxler, P. Kung, C. J. Sun, Z. Bigan and M. Rozeghi, " High quality aluminum nitride epitaxial layers grown on sapphire substrates", *Appl phys Lett.*, **64**, 339, 1993

75. K. B. Sundaram and A. Khan, "Characterization and optimization of zinc oxide films by r.f. magnetron sputtering", *Thin Solid Films*, **295**, 87-91, 1997

76. H. Nakahata, A. Hachigo, S. Hikata and N. Fujimori, " High frequency surface acoustic wave filter using ZnO/diamond/di structure", *Proc. IEEE Ultrason. Symp.*, 377, 1992

77. Irina Diclenko, F. S. Hickernell and F. Naumenko, "The experimental and theoretical characterization of the SAW propagation properties for zinc oxide films on silicon carbide", *IEEE Trans. Ultrason. Ferr. Freq. Contr.*, **47**, 179, 2000

78. S. Minagausa, T. okamoto, T. NIitsuman, S. Mitsutsuka, K. Tsubouchi and N. Mikashiba, "Sezawa wave correlator using monolithic $ZnO/SiO_2/Si$ structure", *Proc. IEEE Ultrason. Symp.*, 298-302, 1984

79. T. Mitsuya, O. Yamazaki and K. Wasa, "An electrostatic voltage sensor using surface acoustic waves", *Proc. IEEE Ultrason. Symp.*, 74-77, 1981

80. C. H. Kao, S. J. Chang, Y. K. Su, C. K. Wong, L. W. Wa, J. K. Sheu, T. C. Wen, W. C. Lai, J. M. Tsai and C.C. Lin, "Nitride-based blue LEDs with GaN/SiN double buffer layers", *Solid-State Electronic*, **47**, 2019-2022, 2003

81. Y. C. Lin, S. J. Chang, Y. K. Su, C. S. Chang, S. C. Shei, J. C. Ke, H. M. Lo, S.C. Chen and C. W. Kao, "High power nitride based light emitting diodes with Ni/ITO p-type contacts", *Solid State Electronics*, **47**, 1565-1568, 2003

82. G. Y. Zhang, Z. J. Yang, Y. Z. Tong, Z. X. Qin and X. D. Hin *et al*, "InGaN/GaN MQW high brightness LED grown by MOCVD", *Optical Mater.*, **23**, 183-186, 2003

83. R. W. Martin, H. S. Kim, Y. Cho, P. R. Edwards and I. M. Watson *et al*, "InGaN/GaN MQW high brightness LED grown by MOCVD", *Mater. Sci. Engineering B.*, **93**, 98-101, 2002

84. H. P. Zhang, F. Ren, T. J. Anderson, C. R. Abernathy, S. R. Singh, P. H. Holloway and S. Peaton *et al*, "High-Power GaN Electronic Devices", *Critical Rev. in Solid State and Mater. Sci.*, **27**, 1-71, 2002

85. H. Shen, J. Pamulapati, M. Taysing, M. C. Wood, R. T. Lareau, M. H. Ervin, J. D. Mackenzie, C. R. Abernathy, S. J. Pearton, F. Ren and J. M. Zavada, "1.55 μ m Er-doped GaN LED", *Solid-State Electronics*, **43**, 7, 1231-1234, 1999

86. H. Morko, A. D. Carlo and R. Cingolari, "GaN-based modulation doped FETs and UV detectors", *Solid State Electronics*, **46**, 157-202, 2002

87. P. Javorka, A. Alam, M. Marso, M. Wolter, J. Kuzmik, A. Fox, M. Heuken and P. Kordoš ,"Material and device issues of AlGaN/GaN HEMTs on silicon substrates", *Microelectronics Journal*, **34**, 5-8, 435-437, 2003

88. J. W. Johnson, A. G. Baca, R. D. Briggs, R. J. Shul, J. R. Wendt, C. Monier, F. Ren, S. J. Pearton, A. M. Dabiran, A. M. Wochack *et al.*, "Effect of gate length on DC performance of AlGaN/GaN HEMTs grown by MBE", *Solid-State Electronics*, **45**, 12, 979-1985, 2001

89. I. Ferguson, C. A. Tran, R. F. Karlicek Jr., Z. C. Feng, R. Stall, S. Liang, Y. Lu and C. Joseph, "GaN and AlGaN metal–semiconductor–metal photodetectors", *Mater. Sci. Engineer. B*, **50**, 1-3, 311-314, 1997

90. Yan-Ru Lin and Shinn-Tyan Wu, "Buffer-facilitated epitaxial growth of AlN on Al_2O_3(0 0 0 1) at room temperature", *Surface Science*, **516**, 3, L535-L539 , 2002

91. Y. Huttel, H. Gomez, A. Cebollada, G. Armelles and M. I. Alonso, "Epitaxial growth of AlN on sapphire (0 0 0 1) by sputtering: a structural, morphological and optical study", *J. Crystal Growth*, **242**, 1-2, 116-12, 2002

92. Masahiro Sakai, Hiroyasu Ishikawa, Takashi Egawa, Takashi Jimbo, Masayoshi Umeno, Tomohiko Shibata, Keiichiro Asai, Shigeaki Sumiya, Yoshitaka Kuraoka, Mitsuhiro Tanaka and Osamu Oda, "Growth of high-quality GaN films on epitaxial AlN/sapphire templates by MOVPE", *J. Crystal Growth*, **244**, 1, 6-11, 2002

93. Y. Ohba and R. Sato, "Growth of AlN on sapphire substrates by using a thin AlN buffer layer grown two-dimensionally at a very low V/III ratio", *J. Crystal Growth,* **221**, 1-4, 258-261, 2000

94. Tomohiko Shibata, Keiichiro Asai, Yukinori Nakamura, Mitsuhiro Tanaka, Kazuyuki Kaigawa, Junko Shibata and Hiroaki Sakai, "AlN epitaxial growth on off-angle *R*-plane sapphire substrates by MOCVD", *J. Crystal Growth,* **229,** 1-4, 63-68, 2001

95. M. Kadota, T. Miura, "Shear bulk wave transducer made of (1120)-plane epitaxial ZnO film on R-sapphire", *Jpn. J. Appl. Phys. Part 1*, **41**, 3281, 2002

96. K. Kondo, M. Harada, N. Shibata, "Epitaxial growth of ZnO/AlN heterostructures on sapphire and Si substrates", *J Ceram. Soc.,* **110**, 343, 2002

97. H. B. Kang, K. Nakamura, Ishikawa, "Growth of ZnO thin films on sapphire substrates by ECR-assisted MBE." *IEEE Epitaxial Oxide Thin Films III. Symposium,* 395, 1997

98. M. A. I. Johnson, S. Fujita, W. H. Rowland, W. C. Hughes, "MBE growth and properties of ZnO on sapphire and SiC substrates", *J. Electr. Mater.*, **25**, 855, 1996

99. B. A. Movchan and A. Z. Demchishin. " Study of the structureand properties of thick vacuum condensates of nickel, titanium , aluminum oxide and zirconium dioxide,' *Phys. Met. Metallogr.,* **28**, 83, 1969

100. B. D. Cullity, "Elements of X-ray diffraction", *Prentice Hall*, 2001

101. C. Hammond, "The basics of crystallography and diffraction", 2nd ed, *Oxford University Press*, 2001

102. V. J. Moris, " Atomic Force Microscopy for biologists", *Imperial College press*, 1999

103. J. Goldstein, "Practical scanning electron microscopy: electron and ion microscobe analysis", Blenum Press, 1975

104. CRC Materials sciences and engineering handbook, CRC Press. 1994

105. W. R. Smith, H. M. Gerard, J. H. Collins, T. W. Redder and H. J. Shaw, "Analysis of interdigital surface acoustic wave trnsducers by use of an equivalent circuit model", *IEEE Trans. Microwave Theory Techniques,* **MTT-**

17, 856-864, 1969

106. H. Liess, A. Sacher, "Voltage coefficient, distortion and noise in carbon resistors, *Radio Mentor*, **34**, 551, 1968

107. H. Sutcliffe, "Current-induced resistor noise not attributable entirely to fluctuations of conductivity", *Electronic. Lett.*, **7**, 160, 1971

108. H. J. Lo, "Relation between quality and current noise in carbon film resistors", *J. Korea institute of Electronics Eng.*, **9**, 253, 1972

109. W. J. Moore, "Statistical studies of l/f noise from carbon resistors", *J. Appl. Phys.*, **45**, 1896, 1974

109. B. K. Jones, "1/f and 1/ Delta f noise produced by a radio-frequency current in a carbon resistor", *Electron. Lett.*, **12**, 110, 1976

110. I. Brodie, "The significance of fluctuation phenomena in vacuum Microelectronics", *Intl. Electron Dev. Techn. Digest*, 521, 1989

111. R. J. Espinosa, H. H. Busta, "Applications of carbon film cold cathodes in vacuum electron devices", *Intl Vac. Electronics Confer 2000*, 2000

112. E. J. P. May, H. M. Aniagyei, "Reply to comment on low-frequency noise in incandescent filaments", *Electron. Lett.*, **10**, 369, 1974

113. T. Musha, "1/f fluctuations", *Oyo Buturi*, **46**, 1144, 1977

114. V. N. Kuleshov, B. E. Leshukov, "Fluctuations in transistor power amplifiers and oscillators", *Radiofizik*, **17**, 840, 1974

115. Van Der Ziel "Flicker noise in electronic devices", *Adv. Electron. and electron phys.*, **49**, 225, 1979

116. J. Nishizawa, T. Terasaki, J. Shibata, "Field-effect transistor versus analog transistor", *IEEE Trans. on Electron Devices*, **22**, 185, 1975

117. M. J. Deen, E. Simoen, "Low-frequency noise in polysilicon-emitter bipolar transistors", *IEE Proceedings-Circuits, Devices and Systems*, **40**, 149, 2002

118. S. Jarrix, C. Deiseny, Y. Mourier, F. Pascal, G. Lecoy, T. Kleinpenning, "Comparison of noise between passivated and unpassivated AlGaAs/GaAs and GaInP/GaAs HBTs", *Semiconductor Science and Technology*, **12**, 1630, 1997

119. B. Hughes, N. G. Fernadez, J. M. Gladstone, "GaAs FET's with a flicker-noise corner below 1 MHz", *IEEE Trans. on Electron Devices,* **34**, 733, 1987

120. A. Mircea, A. Roussel, A. Mitonneau, "1/f noise: still a surface effect", *Phys. Lett. A*, **41A**, 345, 1972

121. R. L. Baer, D. M. Hoover, D. Molinari, E. C. Herleikson, "Phase noise in SAW filters", *Proc. IEEE Ultrason. Symp.*, 30, 1984

122. R. L. Baer, "Phase noise in surface-acoustic-wave filters and resonators", *IEEE Trans. Ultrason. Ferr. And Freq. contr.*, **35**, 421, 1988

123. I. D. Avramov, "Very wide tuning range, low-noise voltage controlled oscillators using ladder type leaky surface acoustic wave filters", *Proc. of the IEEE Intl. Freq. Contr. Symp*, 489, 1998

124. S. Doberstein, A. Martynov, V. Malyukhov, "Hybrid wide-band VCOs using low-loss leaky SAW ring filters", *Proc, of 10th Intl. Confere. on European Freq. and Time*, 420, 1996

125. T. E. Parker, "1/f phase noise in quartz SAW devices", *Electronics Lett.*, **15**, 296, 1979

126. W. J. Tanski, "Elements of SAW resonator fabrication and performance", *Proc. of the Thirty Fifth Ann. Freq. Contr. Symp*, 388, 1981

127. S. S. Elliot, R. C. Bray, "Direct phase noise measurements of SAW resonators", *Proc. IEEE Ultrason. Symp.*, 180, 1984

128. G. K. Montress, T. E. Parker, M. J. Loboda, J. A. Greer, "Extremely low-phase-noise SAW resonators and oscillators: design and performance", *IEEE Trans on Ultrasonics, Ferr. and Freq. Contr.*, **35**, 657, 1988

129. Dai Enguang, "Surface-related phase noise in SAW resonators", *IEEE Trans on Ultrasonics, Ferr. and Freq. Contr.*, **49**, 649, 2002

130. E. Sang, R. Beckman, P. Snow, J. Wright, "Design and manufacture of SAW resonators for low phase noise and low vibration sensitivity applications", *Proc. IEEE Ultrason. Symp.*, 245, 1986

131. A. Mauder, "SAW gas sensors: comparison between delay line and two port resonator", *Sensors and Actuators B*, **B26**, 187, 1995

132. A. S. Luchinin, A. V. Korobeinikov, "Study of noise characteristics of BAW and SAW quartz resonators", *Radiofizika*, 36, 1993

133. T. E. Parker, G. K. Montress, "Low-noise SAW resonator oscillators", *Proc. of the 43rd Ann. Symp. on Freq. Contr.*, 588, 1989

134. T. E. Parker, G. K. Montress, "Frequency stability of high performance SAW oscillators", *Proc. IEEE Ultrason. Symp.*, 37, 1989

135. T. E. Parker, G. K. Montress and D. Andres, "Review of SAW oscillator performance", *Proc. IEEE Ultrason. Symp.* , 43, 1994

136. T. E. Parker, G. K. Montress and M. J. Loboda, "Residual phase noise measurements of VHF, UHF, and microwave components", *Proc. of the 43rd Ann. Symp. Freq. Contr.*, 349, 1989

137. T. F. O'Shea, M. R. Lewis, B. H. Horine, "Low-noise voltage controlled SAW oscillator for phased lock loop application", *Proc. IEEE Ultrason. Symp.*, 53, 1987

138. C. K. Campbell, P. J. Edmonson, P. M. Smith, "The phase noise characteristics of a driven SAW oscillator in the threshold vicinity for injection locking", *Proc. IEEE Ultrason. Symp.*, 283, 1985

139. K. Borst, B. Fleischmann, K. Wacker, "Design of low phase noise UHF-oscillator with advanced SAW-resonator-technology", *Confere. Proc. 20th European Microwave Conference 90*, 1748, 1990

140. E. J. Staples, T. C. Lim, "300 MHz oscillators using SAW resonators and delay lines", *31st Ann. Freq. Contr. Symp.*, 371, 1977

141. I. D. Avramov, "Very wide tuning range, low-noise voltage controlled oscillators using ladder type leaky surface acoustic wave filters", *Proc. of the IEEE Intl. Freq. Contr. Symp.*, 489, 1998

142. C. K. Campbell, J. J. Sferrazza Papa, P. J. Edmonson, "Study of a UHF mobile

radio receiver using a voltage-controlled SAW local oscillator", *IEEE Trans. on Sonics Ultrason.*, **SU-31**, 40, 1984

143. T. F. O'Shea, M. R. Lewis, B. R. Horine, "SAW feedback stabilizes VCO for low noise", *Microwaves & RF*, **27**, 109, 1988

144. P. H. Handel, "New insights on fundamental 1/f noise theory and applications", *Proceedings of International APS/IEEE Conference on Noise in Physical Systems and 1/f Fluctuations*, 584, 2001

145. T. E. Parker, "Characteristics and sources of phase noise in stable oscillators", *IEEE Proc. 41st Annu. Freq. Symp.*, 99, 1987

146. P. H. Handel, "Incoherence and negative entropy in the quantum 1/f effect of BAW and SAW quartz resonators", *IEEE Freq. Contr. Symp.*, 464 -469, 1997

147. P. H. Handel, "Quantum 1/f effect in piezoelectric sensors", *IEEE Freq. Contr. Symp. and PDA Exhibition*, 430 -437, 2001

148. P. H. Handel, "Calculation of incoherent quantum 1/f frequency fluctuations in low-Q BAW and SAW quartz resonators", *IEEE Freq. Contr. Symp.*, 502-506 1998.

149. P. H. Handel, "Quantum 1/f quartz resonator theory versus experiment:, *IEEE Intl. Freq. Contr. Symp.*, **2**, 1192 -1195, 1999

150. R. L. Jungerman, R.L. Baer, R.C. Bray, "Delay dependence of phase noise in SAW filters", *Proc. IEEE Ultrason. Symp.*, 258, 1985

151. T. E. Parker, D. Andres, J. A. Greer, G. K.Montress, "1/f noise in etched groove surface acoustic wave (SAW) resonators", *IEEE Trans. on Ultrason. Ferr. Freq. Contr.*, **41**, 6, 853 -862, 1994

152. T. E. Parker, D. Andres, "Dependence of SAW resonator 1/f noise on device size", *Freq. Contr. Symp.*, 178 -185, 1993

153. D. B. Leeson, "A sample model of feedback oscillator noise spectrum", *Proc. IEEE*, **54**, 329-330, 1996